POLITECNICO DI TORINO

Corso di Laurea Magistrale
in Ingegneria Meccanica

Tesi di Laurea Magistrale

Diamond dressing of vitrified grinding wheels

Relatori:
Atzeni Eleonora (Politecnico di Torino)
Krajnik Peter (Chalmers university of technology)

Candidato:
Vindemmio Stefano

Anno accademico 2021/2022

Preface

This Master's thesis has been carried out as a project formalized by the IGC (International Grinding Centre). The tests have been run in the Materials Processing Laboratory at Chalmers University of Technology, in the period going from January 2022 to June 2022.
A debt of gratitude is owed to my supervisors, Jeffrey Badger (The Grinding Doc) and Peter Krajnik (Professor at Materials and Manufacturing/Industrial and Materials Science, Chalmers University of Technology), for their guidance and assistance along with their expertise throughout the study. The completion of this studies could not have been viable without the support of Philipp Hoier (Researcher at Materials and Manufacturing/Industrial and Materials Science, Chalmers University of Technology).
Furthermore, I would like to express my gratitude to Francesco Nigro, my thesis partner, and Eleonora Atzeni (Associate Professor, Politecnico di Torino) my supervisor at Polytechnic of Turin.
Finally, I would like to thank my family and friends, who have given me emotional support. Without them none of this would have been possible.

Stefano Vindemmio

Contents

1. Abstract

The aim of the work is to provide a detailed description of grinding and dressing, focusing on definitions, involved phenomena during the operations, different kind of machines, applications and main variables to know for complete understating of the processes.
A state of the art on previous tests carried out by Malkin, Murray and Salmon on effects of rotary dressing on grinding wheels performances is presented as well as a definition of Aggressiveness number in finishing processes and studies on utility of acoustic emission signal monitoring during dressing, by Badger et al.
By carrying on the mentioned experiments and expanding the studies to new evaluations, the purpose is to analyse effects of plunge-roll diamond dressing on vitrified grinding wheels performances, establish dressing Aggressiveness number importance in industry for monitoring thermal damage and speeding-up the process (clear correlations between dressing and grinding variables and dressing Aggressiveness number have been noticed), prove the possibility of wheel sharpness assessment and the acoustic emission signal monitoring relevance in dressing.
In order to analyse the effects of the plunge roll dressing on grinding wheel performances, tests on a BLOHM grinding and dressing machine, by using a diamond plunge-roll dresser from Meister Abrasives, an Aluminum oxide grinding wheel and several flat steel workpieces have been performed. First of all, the tests will be run with fixed grinding conditions, and finally with variable grinding conditions as well to see the combined effects of grinding and dressing parameters on heat generation.
Furthermore, scanning electron microscope has been used for assessing the wheel topography after dressing, and differences between dull and sharp dressing have been found out.
Additional studies on the topic are necessary, since further developments on grinding and fine-finishing processes are required for modern and future applications in the industry (Krajnik et al.).

2. Grinding operation

In this chapter, the most important concepts of grinding will be explained. Information are gathered from personal knowledge and [1] [2] [3].

Grinding is an abrasive process in which grits with geometrically undefined cutting edges and with random distribution are shaped in a grinding wheel which will be used for the material removal. Moreover, those cutting edges are way more than in other machining operation such as milling, and the equivalent chip thickness is smaller. In particular, in manufacturing, the terminology grinding refers to the material removal by means of a rotating abrasive wheel. The grinding wheel is composed by many grits bonded together, with a certain porosity as shown in Figure 1.

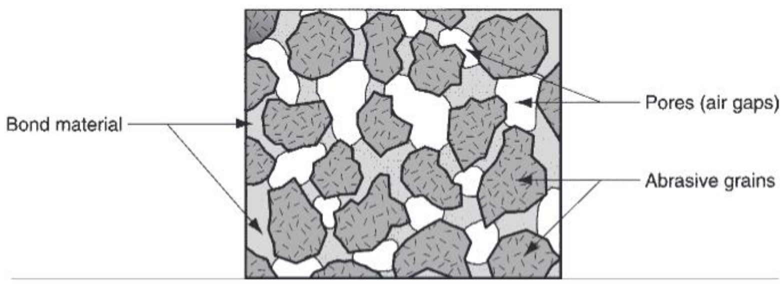

Figure 1: structure of a grinding wheel [1]

The mechanism for material removal is not only cutting as for other machining operations, in this case rubbing and plowing are involved as well (Figure 2), indeed the heat generation in a grinding operation is not to be disregarded.

Cutting consists of chip formation from the cutting action of a single grit into the workpiece.

Plowing occurs in case of the projection of the grit into the workpiece results not far enough, hence cutting is not possible and the workpiece surface is deformed, with heat generation and no material removal.

Rubbing includes the grit contact with the workpiece surface with just rubbing friction, material is not removed and there is heat generation as well.

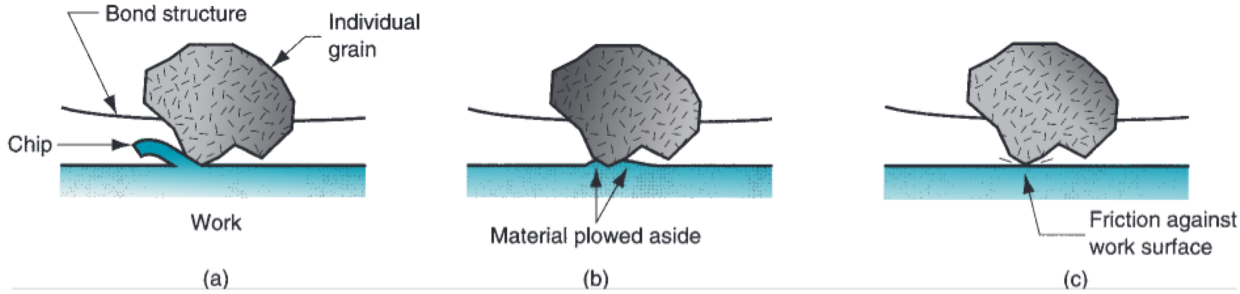

Figure 2: (a) cutting, (b) plowing and (c) rubbing during grinding operation [1]

Given the higher heat generation compared to other operations like turning, milling, drilling, regardless grinding conditions, coolant should always be used at the interface between workpiece and grinding wheel.

More into details, differences between grinding operation and regular machining operations are several:

- The grains are randomly distributed over the grinding wheel surface, and they have irregular shapes.

- An average rake angle is typically negative, hence there is more plastic deformation of chips than in other processes such as milling.
- Not all the grains are acting at the same time on the workpiece, they are in different radial positions.
- Tangential speeds are typically very high (about 30m/s usually, but up to 150m/s).

Nevertheless, the reasons why grinding is a frequently used operation are multiple as well:

- Possible to machine a large variety of materials and materials with high hardness (>50 HRC).
- Fine finishing of the workpiece surface (down to 0.025µm of surface roughness).
- Tight tolerances possible to achieve because of the small amount of stock removed.
- Grinding pressure is not so high, hence workpieces can be hold by magnetic chucks (if ferromagnetic).

During the grinding process different phenomena can occur.
Temperature rise, for instance is relevant and to be taken into account, indeed it could change material properties on the surface, create residual stresses and cause distortions in the workpiece due to expansion and contraction of the latter. Generally, the higher are depth of cut, wheel speed, workpiece speed (feedrate), the higher is the temperature rise.
During the operations, chips are formed, and they help for heat removal, nevertheless temperature can reach peaks of 1600°C.
Since the grinding operation is usually run in atmosphere without inert gas, there is the presence of Oxygen and hence the possibility of exothermic reactions and sparks. The type of sparks depends on the worked material.
Moreover, tempering and softening could occur due to the thermal rising. Grinding fluids should be carefully selected depending on operations and materials.
Excessive temperature could cause burning on the workpiece surface, and residual stresses as well. Burning would ruin the surface and lead to poor metallurgical properties, on the other hand residual stresses would cause a low resistance to fatigue phenomenon.
In order to avoid all these problems is well-practice to adjust grinding parameters and use a grinding fluid during the operation. Usually the fluid is a water-based emulsion. The nozzle is adjusted to the right position to dispense the liquid at high pressure in the direction of the contact point.

Chatter could be another problem of the process. It affects the surface finish of the workpiece.
There are several possible causes: bearings and spindle of the grinding machine, non-uniformities of the grinding wheel or non-uniform wear, poor dressing techniques, non-balanced grinding wheels, external sources. Damping and stiffness are the main parameters to look at when chatter occurs, and for solving it, is possible to reduce material removal rate, change dressing parameters or dressing technique, use a softer-grade wheel, support rigidly the workpiece.

2.1 Grinding machines

The selection of the machine depends on the workpiece shape and features mostly. Many machines nowadays are CNC and with clamping devices or magnetic chucks. Some of them have the possibility to dress in the same station as grinding is performed. There are two different movements of grinding wheel into workpiece: radial or traverse.

2.1.1 Surface grinding

Surface grinding is one of the most common grinding operations, for grinding flat surfaces. The workpiece is hold by a magnetic chuck, and a grinding wheel with a straight profile is typically mounted on a horizontal spindle (Figure 3), however it is possible on a vertical one as well. Traverse grinding occurs with a length and width of work (given by width of the grinding wheel or width of the workpiece if thinner than the previous), a depth of cut (in radial direction) of grinding wheel into workpiece, a selected number of passes, a workpiece feedrate (parallel to workpiece surface), and given revolutions per minute of grinding wheel. For obtaining grooves it is possible to plunge the grinder into the workpiece.

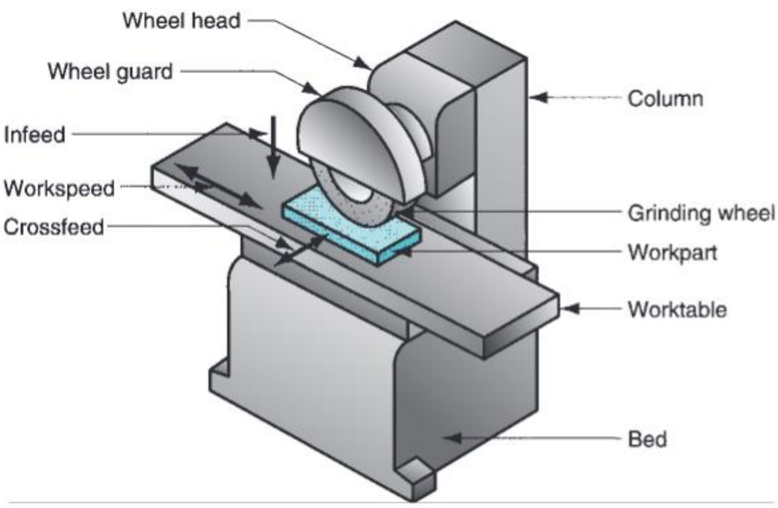

Figure 3: surface grinding machine with horizontal grinding wheel spindle [1]

2.1.2 Cylindrical grinding

Using cylindrical grinding it is possible to grind cylindrical surfaces and shafts' shoulders. The cylindrical workpiece will rotate about its axis and eventually transversely move along its axis. The workpiece is usually hold between two centres.

Different operations of straight cylindrical grinding can be performed, the axis of workpiece and grinding wheel are parallel, and the wheel can eventually be shaped for working shoulders on a shaft. If working a flat workpiece, it is possible to perform traverse grinding over all the length, or plunge grinding (Figure 4). Otherwise, profile grinding for shaped workpieces. Moreover, cams and camshafts can be ground and threads as well with traverse or plunge grinding, depending on the wheel shape.

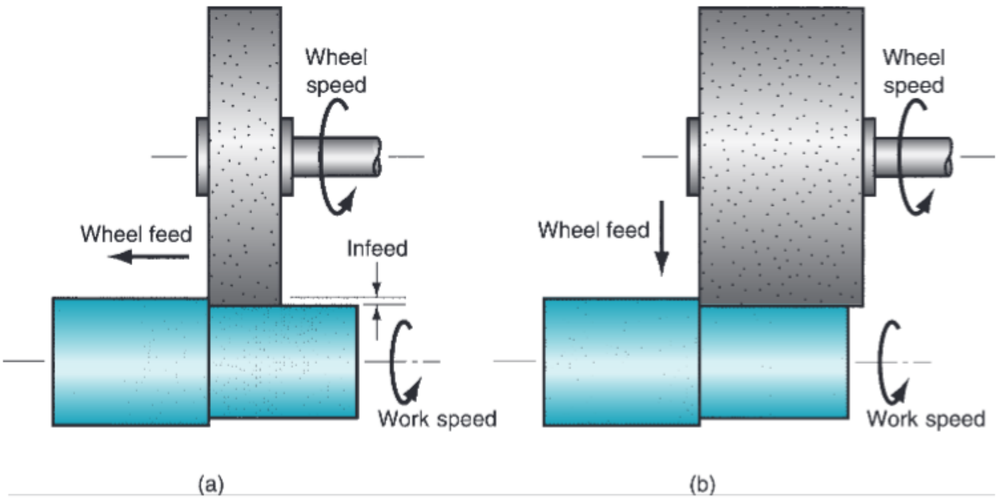

Figure 4: cylindrical grinding, (a) traverse operation and (b) plunge operation [1]

2.1.3 Internal grinding

In order to perform internal grinding, a small wheel is utilized to grind the inside diameter of the part (Figure 5). The workpiece is hold in a rotating chuck and the wheel is mounted on a spindle. It is possible to perform profile grinding by using a shaped wheel. Common for boring operation.

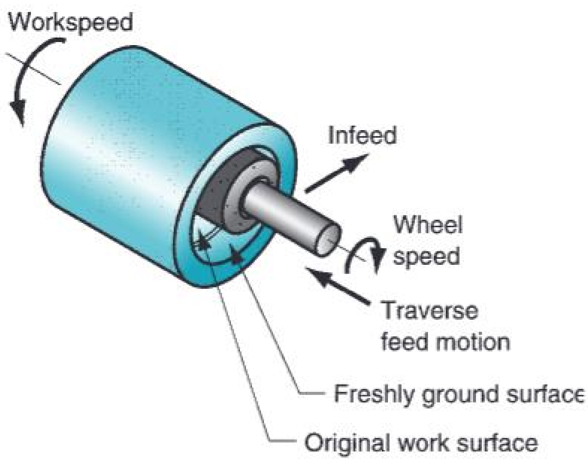

Figure 5: internal grinding operation [1]

2.1.4 Centerless grinding

Centreless grinding is a grinding process used for cylindrical surfaces in which the workpiece is supported by a blade, not by centres as usual. Technique usually performed for grinding parts such as piston pins, engine valves, camshafts. Moreover, components with small diameters can be worked, and with reduction in handling time with respect to conventional cylindrical grinding. As normal traverse grinding, plunge grinding and profile grinding are the options.

Between the most common operations for centreless grinding there are:

- Through-feed grinding, the workpiece is supported by a blade, and placed in between the grinding wheel and a regulating wheel (Figure 6). The purpose of the regulating wheel is to regulate the axial feed of the cylindrical workpiece, and in order to accomplish this function it is tilted with a small angle. The axial feed is parallel to the axis of the grinding wheel. The speed of the regulating wheel is 20 times smaller than the one of the grinding wheel.

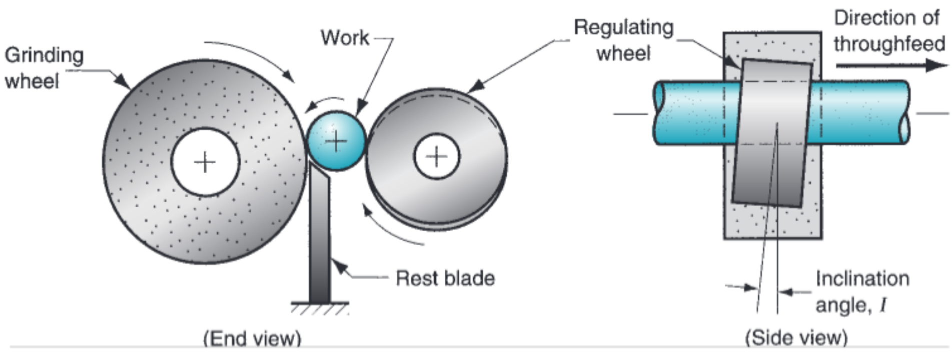

Figure 6: centreless grinding, through-feed operation [1]

- Plunge grinding (or in-feed grinding), used for grinding parts with variable diameters such as shoulders. As for the previous case, there are grinding wheel and a regulating wheel, but in this case no blades. An end stop is also part of the equipment.

- Internal centerless grinding, in this operation 3 rolls are involved (support roll, regulating roll and pressure roll) while a grinder shaft is working the internal diameter of the workpiece (Figure 7).

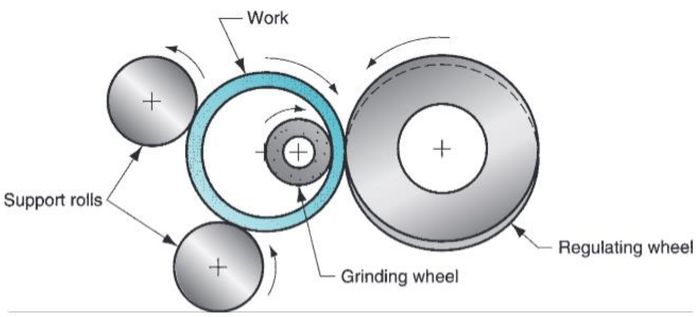

Figure 7: internal centreless grinding [1]

2.1.5 Creep-feed grinding

Creep-feed grinding is a grinding operation associated with small rates of material removal (Figure 8). The depth of cut is from 1 to 6mm (high values) and the workpiece speed (feedrate) is slow: these are the main differences with conventional surface grinding. For avoiding excessing temperature, the wheels have an open structure with many porosities, and they are resin bonded. Furthermore, creep-feed grinding can be applied on cylindrical surfaces as well. Grinders are equipped with devices for continuously dressing.

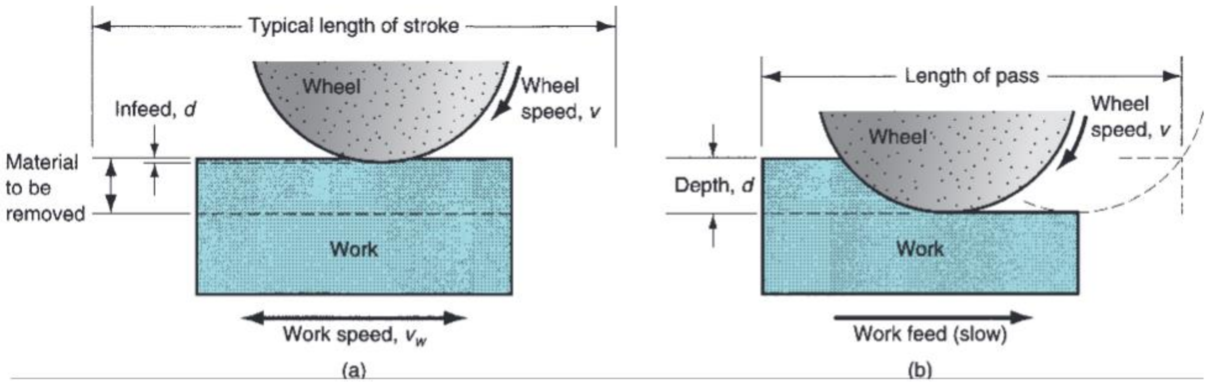

Figure 8: comparison between (a) conventional surface grinding and creep-feed grinding (b) [1]

2.1.6 Heavy stock removal by grinding

Another option given by the grinding operations is for heavy stock removal, indeed by increasing process parameters it is possible to obtain larger stock removals. Sometimes this technique can be preferred over other types of machining processes. Surface roughness is not of primary importance in this case.

2.1.7 Other grinding operations

Several special grinding machines for particular operations are here stated:

- Universal tool and cutter grinders are used for grinding single or multi-point tools and cutters.
- Tool-post grinders, attached on the tool post of a lathe.
- Swing-frame grinders, used for grinding large castings. It is a rough grinding, called snagging.
- Portable grinders, driven pneumatically or electrically. Used for cutting off weld beads.
- Bench and pedestal grinders, for simple and manual operations for small parts.

2.2 Grinding wheel wear

Grinding wheel wear is a similar phenomenon to wear in normal cutting tools for turning for instance. The difference is that there are 3 wear methods: attritious grain wear, grain fracture and bond fracture.

2.2.1 Attritious wear

In this first type of wear, the grains are becoming dull (originally sharp) developing a wear flat area. This is given by chemical and physical interaction between steel workpiece and grinding wheels' abrasive grains, such as diffusion, friction and chemical reaction at high temperatures. If the two materials in contact are chemically inert, the wear will be lower since there will be less tendency for reaction and adhesion. An example of that is using Aluminum oxide grinding wheels on iron workpieces, they are inert with respect to each other, hence the wear is way lower than for instance if using a Silicon carbide or diamond grinding wheel. CBN would be suitable for steels as well.
Thus, the selection of abrasive type is dependent on the reactivity between the two materials that are involved in the operation, and of course the objective is to reduce the attritious wear.

2.2.2 Grain fracture

The grains should break partially while the remaining part stays in the grinding wheel, but at an acceptable rate (not too fast) to allow the presence of sharp edges. Indeed, if too many dull flat areas are present, the grinding operation would not be efficient speaking about the energy and heat generation. The friability of the abrasives influences the self-sharpening processes and affects grinding efficiency. Low friability and high attritious wear are not a good combination and together they would lead to too dull grains, many flat areas and consequently an inefficient process, thus also workpiece surface burning could occur.

2.2.3 Bond fracture

Bond fracture consists of grains being pulled out of the bonding material, and it is mainly regulated by the strength of the bond, given by the grade. If the bond is too strong, the dull grains are not possible to be dislodged from the grinding wheel, preventing the self-sharpening of the latter. However, if the bond is too weak, the wear would result too high since it would be too easy to dislodge a grain. A rule of thumbs suggests using soft grades for hard materials for reducing stresses and thermal damage chances, and hard grades for softer material in order to remove material at a faster rate.

2.2.4 Wear curve

A wear curve can be identified, and the volume of wear wheel can be plotted versus the volume of work material removed (Figure 9). This wear curve will involve all three types of wear. Three regions can be distinguished:

- *First region*: the grains are initially sharp and grain fracture is occurring.
- *Second region*: the wear rate is constant (constant slope). Attritiuos wear together with some grain and bond fracture is occurring.
- *Third region*: the wheel is becoming duller and duller, and amount of plowing and rubbing is increasing compared to the cutting action. Moreover, some chips are stuck in the grinding wheel pores, causing the so-called wheel loading and leading to higher temperatures and inefficiency.

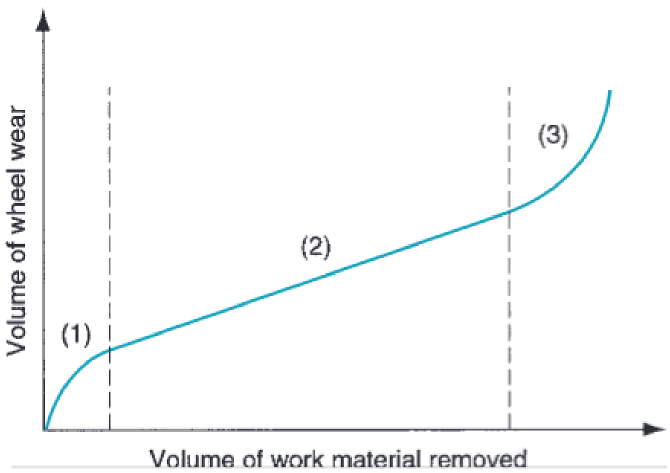

Figure 9: wheel wear curve [1]

The grinding ratio GR represents the slope of the wheel wear curve and is given by the ratio between the volume of work material removed and the corresponding volume of grinding wheel that is worn in the process (1).

$$GR = \frac{V_w}{V_g} \tag{1}$$

Typical values are between 95 and 125, but it can vary between 2 and 200.
Generally, with higher wheel speed, the grinding ratio results higher, furthermore it is influenced by type of wheel, grinding material and grinding fluid. A trade-off should be found since high grinding ratios would indicate grain dulling, and low grinding ratios too much wheel wear.
When a grinding wheel wear curve is approaching the third region, *dressing operation* becomes necessary for breaking of dull grits and removing clogged chips. A more detailed description of the dressing operation will be presented in: 3. Dressing and truing operations

2.3 Grinding wheels designation

Grinding wheels are distinguished one to the other by using a standardized system of letters and numbers for indicating: abrasive type, grain size, grade, structure and bond type. Moreover, there are differences for this standardization depending on if conventional or superabrasives.

2.3.1 Abrasive types

The most common abrasives used for grinding wheels are Aluminum oxide (Al2O3) and Silicon carbide (SiC), known as conventional abrasives, and Cubic boron nitride (CBN) and diamond, known as superabrasives. It is clear that hardness is the main property that is required by an abrasive operation such as grinding, but friability is to be considered as well when choosing the material, because of self-sharpening properties. For instance, Al_2O_3 is less friable than SiC, hence it has less tendency to fragmentation of grains.
Furthermore, shape and size of the grits affects the friability as well.
The above-mentioned materials are synthetically produced since if using common abrasives that is possible to find in nature, there would be many impurities together with the grains.

A more detailed description of each one of them is in the following:

- *Al_2O_3*, it is produced by fusing bauxite, iron filings and coke. There are 3 different classes of fused aluminum oxides: dark (less friable), white (more friable) and single crystal.
  Seeded gel on the other hand is the purest form of unfused Aluminum oxide, known as ceramic Aluminum oxide. One of the main characteristics is the small grain size (about 0.2µm). The grains are sintered for reaching larger sizes. Seeded gel is used for difficult to grind materials since it has high hardness, high friability and high self-sharpening.

- *SiC*, made of silica sand and petroleum coke. Silicon carbides can be distinguished in black (less friable) and green (more friable). Overall, the friability is higher than in aluminum oxides, thus the fragmentation and the self-sharpening are higher.

- *CBN*, it is the second hardest material after diamond, and it is made synthetically with similar techniques used for producing synthetic diamonds. It has high resistance to oxidation and high temperatures, hence it works well when used for grinding hardened ferrous materials

- *Diamond*, it is the hardest known material. It is a form of carbon with a covalently bonded structure. Synthetic diamond was first discovered in 1955, and the process consists in apply high temperatures and pressure to graphite specimens. It is mainly used for working very hard materials or reconditioning grinding wheels by dressing, and it is the more expensive of all the mentioned abrasives.

Furthermore, in order to choose which abrasive to use for a grinding operation, depending on the material to work, the working affinity is to be considered.
In the following there are recommendations:

- Aluminum oxide to be used for ferrous materials, mainly carbon steel.
- Silicon carbide for non-ferrous metals like aluminum, ceramics, glass and cast irons.
- Cubic-boron nitride for steels and cast irons with >50HRC hardness and high-temperature resistant alloys.

- Diamonds for the hardest materials, ceramics and some hardened steels.

2.3.2 Grit size

The grit size gives an indication of the average size of the grits that form the grinding wheel. There is a scatter as not all grits are of the stated size.
A larger number stands for a finer grit size. With finer grits, there are lower grinding forces, lower grinding ratio, better surface finish and lower heat generation during grinding. Mostly, the grit selection depends on surface roughness to achieve. It is possible to combine grit sizes.

2.3.3 Grade (Hardness)

The hardness in the designation is specified as a letter, going from A to Z. It indicates the force required for breaking a grit out of the binding structure. With higher strength brings to less wear (higher GR), however higher forces and temperatures during grinding operation. Ideally the hardness should be tuned in order to have self-sharpening of the wheel, and if the harness results too high the process is prevented. On the other hand, too soft wheel would wear very fast. The surface roughness gets better with larger hardness.

2.3.4 Structure

The structure of a grinding wheel is indicated by a number, going from low to high number the density decreases. It represents indeed the concentration of abrasives grits in the bond. The selection of the structure depends on grinding operation and material to work. More open structures would lead to higher grinding forces and temperatures, as well as higher surface roughness, and lower grinding ratio.

2.3.5 Bond types

Many bonds are possible to use depending on the wanted properties. In the following the different types of bonding are described more into details:

- *Vitrified*: also called ceramic bond, it is the most common bond. It consists of crystalline mineral and clays, mixed with the abrasive and shaped to become grinding wheels. The wheels are the heated for forming a structure with higher strength. Finally, slowly cooled down and finished.
  By using this kind of bond, stiff, porous and resistant to liquid agents grinding wheels are obtained; however of course they are brittle. The colour of the grinding wheel can be modified by using various elements.

- *Resinoid*: the bond is an organic compound, hence the grinding wheel bonded with resinoid are called organic wheels. For manufacturing the grinding wheel, the procedure consists in mixing the liquid or powdered phenolic resin with the abrasive grains, pressing and shaping them in the wanted part, and curing at low temperature. These wheels are more flexible than the ones produced with the vitrified bond. Instead of phenolic resin there is the possibility of using polyimide and moreover, grinding wheels with this bond can be produced with injection moulding.

- *Reinforced wheels*: layers of fiberglass mats are providing additional strength to the resinoid bonded wheels.

- *Thermoplastic*: the bond is a thermoplastic material.

- *Rubber*: the most flexible possible bond is that one. Rubber bonded thin wheels are produced for cutting-off operations. The manufacturing process involves mixing rubber, sulfur and abrasive grits, rolling the mix into sheets and cutting out circles from the sheet, then heating up to vulcanize the rubber.

- *Metal bond*: mostly used for diamond and CBN wheels. Metal powder sintered together with diamond or CBN grits and bonded to the periphery of a grinding wheel for a thickness up to some millimetres.

2.3.6 Designations examples for conventional abrasives and superabrasives

For instance, for *conventional abrasives* [3]:

51-A-36-L-5-V-23

- 51: prefix, manufacturer's symbol, optional.
- A: abrasive type. A for Aluminum oxide, or C for Silicon Carbide.
- 36: abrasive grain size, from low number to higher going from coarser to finer grains. There are 4 classes: coarse, medium, fine and very fine. 36 is a medium size.
- L: grade, from soft to hard going from A to Z, and L is a medium grade.
- 5: structure, from 1 increasing the number going from dense to open structure (more porosities).
- V: bond type. V stands for vitrified, and the other types are B resinoid, BF resinoid reinforced, E shellac, O oxychloride, R rubber, RF rubber reinforced, S silicate.
- 23: manufacturer's record, for identifying the wheel.

On the other hand, for *superabrasives* [3]:

M D 100-P 100-B A 1/8

- M: prefix, manufacturer's symbol, optional.
- D: abrasive type. D for diamond and B for CBN.
- 100: grit size. From low to high number going from smaller to bigger grit size. 100 is a medium size.
- P: grade, going from A to Z from softer to harder grade.
- 100: diamond concentration. 25 50 75 or 100, from low to high concentration.
- B: bond type, B stands for resinoid, M for metal and V for vitrified.
- A: a letter here means a bond modification.
- 1/8: diamond depth in inches, 1/16, 1/8 or 1/4. If not indicated, it is a solid diamond.

3. Dressing and truing operations

In order to control the grinding conditions such as grinding forces and surface finish, dressing and truing are usual processes to apply to a grinding wheel before starting using it.
Truing represents the minimization of the run-out from the theoretical shape.
Dressing is a reconditioning process used for reconditioning the wheel when the latter is not sharp anymore, indeed a dull grinding wheel would lead to higher heat generation and consequently to less efficiency during the process.
Processes are described in a more complete way in [4] and [5].

3.1 Dressing operation for conventional abrasives

Normally, with conventional abrasives, the truing operation is included in the dressing one, while for superabrasive wheels it is possible to separate the processes.
There are several ways of dressing a conventional abrasive dressing wheel (Aluminum oxide or Silicon carbide usually), including the following techniques.

3.1.1 Single-point (or multiple-point) diamond dressing

Consisting in a single-point diamond (or multi-edged) which is transversely fed into the grinding wheel, with a constant depth of cut (Figure 10). Two to five dressing passes are taken in addition to the ones necessary to true the wheel. There is the possibility of a final spark out, meaning passes without increasing the depth of cut. In the following figure, the application can be visualized; a drag angle between 10° and 15° is used between dresser orientation and vertical grinding wheel axis.

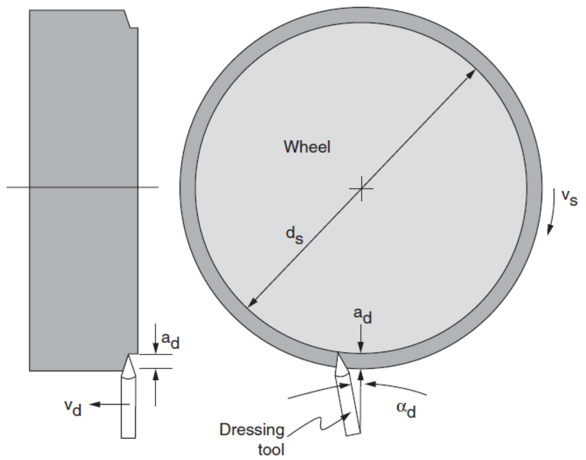

Figure 10: single-point diamond dressing for conventional abrasives [4]

3.1.2 Rotary diamond dressing (plunge-roll dressing)

This technique consists in plunging a dressing roll into a workpiece (Figure 11) and can be utilized also for profiled griding wheels.
A rotary diamond dressing roll, a roll in which diamonds particles are usually bonded in matrix, has the same profile as the one to shape on the workpiece, therefore it will be the opposite as the one on the grinding wheel.
During the dressing operation, one of the two wheels will be fixed and the other one will have the feedrate that will determine how many µm per grinding wheel revolution will be removed during the process. They will both be spinning, with different speeds depending on how sharp the wheel is needed. A good compromise is usually the dressing roll spinning with 80% of the grinding wheel speed, in the unidirectional mode. As said for the single-point diamond dressing, there is an analogous process as the spark out, called dwelling. The previously introduced parameters radial

infeed per wheel revolution, speed ratio, dwell time will be fully explained later on in: 5.2 Main variables in plunge-roll dressing.

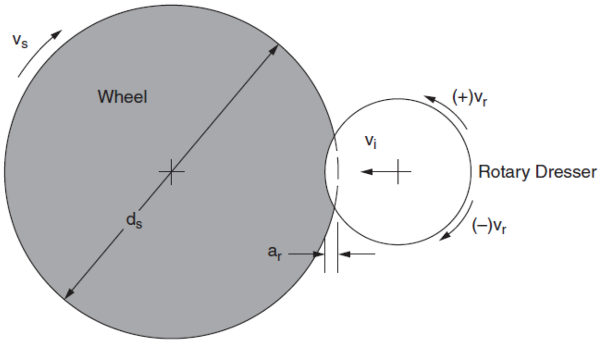

Figure 11: rotary diamond dressing for conventional abrasives [4]

3.1.3 Diamond block dressing

The grinding wheel while rotating is transversely fed through a diamond block shaped in order to achieve the wheel shape necessary for grinding the workpiece.

3.1.4 Crush dressing

The grinding wheel is plunged into a hardened steel or cemented carbide roll, with a reduced speed with respect to the one used in a grinding operation, to avoid the roll wear.

3.2 Dressing and truing for superabrasives

In this case usually the standard procedure advice truing followed by dressing. In the following different truing and dressing operations for superabrasives are described.

3.2.1 Truing of diamond wheels

Vitrified silicon carbide wheels mounted on a brake controlled truing device are used (Figure 12). The grinding wheel once in contact with the silicon carbide one, will lead to motion the latter, which will be braked just in order to have a slip velocity between the two. If the wheel is for peripherical grinding (flat profile), the truing wheel will be transversely fed through the grinding one as shown in the next figure.
If there is not the possibility of a brake-controlled device, the truing wheel should be mounted on motor-driven spindles.

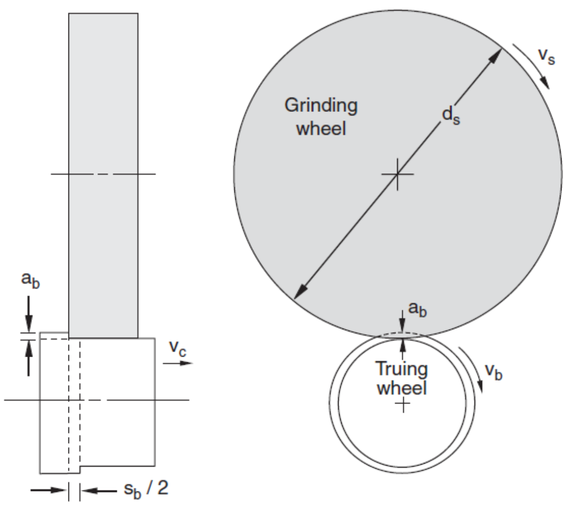

Figure 12: truing of diamond wheels [4]

3.2.2 Truing of metal and resin bonded CBN wheel

Performed with diamond tools. Since CNB is softer than diamond, it is possible to use diamond without having excessive wear. The most used diamond tools are diamond rolls and diamond cup wheels.
Once truing is completed, dressing operation is following.

3.2.3 Dressing of diamond and CBN wheels

The most common way to proceed is to feed fine-grained vitrified abrasive sticks into the wheel surface. The process will 'open up' the surface and expose the grains, by removing binder.
There are differences for diamond wheels and CBN wheels.
For diamond wheels, a silicon carbide stick is used. For CBN wheels an aluminium oxide stick is used.
Vitrified CBN is easier to work than resin bonded CBN.
If a more aggressive method, to obtain a sharper wheel is needed, a thin diamond disk can be considered as ideal dresser, especially for vitrified wheels. In this last case, the disk will transversely work the wheel, with a defined depth of cut and a certain speed ratio, usually unidirectional and with dressing disk speed equals to 40% or 80% of grinding wheel speed (Figure 13).

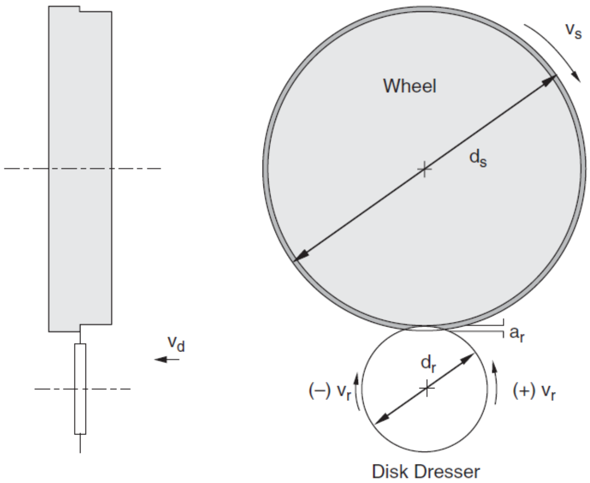

Figure 13: dressing of diamond and CBN wheels [4]

3.3 Continuous dressing

The continuous dressing is a technique which consists in dressing the grinding wheel at the same time as the latter is working on the workpiece, because by keeping regenerating the wheel, there will be less rubbing and thus less heat generation during the operation, as it will be shown in the following.
First of all, continuous dressing is only applied to conventional abrasives like Aluminum oxide and Silicon carbide, because of cost reasons.
There are several ways of implementing this operation.
The simplest one is the single-point diamond dressing (Figure 14). The action in this case will not be properly continuous but intermittent, because the dresser is acting transversely on the grinding wheel until reaching the final width of the latter, and then coming back and starting again the same procedure. There is a major issue though, since the grinding wheel is dressed in a transverse way, the workpiece will be ground with two different depths.

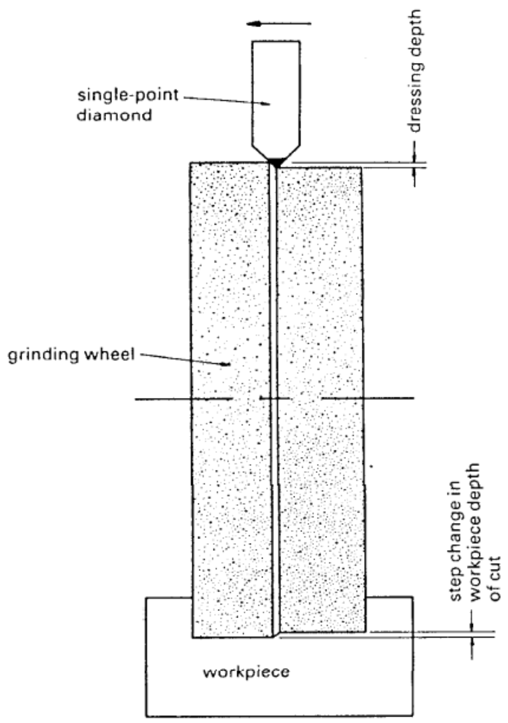

Figure 14: continuous single-point diamond dressing [5]

Another method is the crush dressing, which is the one that produces the sharper wheel profile. Nevertheless, there are a few adjustments to consider in order to be able to apply continuous dressing with this kind of operation, since conventional crush dressing would be done at reduced wheel speeds, but in this case the wheel speed will be the one that will ground the workpiece, then a high speed. The problems are that at such speed there is the possibility of developing chatter phenomena. The condition for chatter is that it will occur if the dresser width is less than a certain limit, then to overcome the issue, the ideal would be to use a thinner dresser which will work transversely on the grinding wheel (but there will be the same problem as the one mentioned for single-point diamond dressing), or a helical dresser (Figure 15).

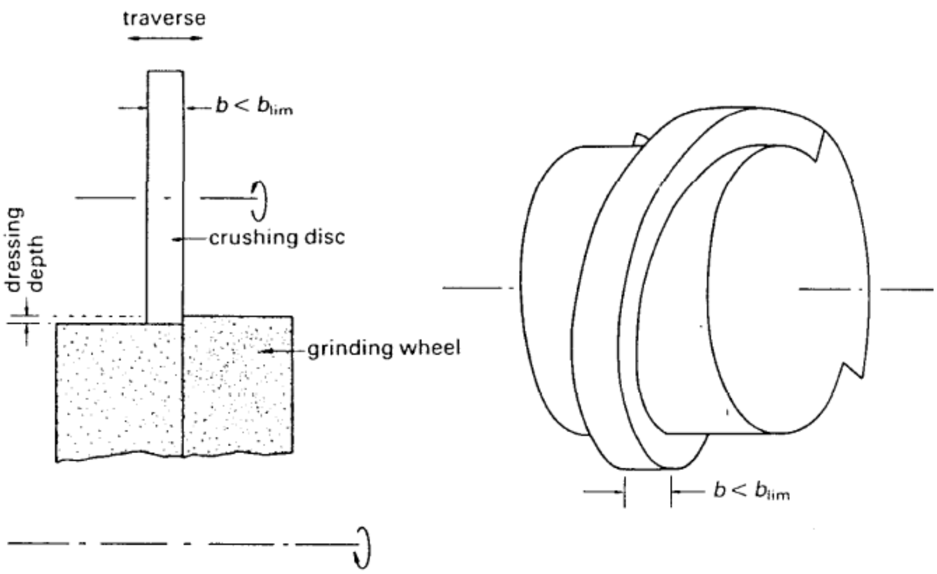

Figure 15: transverse dressing and helical dressing for avoiding chatter in continuous crush dressing [5]

Finally, one of the most suitable types of dressing for continuous operations is the diamond roller dressing (Figure 16). There are no modifications necessary from the normal diamond roller dressing. The diamond roller will be expensive, but if the batch is large enough the purchasing is justified.
In these machines for continuous dressing, the diamond roller is pushed into the grinding wheel by means of an arm. Possibly there is an automatic compensation for wheel wear due to the dressing.

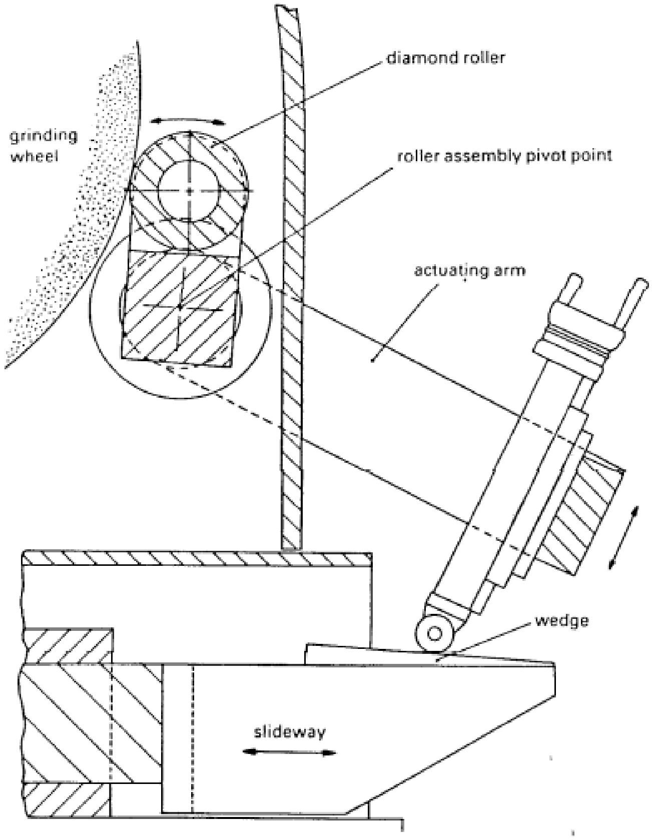

Figure 16: diamond roller continuous dressing [5]

4. Grinding and dressing applications

In the scope of giving a reason to these studies and experiments on dressing and grinding, an example of the importance of these operations in the manufacturing chain nowadays and in the future is presented.

As already mentioned, through grinding it is possible to achieve tight tolerances and low surface roughness, and moreover work a large variety of materials.

On the other hand, dressing is an operation necessary to recondition the grinding wheel, that will determine the performances during grinding, especially heat generation and surface roughness depending on if sharp or dull dressing condition.

Examples of application of grinding and dressing for modern and future applications are proposed by Krajnik et al. in [6].

The automotive industry is one of the main driving forces for finishing operations. Lately, electrification of vehicles and new regulations are pushing the finishing process manufacturing to even higher requirements. Industry professionals have been interviewed by Krajnik et al. about the topic of the future of grinding and finishing processes in the automotive industry, mainly about powertrain components; it turned out that the new requirements for the electrifications will involve stricter requisites regarding noise (e.g. for gears), geometry (e.g. roundness for shafts and bearings), surface integrity and surface roughness (for bearings surfaces). Moreover, grinding will be seen no longer as a finishing method, indeed it will replace traditional machining in some operations, for instance gear skiving (hard machining category).

Examples of requirements for powertrain components are here discussed:

- *Bearings*: they need to achieve long fatigue life, low-torque performances, high wear resistance, low noise emission under contact conditions. For each one of these requirements, finishing processes can really make the difference: for instance, for having long fatigue life a specific residual stress profile is necessary, for low-torque performances achievement surface finishing is the main operation to perform, and finally for controlling the noise the roundness is influencing.

- *Gears*: load carrying capacity, fuel consumption and noise, vibration, harshness (NVH) specifications. For gears production, grinding and dressing play an important role in avoiding twisted tooth flanks, as well as in surface roughness demands, for obtaining Ra down to 0.05µm.

- *Shafts*: even if there are no camshafts or crankshafts in electric vehicles, there are still improvements to carry out since it is an important topic for latest versions of internal combustion engines (ICEs) and for hybrid electric vehicles (HEVs).
  Speaking about camshafts, parallelism and circular run-out between cam lobes and the shaft itself, together with wear resistance and low friction properties are crucial for the correct functioning. According to studies run by Ford Motor Company, finishing processes have been proven as the most effective way to reduce friction by means of improved surface finish, and combined with coatings the effects are even more significant.
  For crankshafts, grinding is a fundamental operation as well since geometric tolerances (perpendicularity, run-out and circularity) and surface roughness have high expectations,

and moreover the process itself should be carefully studied in order to avoid burnings that could lead to crack initiation.

- *New automotive powertrain components*: for instance, hollowed (for cooling reasons) rotor shafts in electric motors, request extremely high surface finishing and tolerances, as well as textured surfaces in order to retain the lubricant and reduce friction, achieved by grind-texturing.

Grinding and dressing together with fine-finishing processes are one of the main portions of the manufacturing chain of the powertrain components and cost-speaking they contribute in about 30% of the total cost for the production (Figure 17).

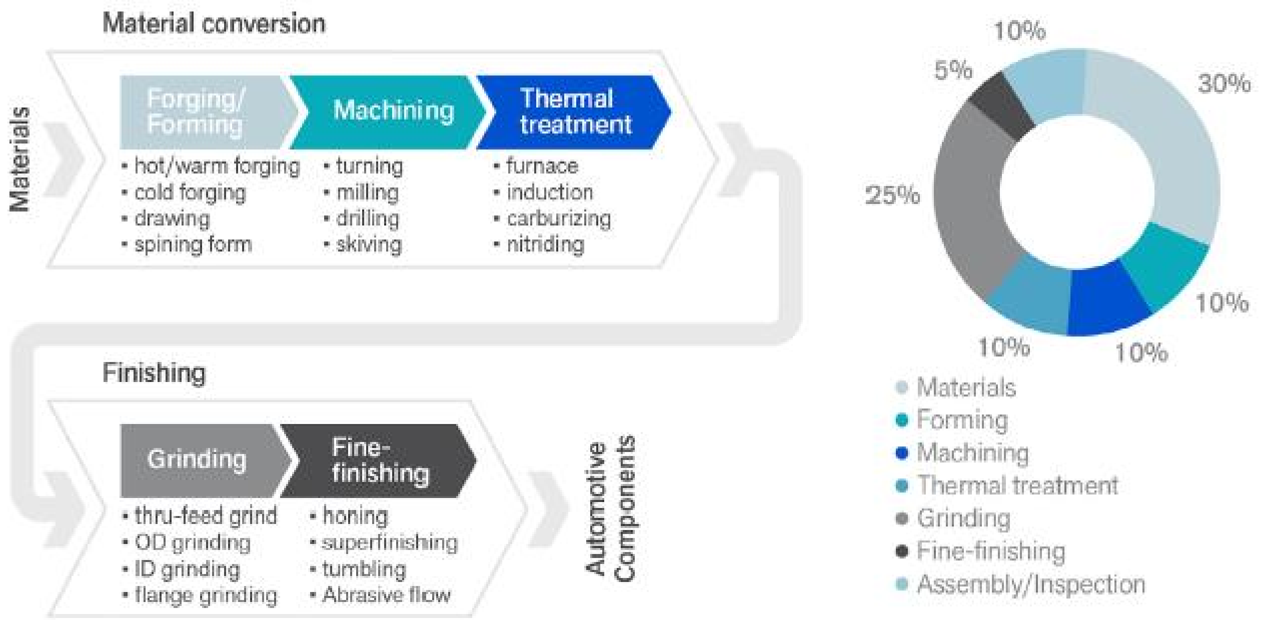

Figure 17: Grinding and fine-finishing in the manufacturing chain for powertrain components and relative costs [6]

Recent advances in grinding and dressing regarding the mentioned powertrain components are presented in the following:

- *Grinding of bearings*, for instance of inner rings of automotive bearings, it constitutes one of the main operations in the production chain, as shown in the following figure.

Figure 18: finishing operations for inner rings of automotive bearings [6]

In specific, double disk through-feed grinders for face grinding, OD grinders, ID grinders and flange shoe-centreless grinders are involved in the process. This finishing lines have a large production volume capability, nevertheless the changeover times are long, therefore they are not ready for innovations in the automotive industry that would lead to low-volume batches.

Examples of high flexibility grinding machines are three axis (two rotary and one linear) grinding machines, allowing multiple grinding operations in the same machine.

- *Grinding of gears*, in particular cylindrical and bevel hardened gears. Discontinuous profile grinding, continuous generating grinding, bevel-gear grinding have relevance.

  Through gear grinding it is possible to achieve improved surface integrity of the tooth flanks, moreover a main focus is on optimization of grinding process for internal gears (growing demand for increased request of planetary gearboxes), reduction of transmission noise (tooth-flank topography is the main parameter influencing the noise emission in gearboxes) and possibility to tailor the surfaces.

  Studies for optimizing the grinding forces for improving surface roughness, avoid burning and reduce wear are necessary, as well as dressing and monitoring for grinding of thermal-treated gears, with hard precipitates, thus reduced grindability given by increased grinding-wheel loading and larger wear rates.

- *Grinding of shafts*, mostly OD-grinding for camshafts and crankshafts are involved, in particular centreless through-feed and centreless plunge operations (for instance, simultaneous grinding of two diameters and a shoulder in a shaft).

  More into details, for camshafts grinding, OD-cylindrical grinding is used for grinding cam lobes; this is a complicated operation involving localized burns and temperature peaks given the complex geometry of the cam lobe itself.

  On the other hand, for crankshafts, many challenges are based on the variable conditions along the grinding wheel profile, since the contact length going towards the sidewall is increasing, causing higher risk of thermal damage. This process can be optimized by changing for example the CBN grinding wheel grits concentration. Moreover, further grinding methods have been patented to overcome this issue, such as radial-plunge grinding for roughing on the sidewall, followed by angle-plunge grinding for finishing, in which the grinding wheel is moving both radially and axially. By considering these two operations, the wear has been proven to be lower and consequently the dressing operation frequency has been reduced.

- *Dressing tools*, of significant importance to determine grinding wheel form, topography and consequently performances.

  The processes governing the dressing operation are not fully understood, hence further studies on how the dressing can influence the grinding wheel performance are necessary.

  Furthermore, new ceramic-metallic hybrid bonds for holding the dressing tool grits have been introduced for reducing the dresser wear and allow higher self-sharpening capabilities. By means of rotary tools for dressing, both conventional and superabrasive wheels can be reconditioned, and in addition complex profiles can be shaped on the wheel itself and consequently on the workpiece.

Tests have been performed on grinding wheel macro-texturing with grooves, and the thermal damage risk has been proven lower. Additionally, for higher performance control, micro-texturing achieved by laser ablation is to be considered.

In conclusion, automotive industry is still leading the machine-tool market, and the focus nowadays is to increase flexibility and capability of grinding and fine-finishing machines, still of major importance in manufacturing.

5. Fundamental variables in grinding and dressing

Talking about the fundamental variables to know in a grinding or dressing process, there are several of them, and they are defined in [7] by Badger and discussed in the following. These are the most important to know for controlling the process, and the discussion will be focused on grinding and dressing, specifically on plunge roll dressing (rotary dressing).

5.1 Common variables to know about grinding and dressing

5.1.1 The material removal rate

This variable represents the volume of material ground (or dressed) away in a unit time. It is measured in mm^3/s. Usually it is named Q or MRR.
For surface grinding for instance, the formula is (2):

$$MRR\left[\frac{mm^3}{s}\right] = Q = depth\ of\ cut\ [mm] \cdot feedrate\ \left[\frac{mm}{s}\right] \cdot width\ of\ cut\ [mm]. \tag{2}$$

On the other hand, the specific material removal rate is named Q' and is given by (3):

$$Q' = \frac{Q}{width}\ [\frac{mm^2}{s}] \tag{3}$$

5.1.2 The specific energy

The specific energy, called SE most of the time, is measured in J/mm^3 and represents the energy during the operation per unit volume. It is obtained by (4):

$$SE = \frac{P}{Q}\left[\frac{J}{mm^3}\right] \tag{4}$$

in which P is the grinding (or dressing) power in Watts, given by (5):

$$P = P_{total} - P_{idle}\ [W] \tag{5}$$

and Q is the material removal rate.

The higher is the power, and consequently the specific energy, the more inefficient will be the process (there will be a lot of rubbing) (Figure 19).
For all kinds of dressing, there is a trade-off to make between heat generation and surface roughness obtained during grinding. In detail, a sharper dressing will give less heat generation during grinding but worse finish, and the opposite for a dull dressing condition.

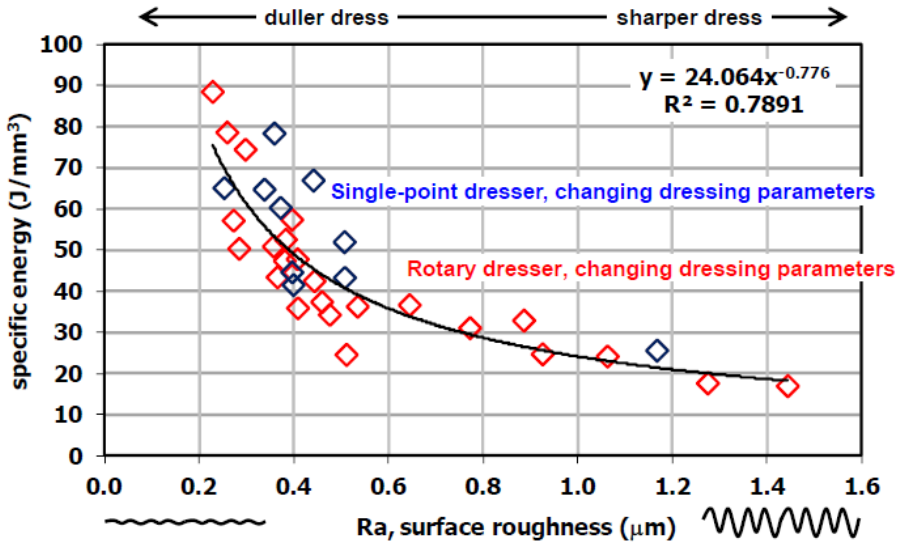

Figure 19: specific energy vs surface roughness for different dressing operation [7]

There is an unwritten rule for this trade-off: it is generally better to have less heat generation and worse surface roughness. If the last parameter is relevant, then a smaller grit size for the grinding wheel should be used to get a good-enough surface finish.

5.2 Main variables in plunge-roll dressing

For rotary dressing the following three variables are the ones that during the experimental part will cover a role of greater importance:

- Speed ratio.
- Plunge-roll effective depth.
- Dwell time.

5.2.1 Speed ratio

It is possible to have unidirectional or anti-directional dressing operation depending on rotation direction as shown in the next figure (Figure 20).
The speed ratio is the ratio between dressing roll speed and grinding wheel speed (6). It can be higher or lower than 1 if unidirectional dressing, and negative if anti-directional dressing.

$$q = \frac{v_{roll}}{v_{wheel}} \; [-] \tag{6}$$

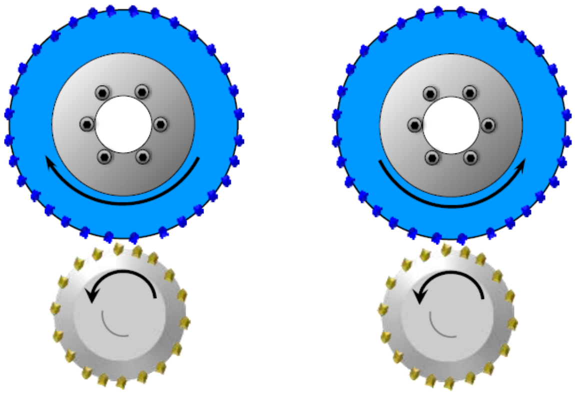

Figure 20: unidirectional and anti-directional dressing [7]

For a unidirectional dressing operation, the grits of the grinding wheel will be sharper and thus there will be less heat generation during grinding; the opposite will be for the anti-directional dressing, in which the wheel will be dull and not sharp. This is due to the way in which the diamond grits are interacting with the grinding wheel grits, indeed there is more like a "skim dressing" if considering an anti-directional case. On the other hand, for a unidirectional case the grit action will result more aggressive.

If the speed ratio is equals to one, then during the dressing operation the two speeds will be the same, and the normal forces during dressing will be too high. This condition is usually avoided.
The most used values for the speed ratio in industry are unidirectional, in particular +0.8 and +0.4.

To prove the point there is a plot showing the difference in grinding power after a uni or anti-directional dressing. The difference is about 30% during a finishing process, and even higher for a coarser grinding (Figure 21).

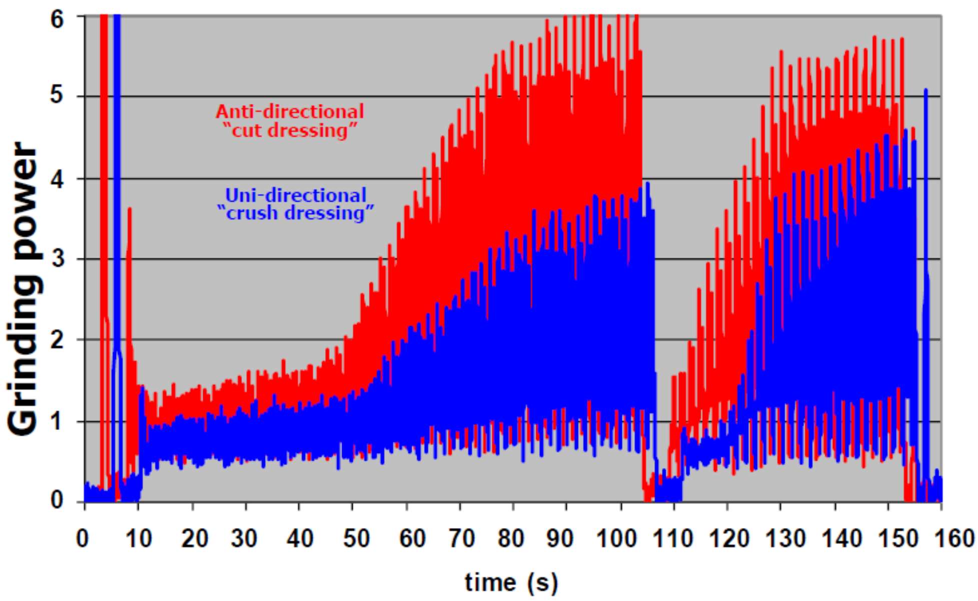

Figure 21: grinding power vs time for unidirectional and anti-directional dressing [7]

5.2.2 Plunge-roll effective depth

The plunge-roll effective depth represents how much the dresser is plunged into the grinding wheel (or vice versa) per each grinding wheel revolution (Figure 22).

The unit is µm/rev.

When the grinding wheel is plunged into the dressing roll, it acts like a spiral from the material removal point of view. In the following figure it is possible to identify the dressing depth per revolution.

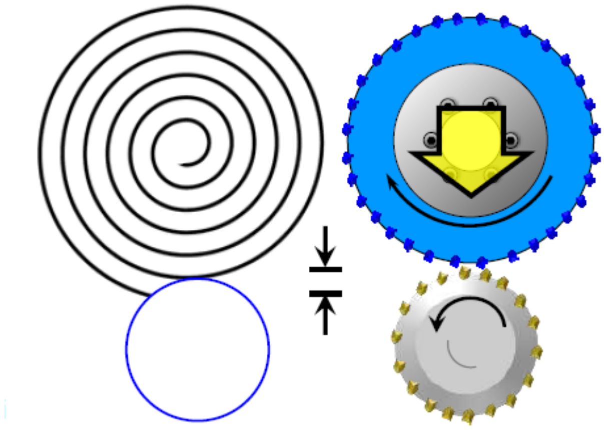

Figure 22: plunge-roll effective depth. Sprial effect [7]

It is possible to identify a threshold value for which the wheel will not get any sharper (Figure 23). This value is for about 1 µm/rev. As it can be seen subsequently, the power will not decrease importantly after it. On the other hand, the heat generation will increase rapidly by decreasing the infeed rate, and consequently, the wheel will result dull.

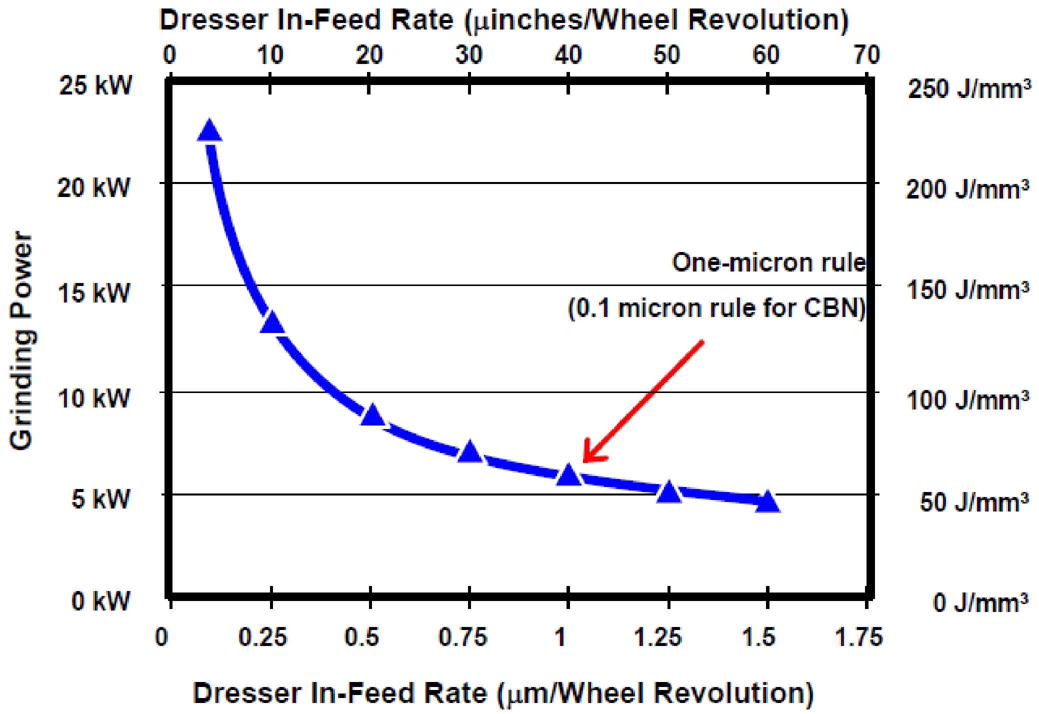

Figure 23: grinding power vs dresser infeed rate. 1 µm rule [7]

5.2.3 Dwell time

The dwell time is the time necessary to have a grinding wheel which has a perfect circular shape and consequently avoiding the roundness to be affected by the spiral effect (see Figure 22).
It is not possible to finish the dressing operation and immediately reverse the radial plunging motion, otherwise the wheel shape will be influenced by the way in which the material is removed. In other words, the spiral given by the material removal mechanism will be detrimental for the successive grinding operation.

Dwelling is necessary, and not only for one revolution, but usually for a few more.
A rule of thumbs suggests dwelling for 20-40 wheel revolutions for a unidirectional dressing and for 10-20 wheel revolutions for an anti-directional dressing.
It is important dwelling only for the necessary time, otherwise the heat generation will increase in the subsequent grinding operation. Many studies have proved this point (Figure 24).

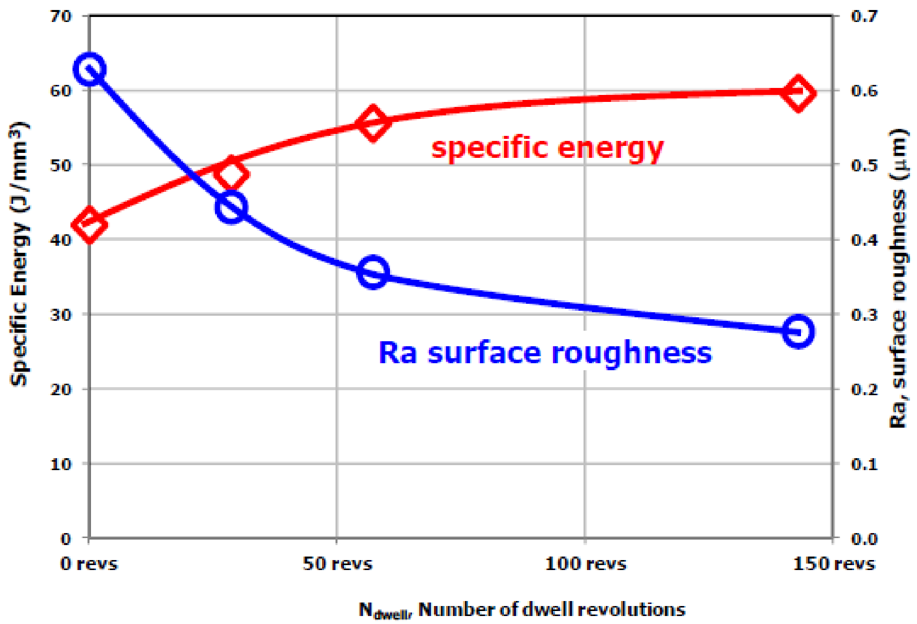

Figure 24: specific energy and surface roughness vs dwelling revolutions [7]

6. State of the art

6.1 Effects of rotary dressing on grinding wheel performance

The most important milestone for grinding and dressing are Malkin and Murray's studies carried out in [8] and [9].

In the following, the results on effects of rotary dressing (Figure 25) on grinding wheel performance are reported. Usually, rotary dressing is performed by radially plunging the grinding wheel into the dressing roll, nevertheless in this case a different configuration has been set. Anyways, given negligible table speed v and depth d_r, the operation is considered kinematically identical to standard plunge-roll dressing with only radial motion.

In particular, the grinding performance in terms of grinding forces and ground workpiece surface roughness are evaluated. The main parameters to vary in the dressing operation are the speed ratio between dresser roll and grinding wheel, the radial infeed per revolution of grinding wheel and the dwell time.

The dressing operation was carried out with these different parameters and different dressers.

The grinding wheel consisted of single crystal Aluminum oxide abrasive in a vitreous binder of diameter 355.6mm and width 12.7mm. Seven different dressers were used, all manufactured using an infiltrated powder metal matrix to hold the diamonds; the difference between them was the diamonds pattern. The dressers diameters were 69.85mm and the widths 19.1mm. The successive results are presented for the dresser number five out of the seven, with irregular diamond grits setting pattern.

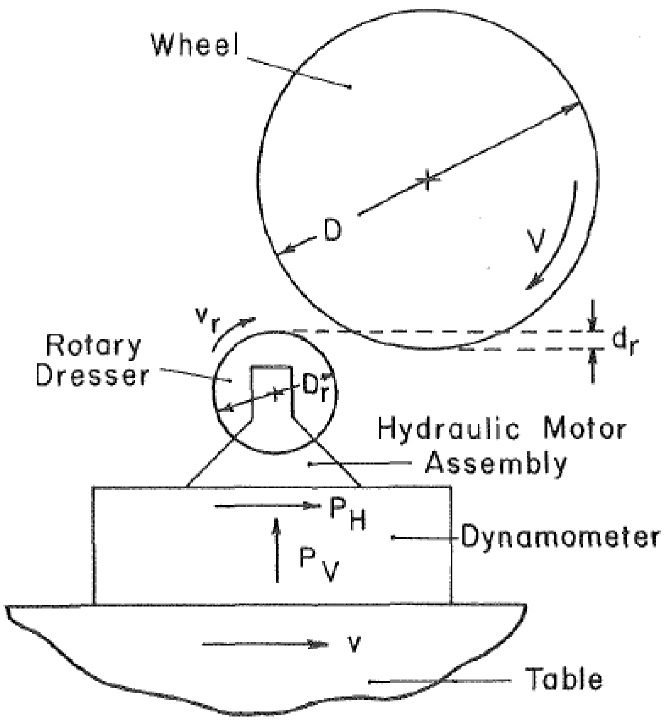

Figure 25: plunge-roll dressing operation for Malkin's experiments [7]

Once the dressing operation was completed with the different set of parameters and different dressing rolls, the surface grinding was performed (Figure 26).
The conditions were:

- Grinding wheel tangential speed of 32m/s.
- Workpiece velocity of 142.24 mm/s.
- Wheel depth of cut 25.4 µm.
- Workpiece (AISI 1090 hot rolled steel of hardness Rockwell 34C) width 9.575 mm.

During the grinding operation, forces were measured, and afterwards surface roughness as well.

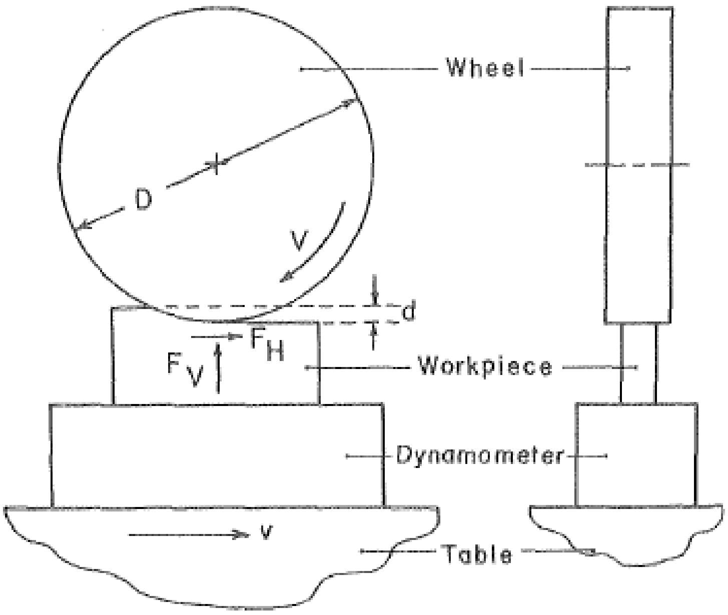

Figure 26: surface grinding operation for Malkin's experiments [7]

Vertical and horizontal forces during grinding for different dressing conditions (speed ratios or radial infeeds) are shown (Figure 27 and Figure 28).

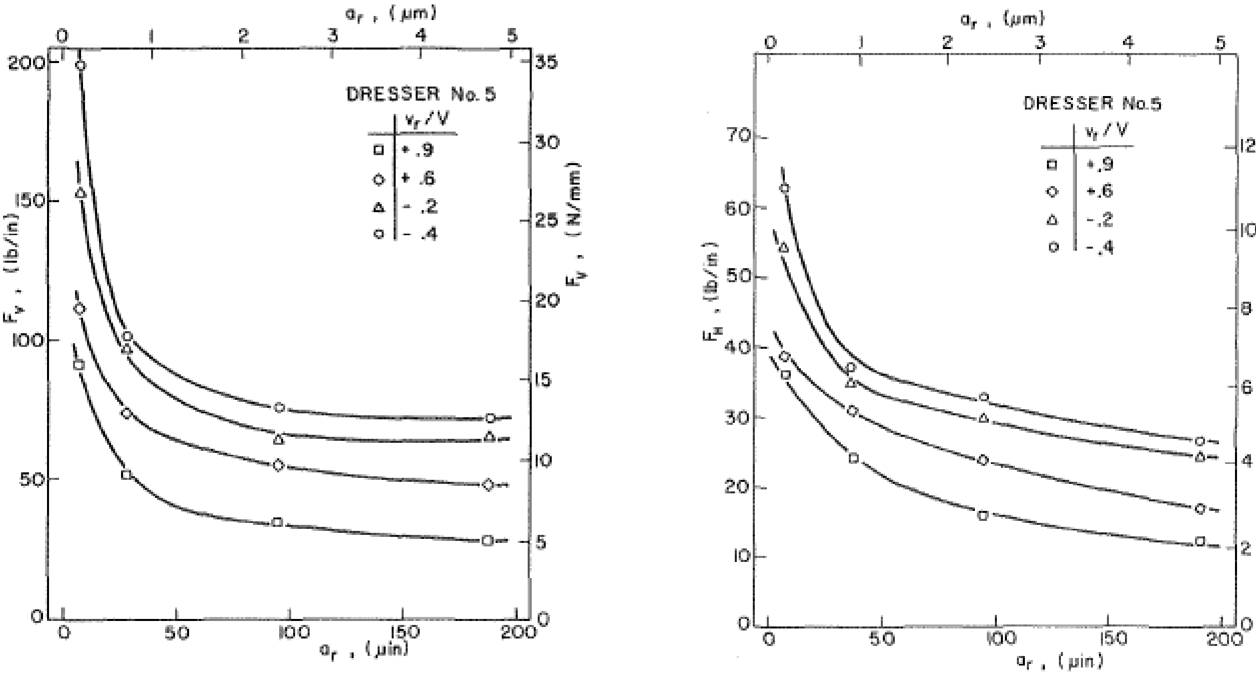

Figure 27: vertical and horizontal grinding forces per unit width vs radial infeed [8]

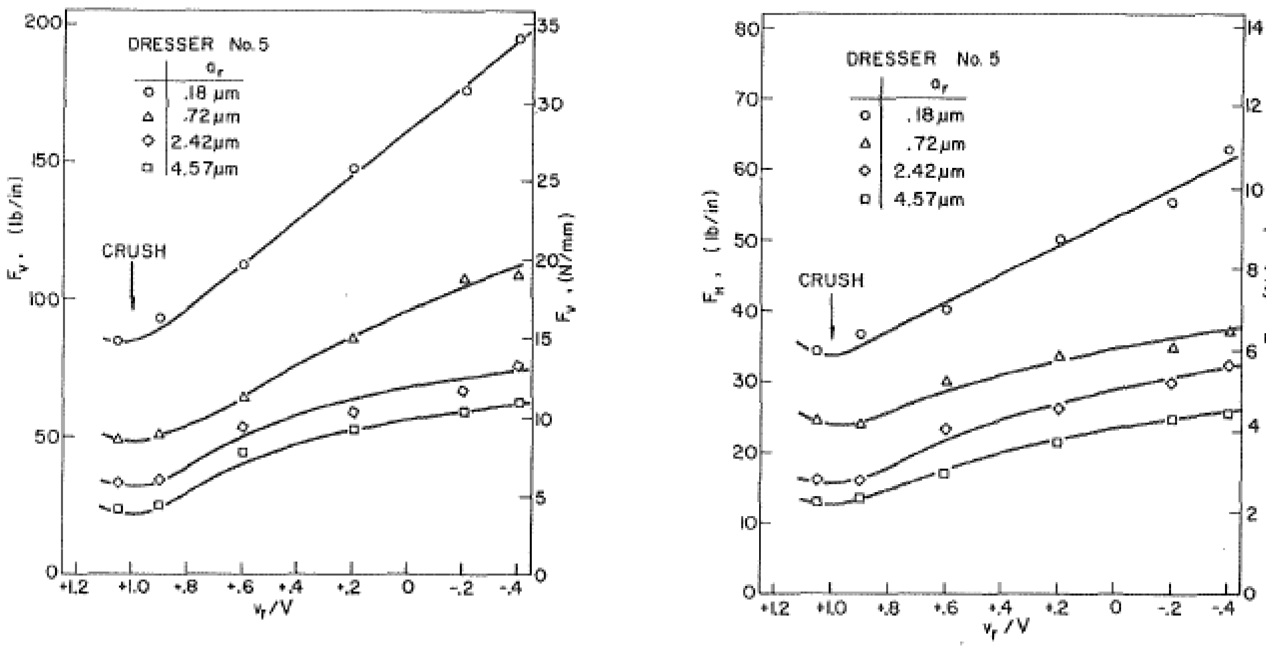

Figure 28: vertical and horizontal grinding forces per unit width vs speed ratios [8]

As it can be seen, the grinding forces have a similar trend, and for increasing radial infeed and increasing speed ratio are getting lower. A minimum in the forces trend, for a given radial infeed, could be reached for speed ratio equals to 1 (crush condition), but it would lead to a high dressing roll wear rate.

Surface roughness correspondent to the forces in the previous figure is here shown (Figure 29).

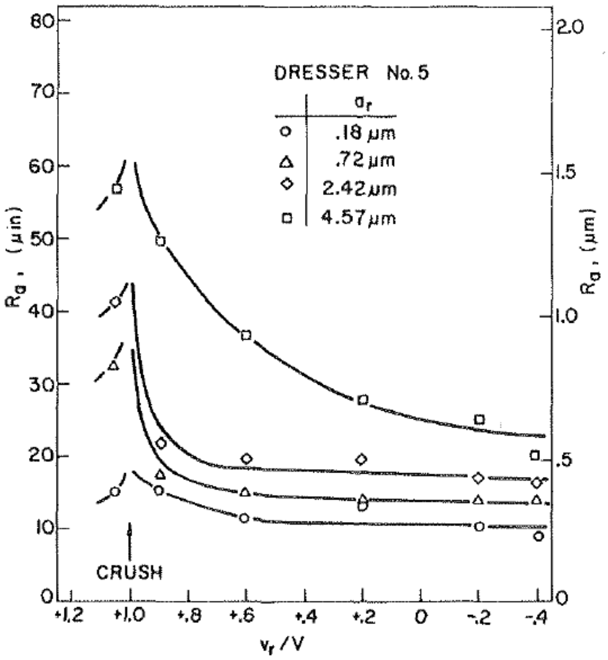

Figure 29: ground workpiece surface roughness vs speed ratio for different radial infeeds [8]

The trend is opposite to the one of the forces: lower (better) surface finish for lower speed ratio and lower radial infeed.

Hence, usually an acceptable trade-off between low forces and low surface finish is given by a unidirectional speed ratio of 0.8. If a better surface finish is required, a smaller diamond grit size should be used.

As already mentioned, another important parameter is the dwell time (Figure 30).

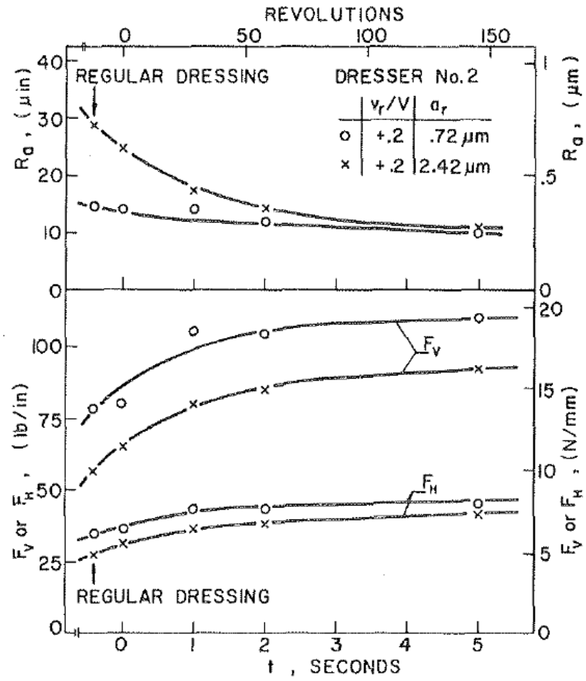

Figure 30: vertical and horizontal forces, and surface roughness vs dwell time [8]

The plot shows as expected that for increasing dwelling seconds (or dwelling revolutions), the grinding forces will be higher, and the surface finish will be lower. This trend is indicating that only for the necessary seconds dwelling should be applied, otherwise the properties would get worse.

Furthermore, SEM analysis has been carried on, for looking at grinding wheel morphology differences between coarse (low specific energy) and fine (high specific energy) dressing conditions. For this purpose, a 65°-75° tilt angle on the SEM has been used.
In the following Figure 31, a difference between coarse and fine dressing conditions is presented.

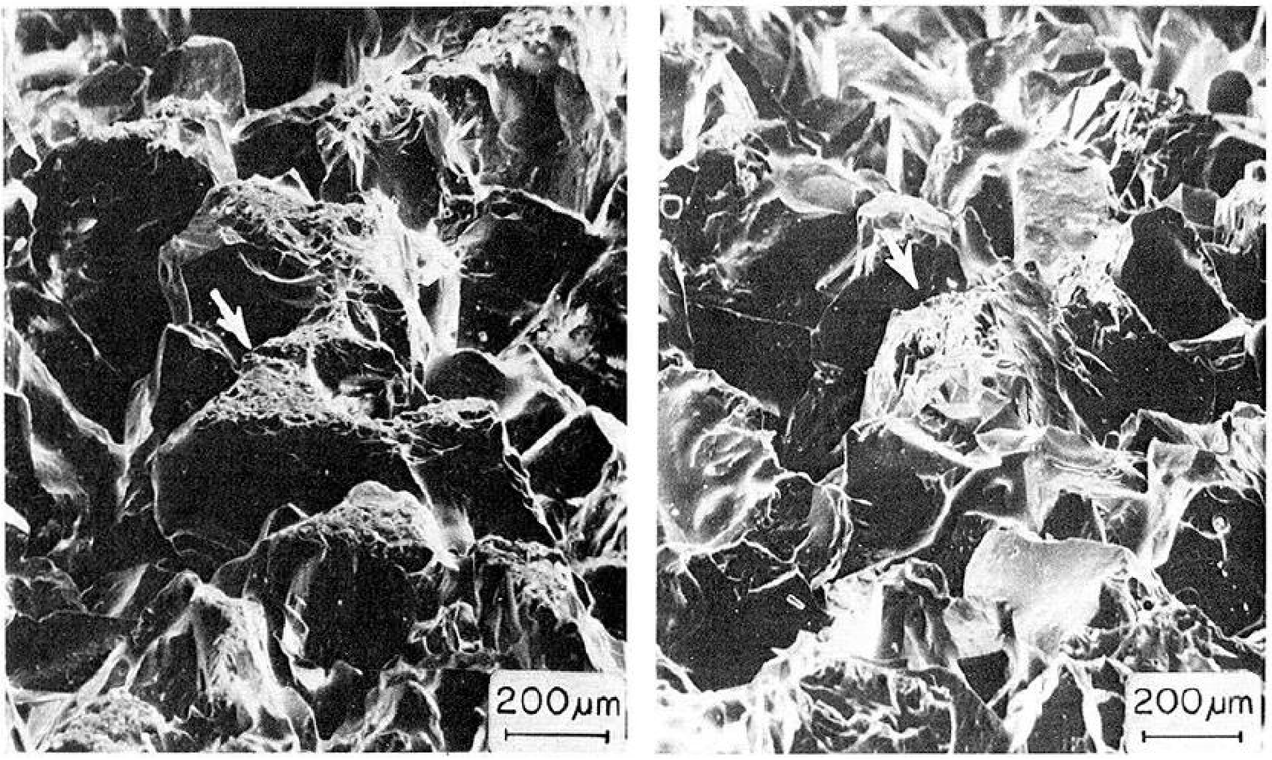

Figure 31: SEM micrographs for dull condition (left) and sharp condition (right) [8]

A clear difference can be observed: on the left the finer condition presents more flattened areas, hence during the dressing operation larger deformation of Aluminum oxide grains has occurred, and consequently more specific energy (power and forces as well) has been generated.
On the other hand, on the right it is possible to look at a coarser dressing condition: greater grain fracture and lower deformation is involved in this process, moreover less flattened areas can be seen.

6.2 Effects of dressing on grinding performance, continuous dressing

More studies on effects of dressing on grinding performance were carried out by Salmon.
In particular, the analysis is on continuous dressing, presented in [5].
Effects of dressing parameters on grinding operation performance in terms of grinding specific energy are displayed in the following (Figure 32 and Figure 33).
Both the tests were run with the same dresser, grinding wheel and workpiece.
The grinding wheel was coded as WA 60 80 F P2 V, and the workpiece was C 1023 nickel-base alloy.
For both cases, the wheel speed was 30 m/s, and speed ratios and radial infeeds of dresser per wheel revolution were varying. The dresser was a diamond roller dresser coded DIAMESH 82971 IPE DD150.
Grinding wheel diameter was 600mm, and dressing roll diameter was 100mm.

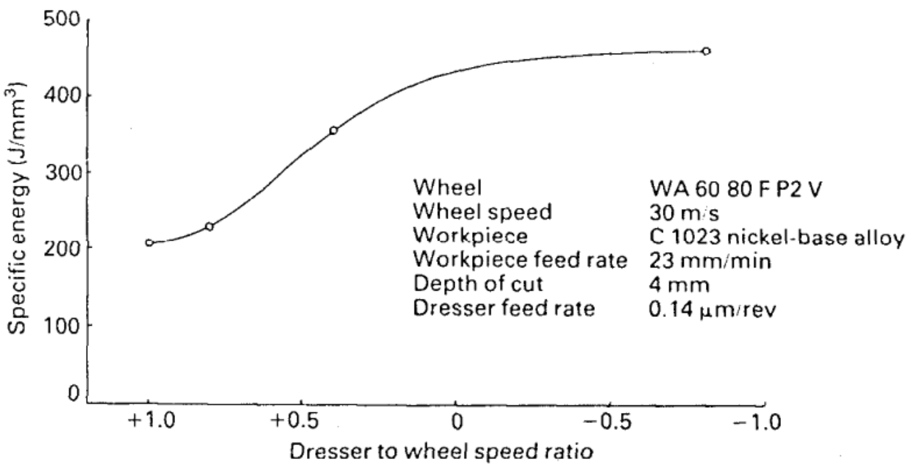

Figure 32: effect of dresser to wheel speed ratio on specific energy in continuous dressing [5]

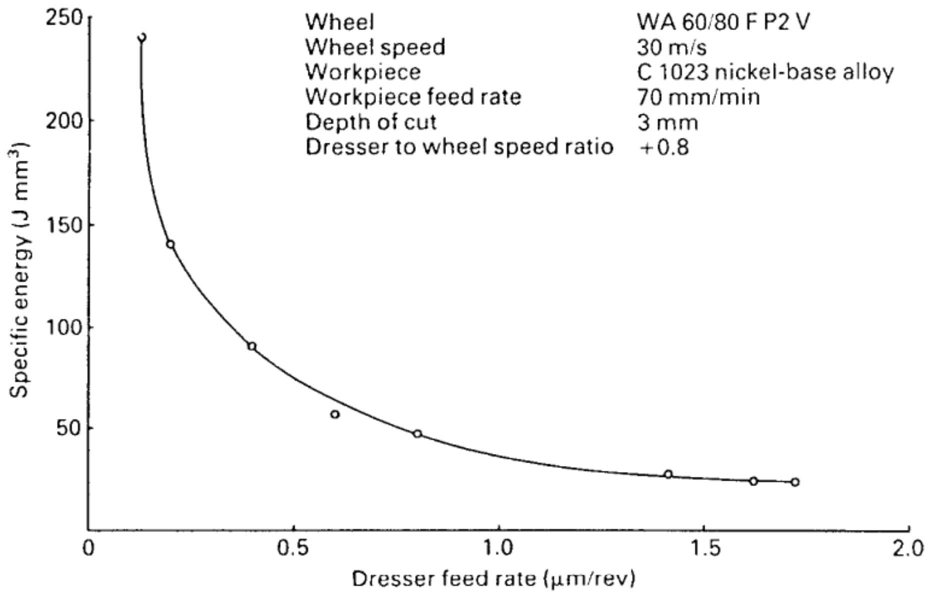

Figure 33: effect of dresser radial infeed per wheel revolution on specific energy in continuous dressing [5]

These results will be discussed later on during the data analysis: 7.3 Grinding specific energy analysis, continuous dressing, Salmon, but a comment on these trends can already be proposed: by increasing speed ratio and radial infeed per wheel revolution, the specific energy gets lower. Moreover, for radial infeeds larger than 1.5 μm/rev, the specific energy is not getting any lower.

6.3 Aggressiveness number definition

The Aggressiveness number (definition in [10]) was named for the first time in 2008, even if already previously known.

It is a dimensionless number of relevant importance for abrasive operations like grinding and dressing. The purpose is to substitute the concept of chip thickness, which is difficult to detail in this kind of machining in which the chip is not as defined as in turning or milling for instance. This is due to the undefined cutting tool geometry.

Initially, over the years, different definitions for equivalent chip thickness were proposed.

The first one was in 1974 with Snoeys and Peters ([10]) in (7):

$$h_{eq} = a_e \cdot \frac{v_w}{v_s} \ [mm]$$

(7)

in which a_e represents the depth of cut in mm, and v_w and v_s are respectively feedrate (e.g., workpiece speed for grinding) and wheel speed in mm/s.

There was a problem though: failure in considering of arc length that would give a not neglectable difference in operations such as cylindrical outer-diameter operation and creep-feed operation for instance.

To overcome this issue, there is a parameter called maximum undeformed chip thickness ([10]), h_m is presented in (8):

$$h_m = \sqrt{\frac{4}{C \cdot r}\left(\frac{v_w}{v_s}\right)\sqrt{\frac{a_e}{d_{eq}}}} \ [mm]$$

(8)

In which C represents the cutting point density, r the chip shape factor and d_{eq} is the equivalent diameter for cylindrical grinding, or the grinding wheel diameter for surface grinding. Nevertheless, there is the introduction of variables like C and r, that are of difficult choice, and other doubts connected to restrictions to grinding operation and to the geometry of plunge grinding.

In 2008 Jeffrey Badger proposed the Aggressiveness number ([10]), a dimensionless parameter in which only relevant variables are used: depth of cut, feedrate (workpiece speed), wheel speed and wheel diameter or equivalent diameter (9):

$$Aggr = 10^6 \cdot \frac{v_w}{v_s}\sqrt{\frac{a_e}{d_{eq}}} [-]$$

(9)

In this way, the parameter was still limited to the two restrictions mentioned before (grinding operation and geometry of plunge grinding).

Finally, in 2020, all the theories have been unified under a theory of Aggressiveness ([10]).

The point Aggressiveness was defined as in (10):

$$Aggr^* = \frac{v_{w,N}}{v_s} \ [-]$$

(10)

with $v_{w,N}$ component of velocity acting normal to the point of contact, and v_s component acting tangentially.

Aggr’ was set out as the line Aggressiveness: average Aggressiveness along a line of contact.

The application field of this dimensionless number is very wide, indeed with a few adjustments it is possible to find a definition for it for various types of grinding (e.g. surface grinding, cylindrical grinding) and dressing operations (e.g. inner-diameter and outer-diameter dressing).
Through the most interesting advantages of the latter, there is the possibility of plotting surface roughness and specific energy, for different dressing parameters (as speed ratio or radial infeed per wheel revolution) and obtaining a clear and only trend for all data.
For instance, in the following, two different plots are shown, the first one for the workpiece surface roughness vs the grinding Aggressiveness number for different radial infeeds and wheel speed, for cylindrical grinding of steel (Figure 34), and the second one for dressing specific energy vs dressing Aggressiveness number for different speed ratios in rotary diamond dressing (Figure 35).

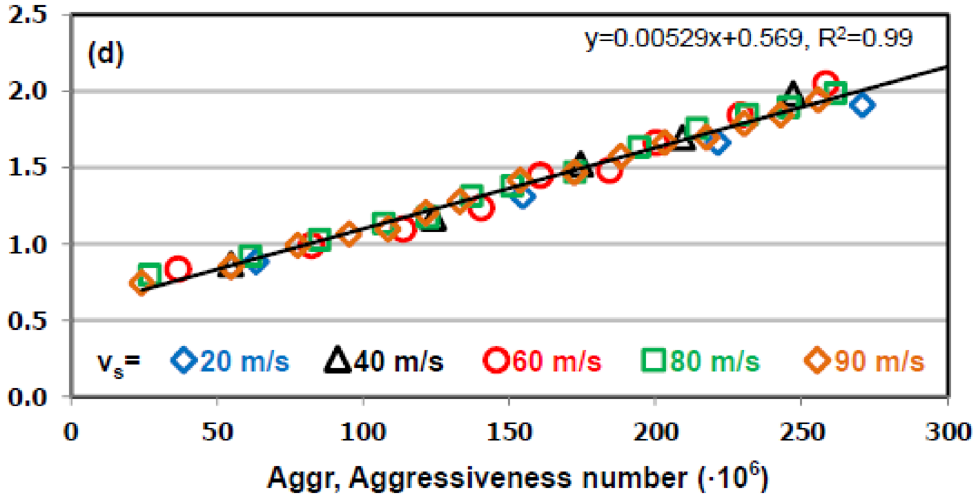

Figure 34:workpiece surface roughness vs grinding Aggressiveness number, surface grinding [10]

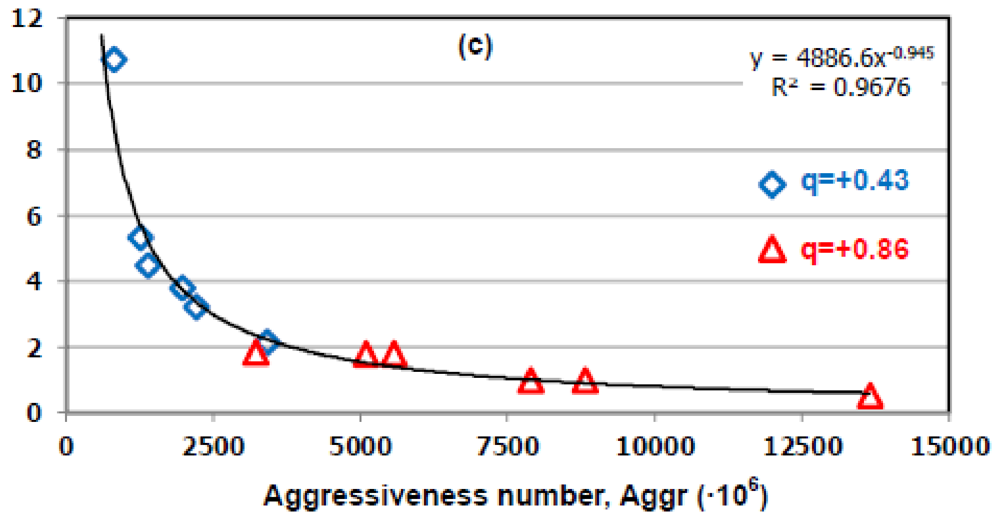

Figure 35: dressing specific energy vs dressing Aggressiveness number, diamond dressing [10]

As it is shown, it is easier to find correlations and trends between these variables like surface roughness, specific energy with the Aggressiveness number than with other parameters such as speed ratio or radial infeed per wheel revolutions.

Second of all, speaking about production, it has been proven useful to keep constant the Aggressiveness number, but for example increasing feedrates in order to reduce cycle times.

6.4 Acoustic emission in dressing of grinding wheels

The following study carried on by Badger et al. in [11], is focused on acoustic emission during dressing for single-point diamond dressing.

Generally, acoustic emission (AE) has been used in order to detect contact between dresser and grinding wheel, and thermal damage as well; indeed, in the first case, speaking about the contact, when this happens a sudden increase in the AE RMS value occurs, and basically the same principle can be observed regarding thermal damage.

Malkin and Murray found out a correlation between dressing specific energy and grinding specific energy, indeed if one is increasing, the other one is increasing as well.

The purpose of this work is proving that dressing acoustic emission could be used for predicting dressing power thus consequently wheel sharpness and grinding specific energy, a fundamental variable linked to heat generation and thermal damage.

Grinding and dressing tests have been carried on a Jones and Shipman 540 surface grinder, and a single-point diamond dresser has been mounted on a holder.

Two grinding wheels have been utilized: a vitrified bond, monocrystalline, Aluminum-oxide, 60-mesh, J-grade wheel (32A60JVBE) and a vitrified bond, 50% ceramic-grit, 60-mesh, J-grade wheel (5SG60JVS).

First of all, idle acoustic emission had to be identified: indeed only the 70% of the dressing pass was considered for collecting the data, disregarding entry and exit of the diamond dresser in the grinding wheel, as shown in the following (Figure 36).

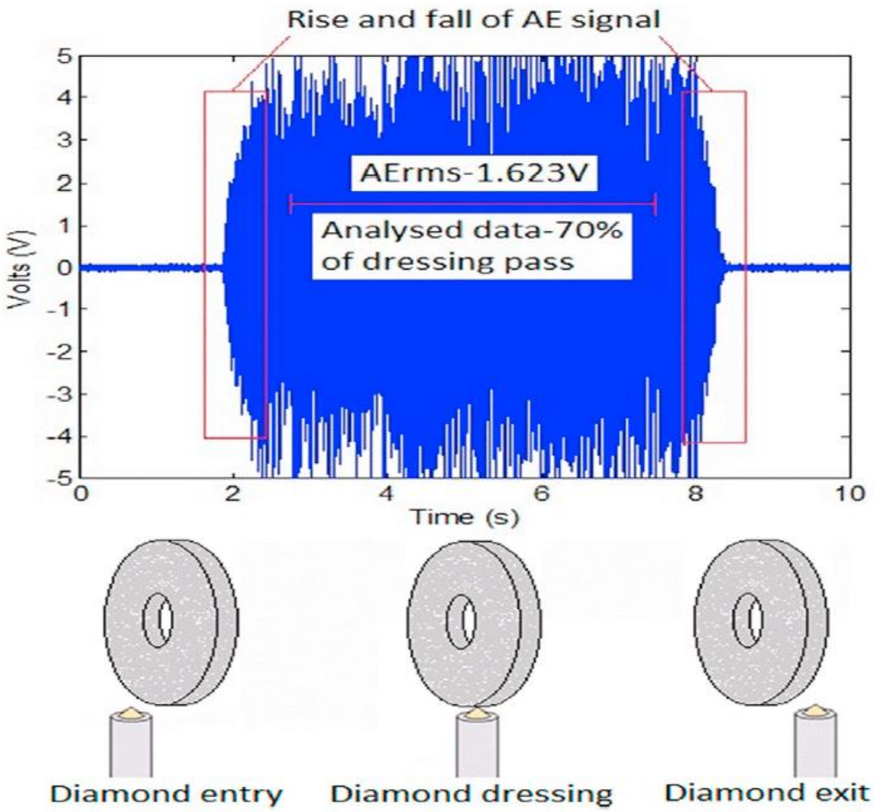

Figure 36: dressing acoustic emission definition [11]

In the next figure (Figure 37) it can be observed as for single-point diamond dressing the AE value in Volts results directly proportional with the dressing power in Watts (disregarding the intercept, with a value close to zero). Given this relationship, it is possible to determine an acoustic emission - power factor, which can be used starting from the acoustic emission value to determine in an enough-accurate way the dressing power value, and eventually wheel sharpness considering that the latter is related to the power value.

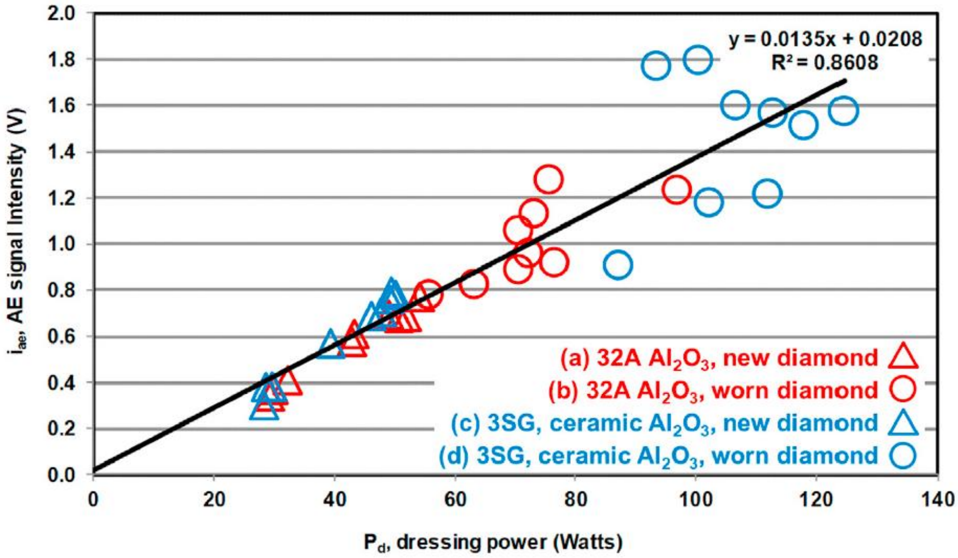

Figure 37: dressing acoustic emission versus dressing power for different grinding wheels for different dressing parameters [11]

Furthermore, a new variable has been introduced and named: *acoustic emission specific energy*, measure in mV/mm^3/s and given by ratio between acoustic emission value and dressing material removal rate (MRR defined in: 5.1.1 The material removal rate). By knowing the acoustic emission specific energy and the acoustic emission – power factor, dressing specific energy can be identified. In addition, the new variable has been proved to be related to grinding specific energy with a power-law equation, and as it can be seen in the next image (Figure 38), the behaviour of grinding specific energy and surface roughness plotted against acoustic emissions specific energy, is opposite as usual: if one is increasing, the other one is decreasing.

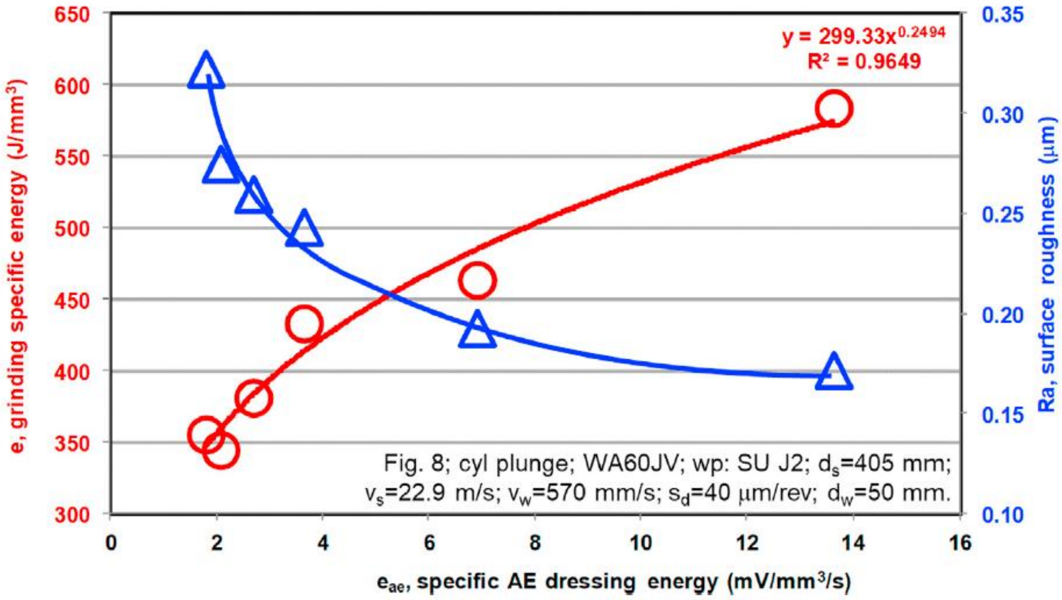

Figure 38: grinding specific energy and surface roughness against dressing AE specific energy [11]

7. Data analysis

The following data points are taken from Malkin and Salmon's experiments, discussed in: 6.1 Effects of rotary dressing on grinding wheel performance and 6.2 Effects of dressing on grinding performance, continuous dressing. Plots from the mentioned papers are remade by means of WebPlotDigitizer (https://automeris.io/WebPlotDigitizer/), and new considerations are drawn by plotting variables against Aggressiveness numbers and finding new correlations.
Moreover, a plot for relating dressing specific energy and grinding specific energy is presented.

7.1 Surface roughness analysis, Malkin and Murray

This first analysis is about ground workpiece surface roughness, coming from Malkin and Murray's data mentioned in 6.1 Effects of rotary dressing on grinding wheel performance.

In (11), the definition of dressing Aggressiveness number is expressed for rotary (plunge-roll) dressing case:

$$Aggr_d\,[-] = \frac{1}{1-\left(\frac{v_r}{V}\right)} \cdot \sqrt{\frac{a_{eff}}{d_{eq}}} \cdot 10^6 \tag{11}$$

It is possible to recognize dressing roll to grinding wheel speed ratio, radial infeed of dresser per wheel revolution (a_{eff}), and equivalent diameter calculated in (12) for outer diameter dressing operation for Malkin and Murray's case:

$$d_{eq} = \frac{d_{roll} \cdot d_{wheel}}{d_{roll} + d_{wheel}} = \frac{69.85 \cdot 355.6}{69.85 + 355.6} = 58.382\ [mm] \tag{12}$$

In this Aggressiveness number definition, remind the equivalence here shown in (13) and valid for the first term of $Aggr_d$:

$$\frac{1}{1-\left(\frac{v_r}{V}\right)} = \frac{V}{V-v_r} \tag{13}$$

Data points are for six different speed ratios and four different radial infeeds, for 24 data points in total. In the successive table, the conditions are shown together with the relative dressing Aggressiveness number.

speed ratio [-]	ar [µm]	$Aggr_d$ [-]
1.05	4.57	176949
1.05	2.42	128765
1.05	0.72	70236
1.05	0.18	35118
0.90	4.57	88475
0.90	2.42	64383
0.90	0.72	35118
0.90	0.18	17559
0.60	4.57	22119
0.60	2.42	16096
0.60	0.72	8779
0.60	0.18	4390
0.20	4.57	11059
0.20	2.42	8048
0.20	0.72	4390
0.20	0.18	2195
-0.20	4.57	7373
-0.20	2.42	5365
-0.20	0.72	2926
-0.20	0.18	1463
-0.40	4.57	6320
-0.40	2.42	4599
-0.40	0.72	2508
-0.40	0.18	1254

First of all, as it can be seen from Figure 39, the higher are radial infeed per revolution and speed ratio, the higher (worse) will be the correspondent surface roughness on the ground workpiece.

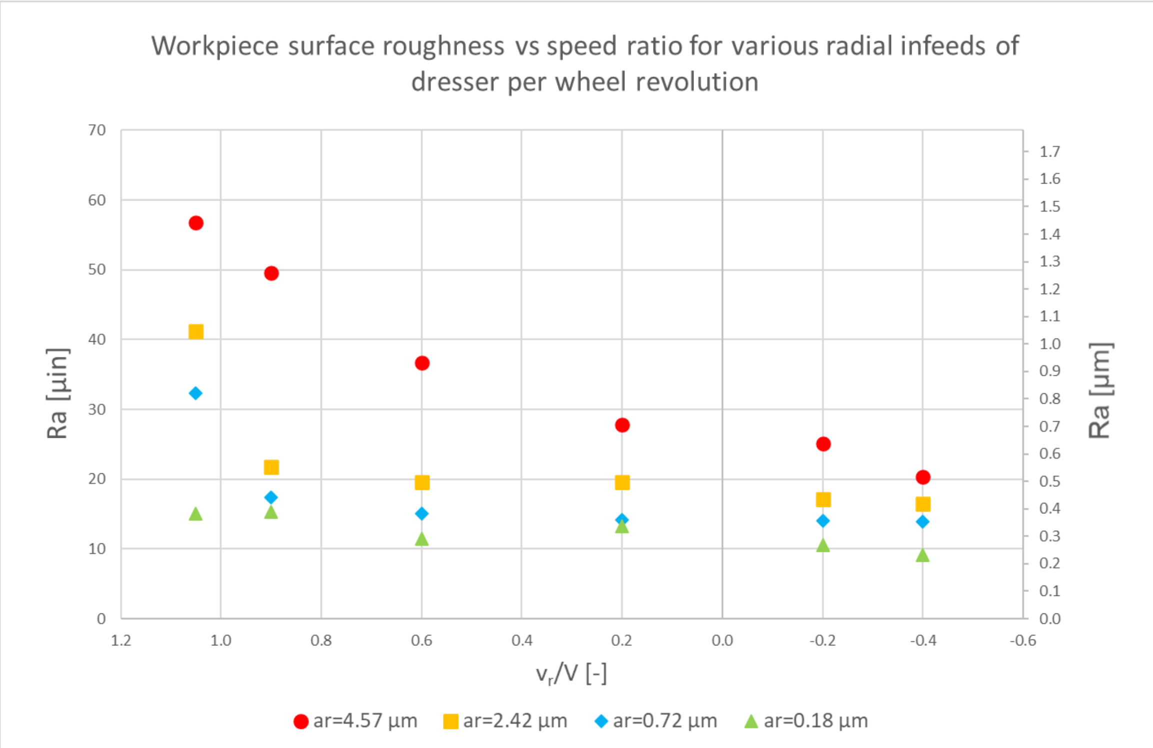

Figure 39: Surface roughness plotted against the speed ratio between dressing roll velocity and grinding wheel velocity

In Figure 40, the same variable can be plotted against the ratio between grinding wheel velocity and difference between grinding wheel and dressing roll velocity (useful for dressing Aggressiveness number definition as shown in (11) and (13)), but still no trend is visible, and it would result the same if plotting against radial infeed per wheel revolution.

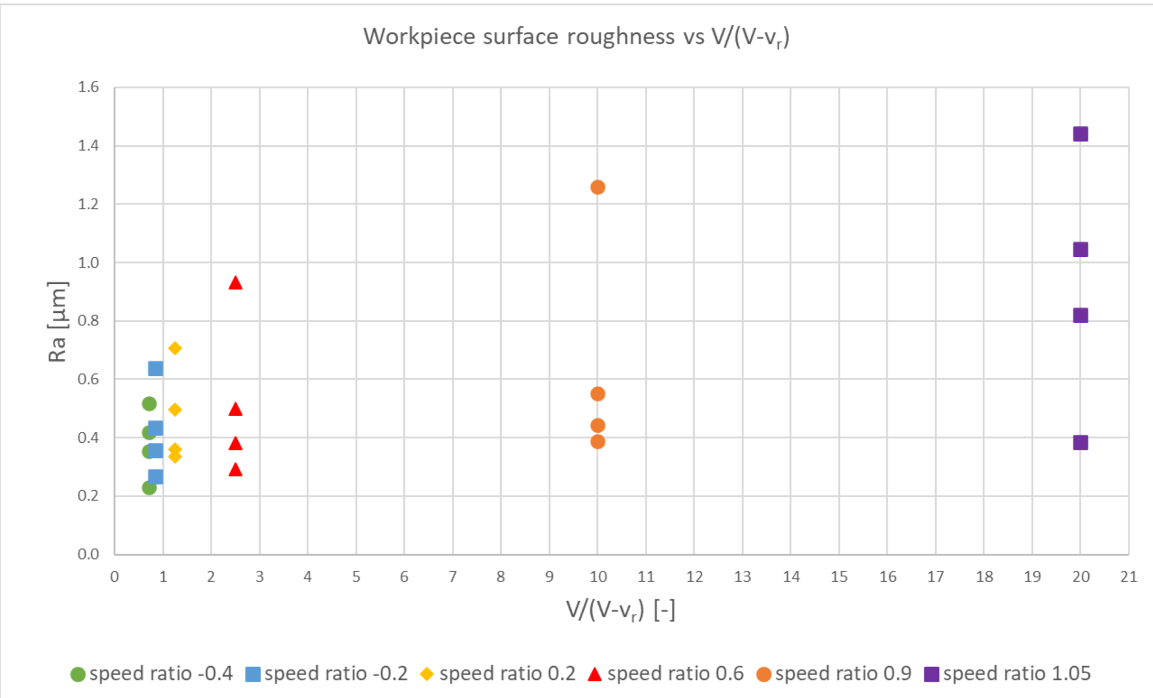

Figure 40: Surface roughness plotted against the ratio between grinding wheel velocity and difference between grinding wheel and dressing roll velocity

On the other hand, by means of the dressing Aggressiveness number, dimensionless number defined to combine the most important dressing parameters under a single variable ((11)), it is possible to obtain a plot in which a trend can be visualized (Figure 41). In particular, the higher is the dressing Aggressiveness, therefore the higher are speed ratio and radial infeed of dresser, the higher (worse) will be the workpiece surface roughness.

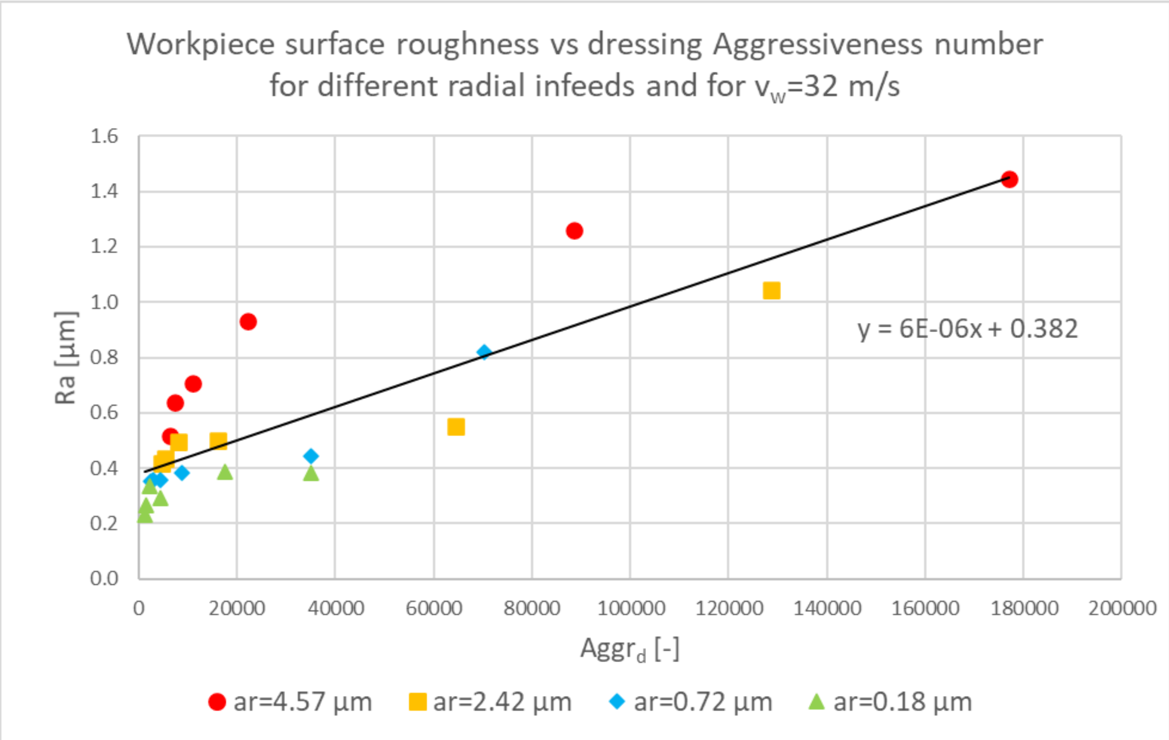

Figure 41: Surface roughness plotted against the Aggressiveness number

7.2 Grinding specific energy analysis, Malkin and Murray

A similar analysis to the previous one can be carried out on another fundamental variable in grinding: the grinding specific energy. To get this value, the maximum horizontal force during grinding is needed. Data are taken from 6.1 Effects of rotary dressing on grinding wheel performance and data points are for the same four radial infeeds as for 7.1 Surface roughness analysis, Malkin and Murray, and for same speed ratios (just data for speed ratios 1.05 and 0.2 are missing, hence there are 16 data points in total).

Once F_H is known, it is possible to get the grinding power, and finally, knowing the material removal rate, the grinding specific energy.

For the grinding power, since the horizontal force is measured per unit width in the experiments, it is necessary to multiply by the workpiece width as well, as shown in (14).

$$P_{grinding}[W] = F_H \left[\frac{N}{mm}\right] \cdot V_{wheel} \left[\frac{m}{s}\right] \cdot width\ [mm] \tag{14}$$

In order to obtain the grinding specific energy, MRR for surface grinding is calculated (15):

$$MRR \left[\frac{mm^3}{s}\right] = feedrate \left[\frac{mm}{s}\right] \cdot depth\ of\ cut\ [mm]\ \cdot width[mm] \tag{15}$$

Finally, the grinding specific energy can be obtained through (16):

$$SE_g \left[\frac{J}{mm^3}\right] = \frac{P_{grinding}\ [W]}{MRR \left[\frac{mm^3}{s}\right]} \tag{16}$$

For the same ground workpiece, grinding wheel and dresser as for the previous surface roughness discussion, there are the plots for vertical and horizontal forces during grinding, by varying the radial infeed and for different speed ratios reported in Figure 42.

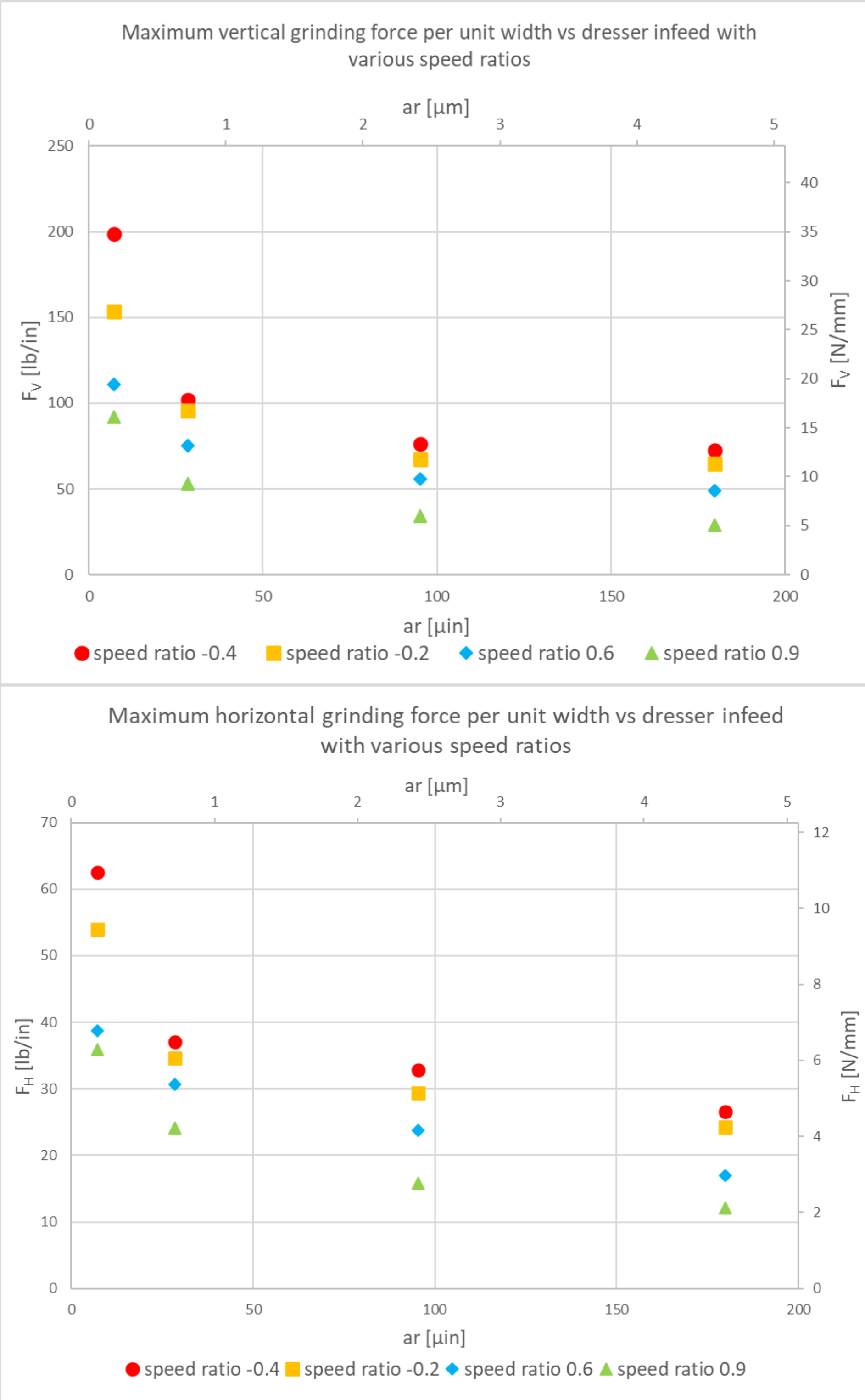

Figure 42: Vertical (above) and horizontal (below) forces during grinding plotted against the radial infeed for different speed ratios

From this last figure, it is possible to get the F_H values and evaluate the grinding specific energy. The grinding material removal rate is calculated with (15), and in particular for this case:

$$MRR = 142.24 \left[\frac{mm}{s}\right] \cdot 0.0254\ [mm]\ \cdot 9.525\ [mm] = 34.41 \left[\frac{mm^3}{s}\right]$$

If interested in the specific material removal rate, it can be evaluated simply by dividing the material removal rate by the width, as shown in (17) for the case in analysis.

$$Q' = \frac{MRR}{width} = \frac{34.41}{9.525} = 3.61 \left[\frac{mm^2}{s}\right] \tag{17}$$

The dressing Aggressiveness number has been calculated in the same way as in the surface roughness analysis ((11)).

In Figure 43 the grinding specific energy is plotted against the dressing Aggressiveness number: a power law trend can be identified, and it will be similar to the one found in the following experimental part: 9.1.1 Grinding power and grinding specific energy (SE_g).

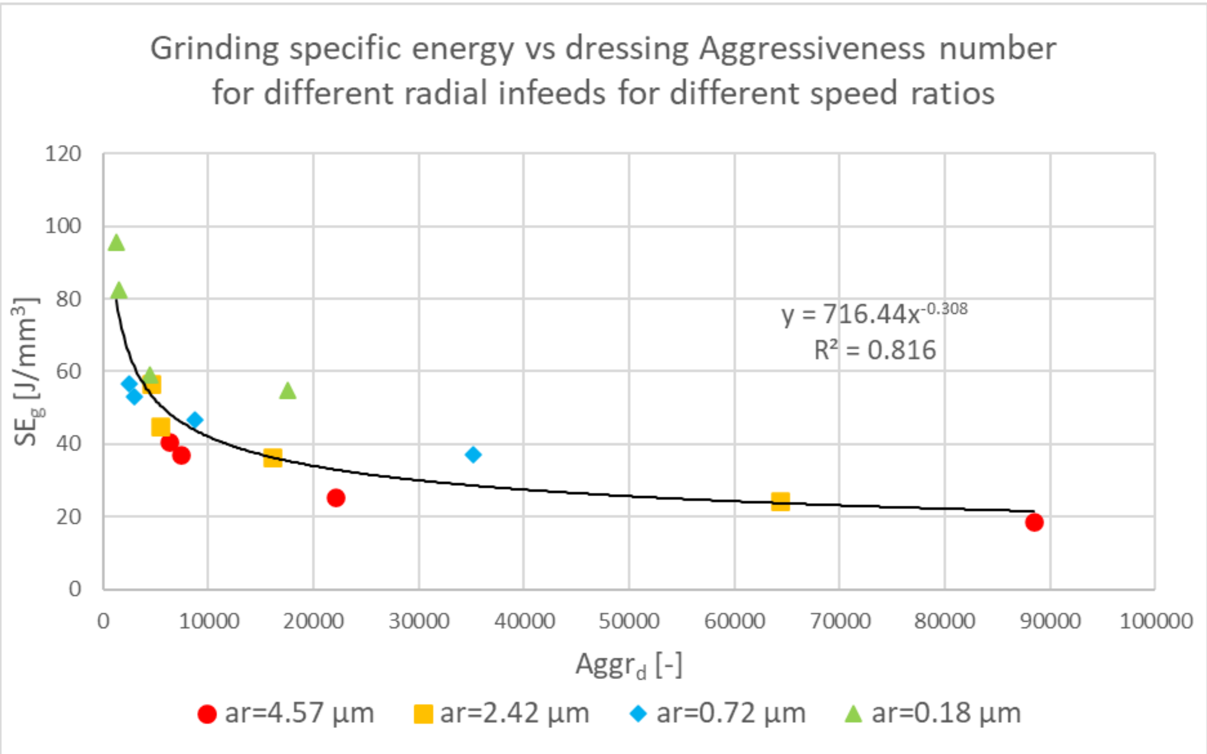

Figure 43: Grinding specific energy is plotted against the dressing Aggressiveness number: a power law trend can be seen

7.3 Grinding specific energy analysis, continuous dressing, Salmon

The topic is still the rotary dressing, and in the following discussion, data from Salmon's experiments on continuous rotary dressing effects on grinding specific energy (6.2 Effects of dressing on grinding performance, continuous dressing) are analysed.

First, the effect of dressing speed ratio on grinding specific energy is shown. In Figure 44 (same as Figure 32, but only with data points), the radial infeed of dresser per wheel revolution was fixed at 0.14 µm/rev and the speed ratio was varying.

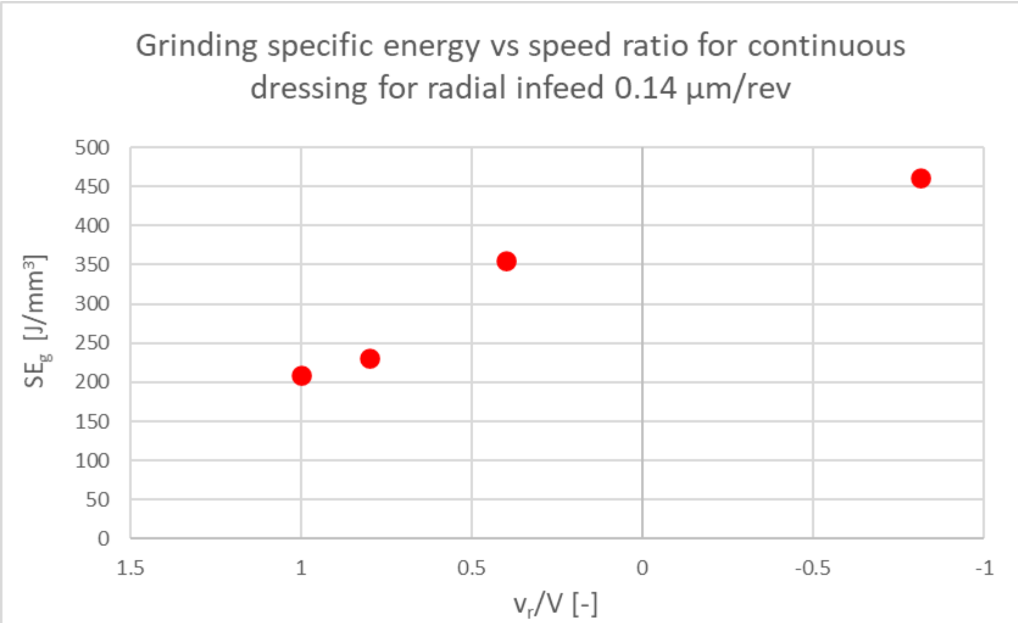

Figure 44: Grinding specific energy is plotted against the speed ratio for continuous dressing with fixed radial infeed 0.14 µm/rev

Moreover, another test was run now by fixing the speed ratio (+0.8) and changing the radial infeed of dresser per wheel revolution. From this following chart, reported in Figure 45 (same as Figure 33, but only with data points) , it is clear that increasing the radial infeed over 1.5 µm/rev will not lead to a significant decrease in grinding specific energy as already mentioned.

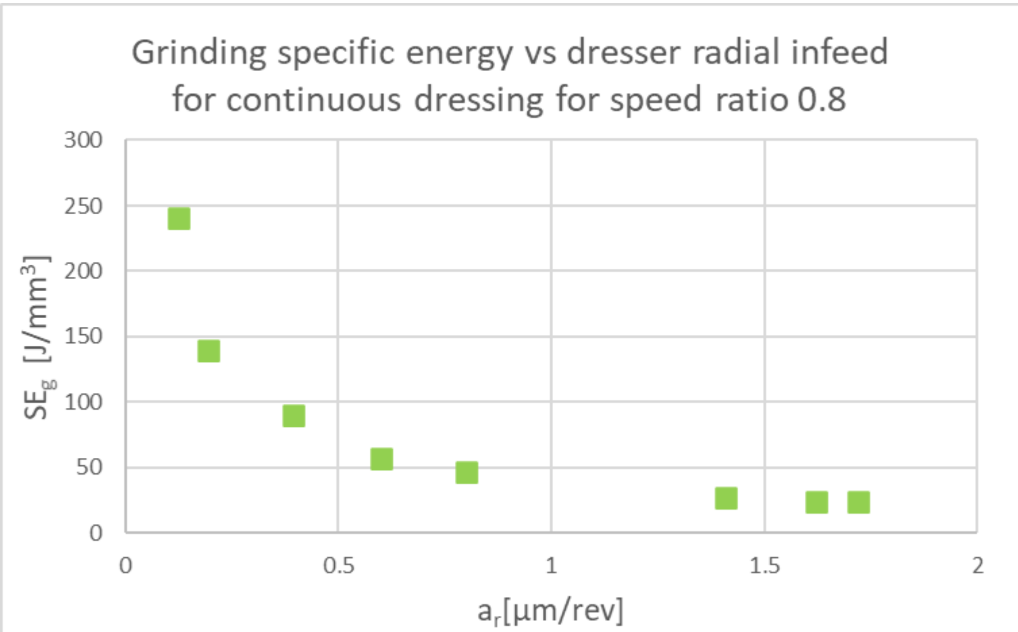

Figure 45: Grinding specific energy is plotted against the dressing radial infeed for continuous dressing with fixed speed ratio 0.8

Equivalent diameter and consequently dressing Aggressiveness number have been gotten respectively through (12) and (11).
In this case, the equivalent diameter was:

$$d_{eq} = \frac{d_{roll} \cdot d_{wheel}}{d_{roll} + d_{wheel}} = \frac{100 \cdot 600}{100 + 600} = 85.714\ [mm]$$

Finally, the two previous charts are combined in only one in Figure 46, in which the grinding specific energy is plotted versus the dressing Aggressiveness number.

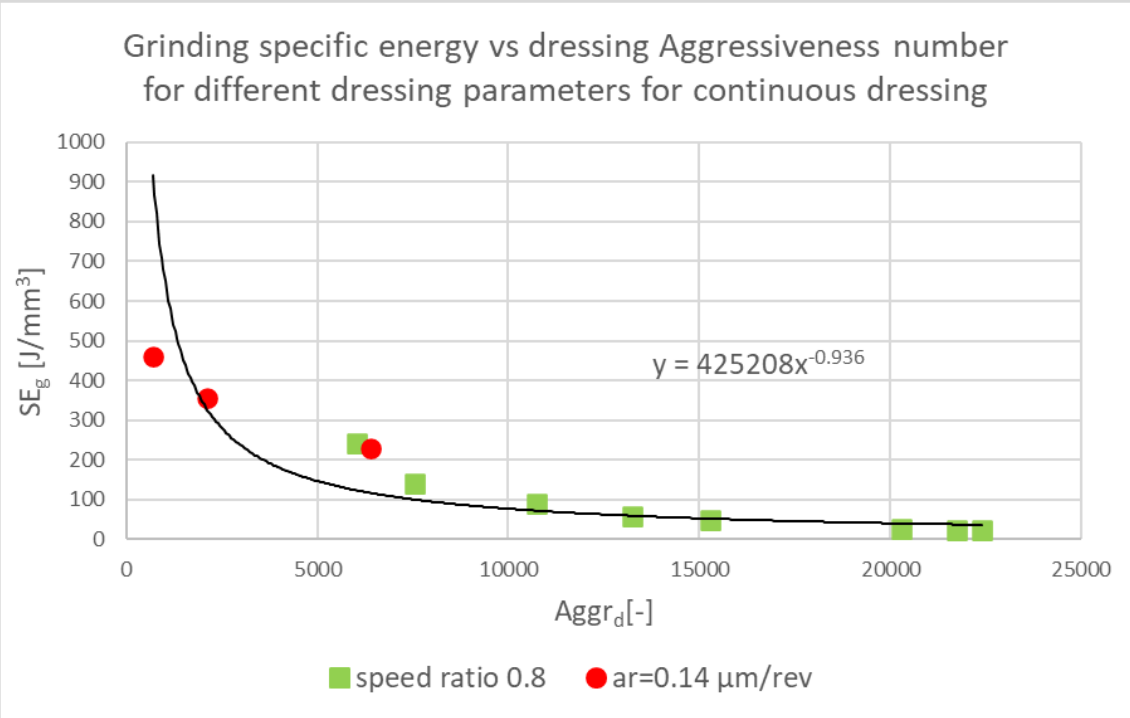

Figure 46: Grinding specific energy is plotted against the dressing Aggressiveness number for different dressing parameters for continuous dressing: a power law trend can be observed

The point correspondent to speed ratio equals to 1 in Figure 44 is missing in this Figure 46, since this would lead to an infinite Aggressiveness number value, given the definition of the dimensionless number.
A power law trend can be recognized, however the specific energy values for the grinding operation result different from the ones presented in Figure 43, and the reason is that the previous tests were run with different dressing roll, Aluminum oxide grinding wheel and workpiece. All these variables are influencing the results of course.

7.4 Surface roughness against grinding specific energy analysis, Malkin and Murray

Continuing the above work in 7.1 Surface roughness analysis, Malkin and Murray and 7.2 Grinding specific energy analysis, Malkin and Murray, since the data points were taken from the same speed ratios (+0.9 +0.6 -0.2 -0.4) and radial infeeds of dresser (4.57 2.42 0.72 0.18 [µm/rev]), surface roughness and grinding specific energy can be plotted together in the same chart for different radial infeeds (Figure 47). A power law trend is recognized. This result is showing what already mentioned several times, the higher is the grinding specific energy, the lower is the surface roughness, hence a compromise should be reached for having low grinding specific energy but still acceptable surface roughness according to the objective of the workpiece.

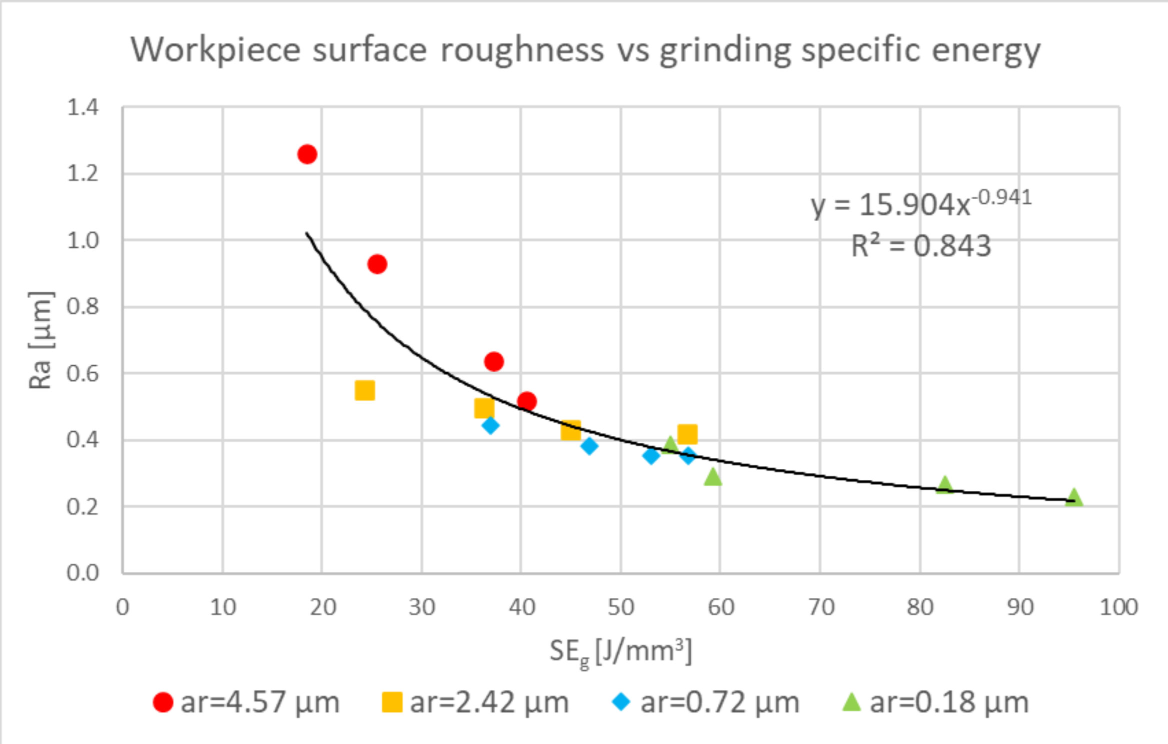

Figure 47: Surface roughness is plotted against the grinding specific energy: a power law trend can be identified

7.5 Force ratio during grinding: (F_V/F_H) analysis, Malkin and Murray

The next evaluation is about the ratio between maximum vertical grinding force and maximum horizontal grinding force. The data points shown in the previous figure for these forces (Figure 42), were both given for the same speed ratios (+0.9 +0.6 -0.2 -0.4) and radial infeeds (4.57 2.42 0.72 0.18 [µm/rev]), thus a new chart in which the ratio between the forces is plotted versus the dressing Aggressiveness number for different radial infeeds, it is presented in Figure 48. The higher will be the dressing Aggressiveness, the lower will be the ratio between the two forces.

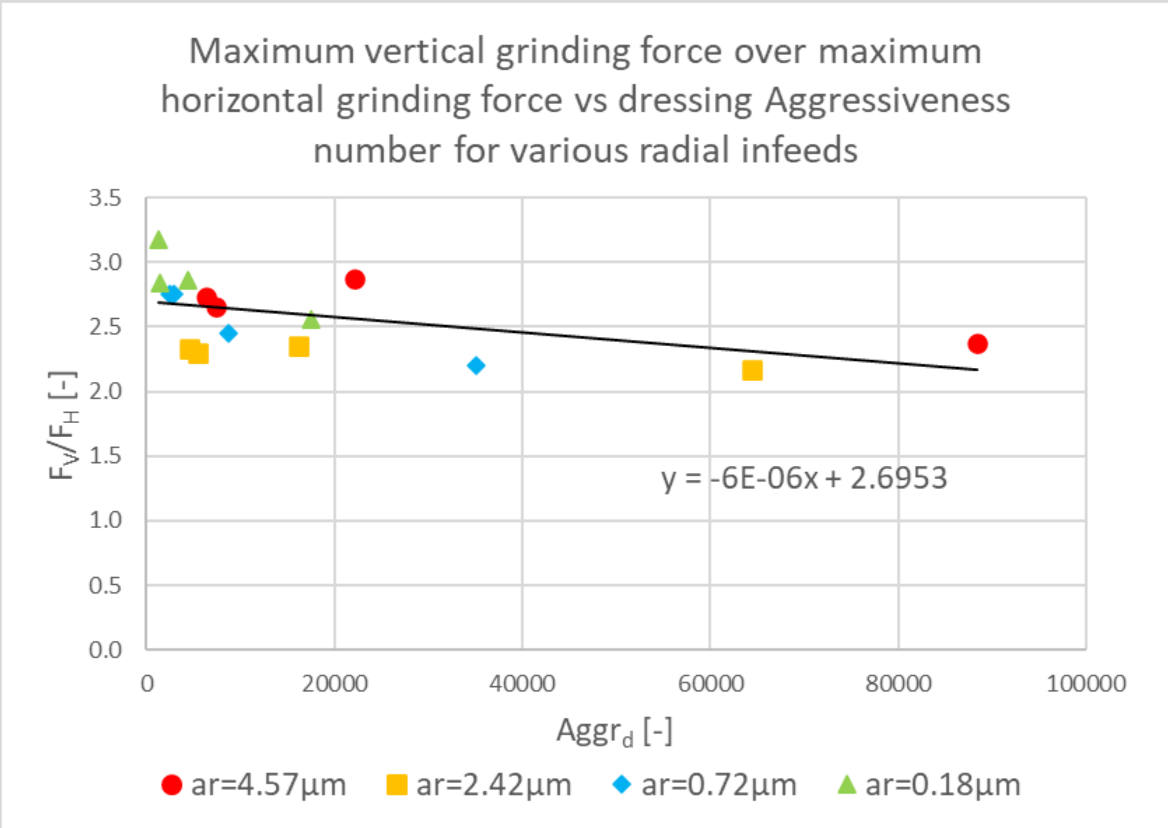

Figure 48: The ratio between the maximum vertical and horizontal grinding forces is plotted against the dressing Aggressiveness number

7.6 Grinding specific energy versus dressing specific energy analysis, Malkin and Murray

One last plot obtained by means of WebPlotDigitizer is taken from Malkin and Murray's studies about rotary dressing and single-point dressing [12]. Basically, they proved that grinding conditions after these two different types of dressing are similar between each other.

Coming to the relevant part, in Figure 49 there is a plot for grinding specific energy vs dressing specific energy for rotary dressing. They result proportional as mentioned in: 6.4 Acoustic emission in dressing of grinding wheels, specifically there is a power-law trend. Nevertheless, there are differences in specific energies values from the previous case since dressing tool, abrasive wheel and workpiece are changing.

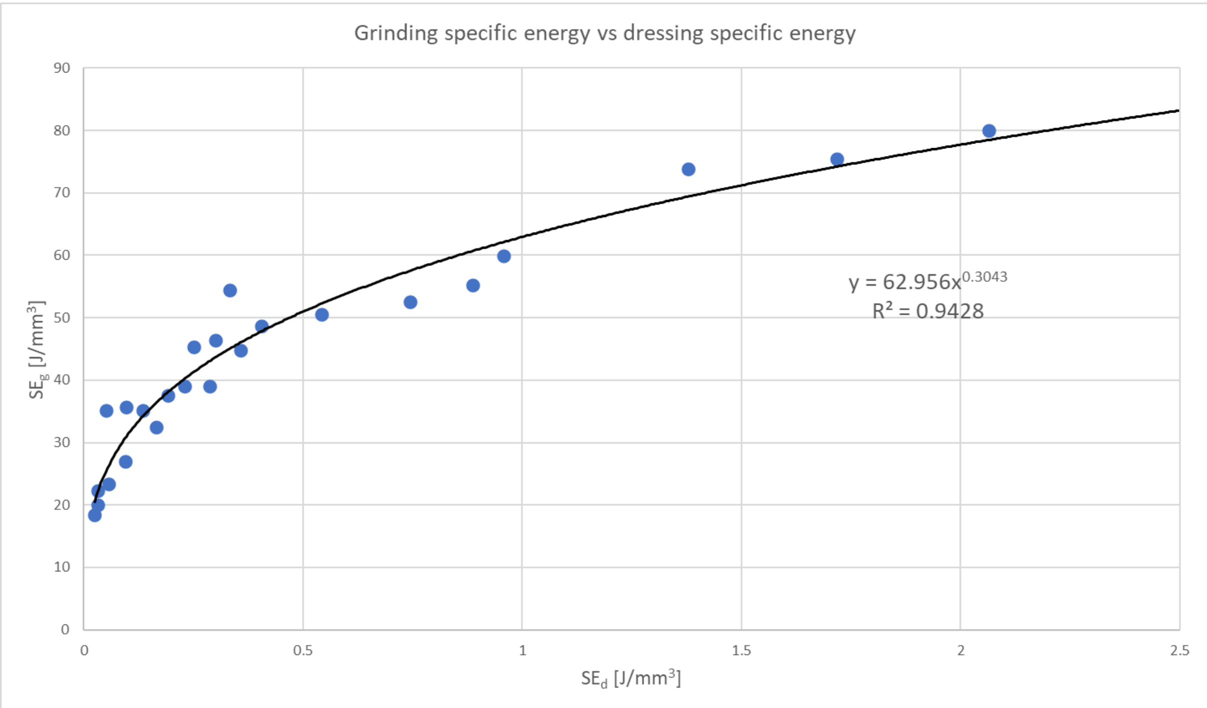

Figure 49: Grinding specific energy is plotted against the dressing specific energy: a power law trend can be identified

8. Experimental setup

In the following sections, the previously discussed results are compared with new ones, and more detailed analyses are carried on.
First of all, the effects on grinding wheel performance in surface grinding after plunge-roll dressing have been evaluated, together with considerations on using the acoustic emission data and on their reliability and benefits. These first tests, in order to investigate different properties given by different dressing conditions, are run with fixed grinding conditions for all the cases.
Secondly, effects of different grinding conditions are drawn, and effects of dwell time as well.

8.1 Machine description

In the scope of completing the necessary dressing and grinding tests, a CNC BLOHM machine has been used and it is presented in Figure 50.

Figure 50: PLANOMAT HP 408 [13]

In specific the machine is a BLOHM PLANOMAT HP 408, a profile grinding machine with excellent speed, robustness and efficiency. There is the possibility of dressing station attachment, indeed a spindle for a diamond roll dresser has been mounted.
Furthermore, between the accessories, there are:

- A magnetic chuck for holding the workpiece while grinding.
- An automatic balancing system for the grinding wheel.
- Acoustic sensors for acoustic emission data collection during dressing operation.
- Coolant filtration units.

The machine has liner guideways, and as shown in Figure 51 there are three driven axes for reaching all working points in the machine workspace.

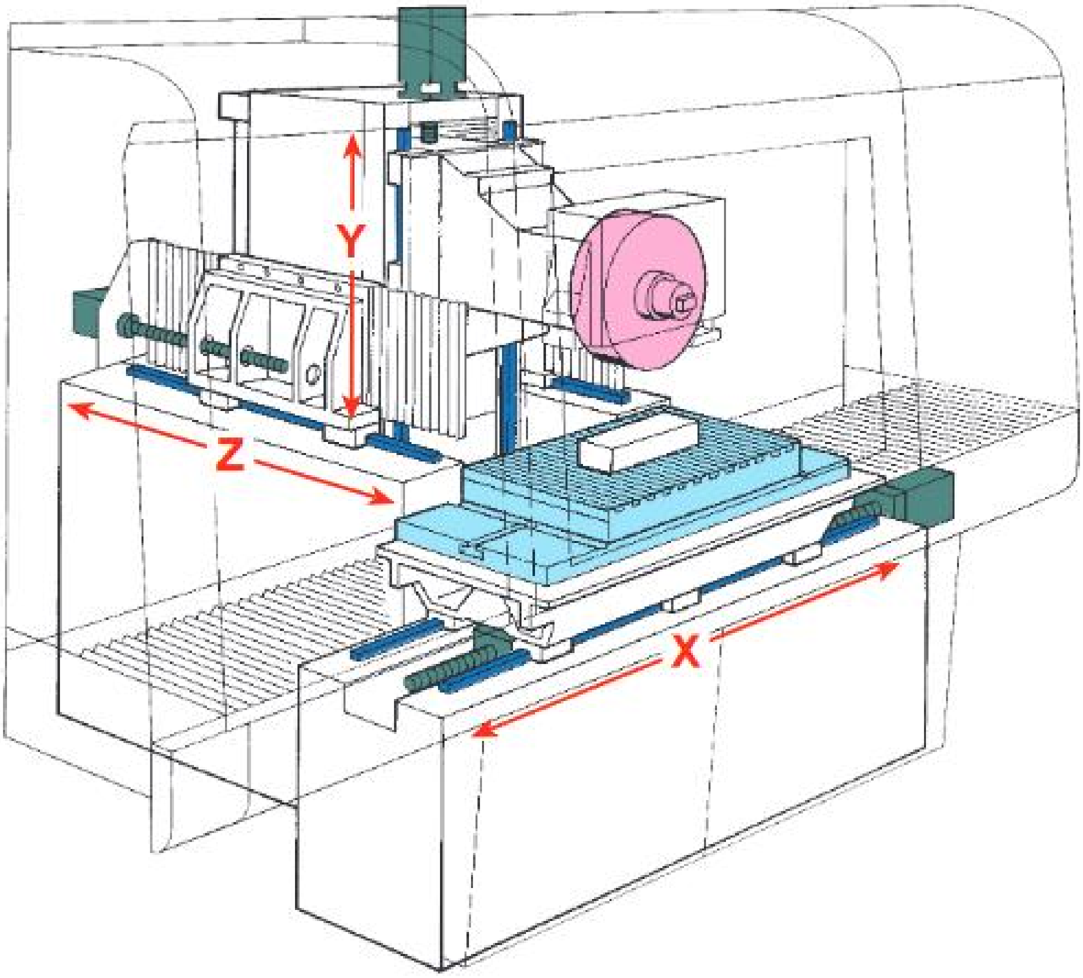

Figure 51: PLANOMAT HP 408 sketch [13]

In the following, a picture with some of the main components of the machine is shown (Figure 52).

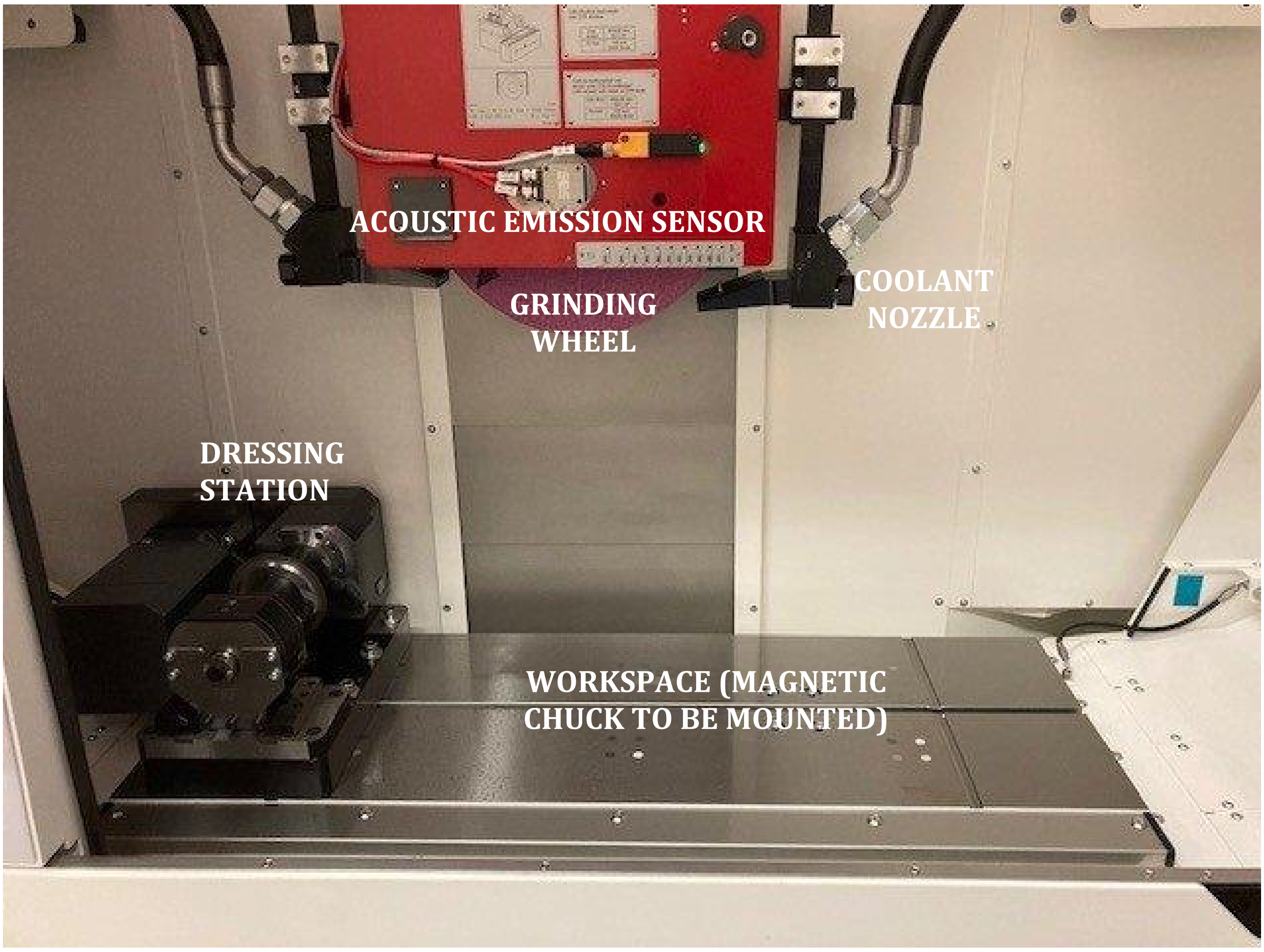

Figure 52: BLOHM machine setup and accessories

About technical data, taking some of the most important from the datasheet available in the BLOHM website [13]:

- Maximum travel speeds in X-Y-Z axis are respectively: 4000, 6000 and 6000 mm/min.
- Maximum spindle power: 24kW.
- Maximum spindle rpm: 6000 rpm.
- Spindle stiffness: 30000N/mm.
- Maximum grinding wheel diameter: 400mm.
- Maximum grinding wheel width: 100mm.
- Maximum workpiece weight: 800kg.
- Table size: 800x400mm.

A user interface on a Siemens platform with a touch screen allows to simplify the machine use (Figure 53).

Figure 53: BLOHM machine interface [13]

8.2 Tools description

Between the main tools that have been used there are: dressing rolls and disks, a grinding wheel and flat workpieces.

8.2.1 Diamond dressing roll from Meister Abrasives

The plunge-roll dresser has been purchased from Meister Abrasives. The roll diameter is 150mm and the roll width 12.83mm.
A diamond coating 5mm radially thick is mounted on a steel body. The bond for the diamond grits is an innovative hybrid bond: in the matrix of the dressing coating there is a selected combination of metal and ceramic properties. Moreover, by means of this bond, the wear resistance is improved.

Figure 54: diamond dressing roll from Meister Abrasives [14]

8.2.2 Diamond dressing disk for traverse dressing from Meister Abrasives

The diamond disk was used for performing profile dressing and traverse dressing and purchased from Meister Abrasives as well. As for the dressing roll, the diamond coating is 5mm radially thick, and mounted on a steel body. The diamond grits are held by the same hybrid bond described for the previous case. The diameter is 125mm and the diamond coating width is 2mm.

Figure 55: diamond disk for traverse dressing from Meister Abrasives [14]

8.2.3 Aluminum oxide grinding wheel from Hermes

The Aluminum oxide grinding wheel was acquired form Hermes Abrasives.
Following the grinding wheel designations, the wheel is coded EWD46G7VHK. Wheel width is 50mm and initial wheel diameter is 400mm.
By clarifying the wheel specifications:

- EWD: friable Aluminum oxide with mixtures.
- 46: medium grit size (Figure 56).

Figure 56: grit size for the Hermes grinding wheel [15]

- G: very soft regarding hardness.
- 7: medium density for the structure.
- VHK: vitrified-high performance bonds.

As already mentioned, the wheel has been profiled for obtaining a step as wide as the dressing roll.

8.2.4 Flat steel workpieces

The workpiece that will be ground are taken from a bigger bar made of 38MnSiVS5 with hardness 217 HV5. The thickness for this surface grinding operation is not a relevant parameter, the length was 68mm.

8.3 Main programs in the BLOHM machine

8.3.1 Plunge-roll dressing

This program is the most important for the studies to perform. The plunge-roll dressing operation is run with different dressing conditions in order to evaluate the effects on the grinding wheel performance.

By simply input the main parameters on the interface presented in Figure 53, it is possible to select the conditions and start the operation.

Specifically, the variables are:

- radial infeed per wheel revolution in mm/rev.
- Speed ratio and dressing mode (unidirectional or anti-directional).
- Total radial dressing amount in mm.
- Number of dwell revolutions in rev.
- Wheel speed in m/s.
- Coolant pressure, going from level 1 to level 7. Level 2 was chosen for running the tests.
- Stand-off amount in mm (for safety reasons, it represents radially how many millimetres before reaching the theoretical contact point the machine will start the dressing operation with the given radial infeed per wheel revolutions as feedrate into the grinding wheel).

A sketch of the operation is proposed in the following (Figure 57).

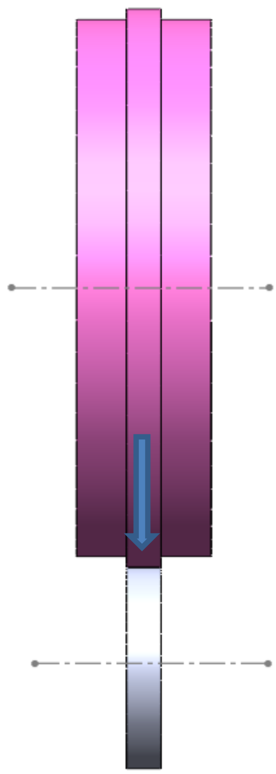

Figure 57: plunge-roll dressing sketch

8.3.2 Profile dressing

In order to be able to perform plunge-roll dressing, it is necessary to shape the grinding wheel by introducing a step as wide as the dressing roll, indeed the dressing roll is 12.83mm wide and the grinding wheel is 50mm wide.

By means of this program, the step will be created in the grinding as shown in the following sketch (Figure 58).

The G-code consists in repeating the operation and the same path with very low depths of cut in the grinding wheel, until the grinding wheel step results 4 mm radially deep and the part of the step with larger diameter is machined for 0.03mm radially.

The G-code and a brief explanation are here presented.

```
G0 G90 Z-5
Y0
Y-2.5
G1 Z7.035 F=R8
Y0
Z22.965
Z35
G0 Z37
```

Starting from rapid motion and absolute coordinates, the grinding wheel moves closer to the dressing roll. Afterwards, coordinated motion is set, as well as the Z-coordinate for indicating the first side of the step starting from the left, and the feedrate for the grinding wheel movement in the Z-axis.

Finally, the grinding wheel motion will follow the profile shape as shown in Figure 58.

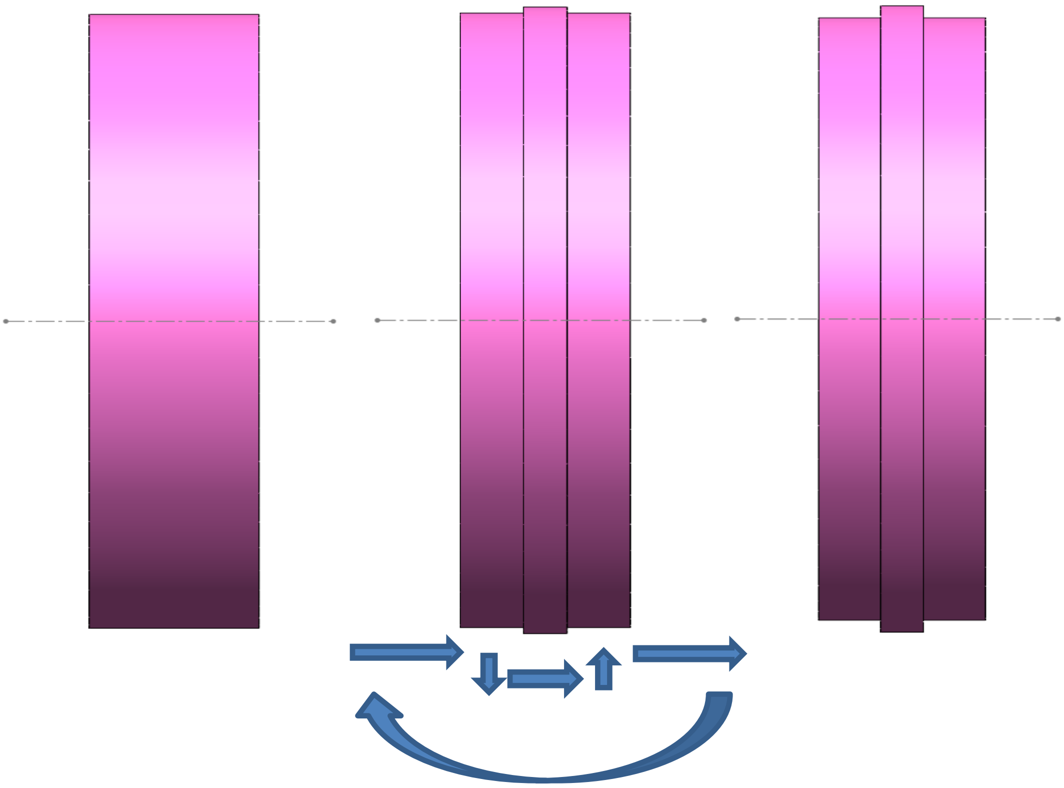

Figure 58: profile dressing operation sketch

8.3.3 Traverse dressing

This operation is to be considered as a side operation, and it is to run after a profiling operation and before a plunge-roll dressing. The purpose is to determine in an accurate way the grinding wheel radius. A function of the BLOHM machine is to automatically calculate the grinding wheel dimeter after a dressing operation, in this way once the zero position for dressing and grinding is set and the radius continually updated, there should not be problems for continuously running the programs. On the other hand, slight errors on the grinding wheel diameter have been noticed, therefore once in a while it has been proved useful to run the described program, just by increasing manually the grinding wheel diameter, starting the traverse dressing operation with the dressing disk and with parameters in order to reduce the wear on the diamond disk, and run this traverse dressing until contact on the dressing acoustic emission sensor can be detected: thus the grinding wheel has an extremely accurate diameter, correctly shown in the interface. An example of the operation and consequent dressing disk motion in presented in Figure 59.

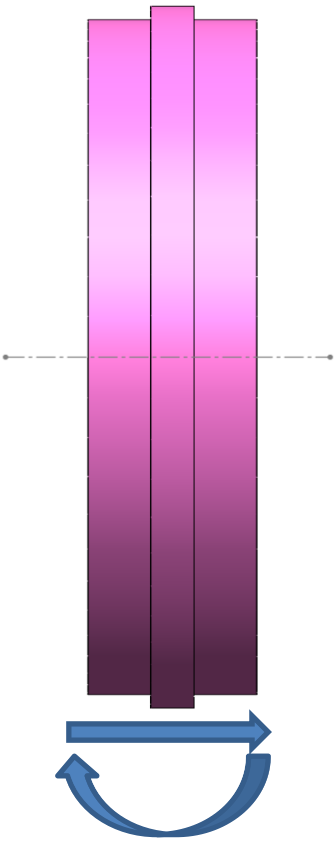

Figure 59: traverse dressing operation sketch

8.3.4 Surface grinding

Surface grinding (Figure 60) is another key operation, indeed after plunge-roll dressing is performed, the effects of dressing are evaluated.

The variables to set are:

- number of passes.
- Depth of cut per pass in mm.
- Total depth of cut in mm (should be equals to number of passes times depth of cut per pass).
- Workpiece feedrate in mm/min and mode (upcut or downcut).
- X-axis overrun in mm.
- Length of workpiece in mm.
- Z position of the grinding wheel on the workpiece.
- Wheel speed in m/s.

In order to set the number of passes, a folder in the program is dedicated for starting a loop, and consequently one for finishing the loop.

The number of passes has been defined depending on grinding conditions: with lower depths of cut, more passes are required for overcoming eventual transients and establish the grinding power in the most accurate possible way.

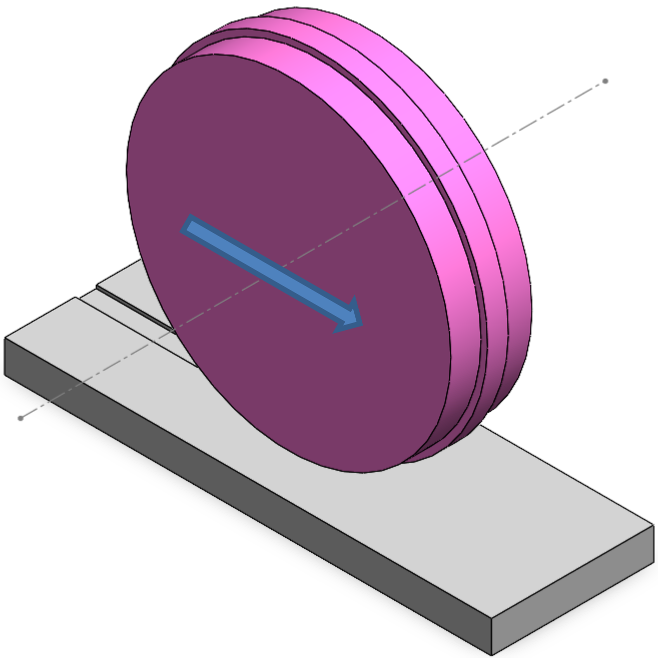

Figure 60: surface grinding operation sketch

8.4 Operations list

Finally, after presenting the different possible operations to run with the machine and the tools, a list of the main important functions to implement for running the tests, and in which order, is stated in the following:

- turn on the machine.
- Run safety checks.
- Start the grinding wheel spindle and run the automatic balance program in order to reach a run-out around 0.10 µm/rev.
- Mount the disk dresser.
- Check dressing zero position by positioning the grinding wheel close to the dressing disk and comparing the values on the Siemens interface.
- Run the profile dressing program for shaping or reshaping a step 4 mm radially deep and 12.83mm wide in the grinding wheel, in order to have a grinding wheel step as wide as the dressing roll for the following plunge-roll dressing.
- Dismount the disk dresser.
- Mount the plunge-roll dresser.
- Check once again the grinding wheel balancing.
- Check the dressing zero position for avoiding unwanted crushes between dressing roll and grinding wheel during plunge-roll dressing operation.
- Run the plunge-roll dressing operation with one of the dressing data points.
- Mount the workpiece on the magnetic chuck.
- Check the grinding zero position.
- Perform the surface grinding operation with selected parameters.
- Ventilate the machine environment.
- Eventually take a look to the workpiece ground track.
- Run once again a plunge-roll dressing program with different parameters.
- Run the surface grinding operation by setting another Z-position for obtaining another grinding track.

9. Experiments and results

In this section, the results of the experimental activities are presented and discussed in detail. The tests are focused on varying dressing conditions and keeping fixed grinding conditions, to see effects of dressing on grinding performance (by analysing several variables' behaviours), and finally varying both dressing and grinding conditions to observe combined effects.

9.1 Plunge-roll dressing effects on Aluminum oxide grinding wheel performances

Twenty plunge-roll dressing conditions have been performed with the Meister Abrasives dressing roll on the Hermes Abrasives friable Aluminum oxide grinding wheel, and the dressing amount has been set at 0.2mm radially for each condition.

One of the main parameters to calculate is the dressing Aggressiveness number, given by (18):

$$Aggr_d = \frac{1}{1-\left(\frac{v_r}{V}\right)} \cdot \sqrt{\frac{a_r}{d_{eff}}} \cdot 10^6$$

(18)

With d_{eff} obtained through (19):

$$d_{eff} = \frac{d_{roll} \cdot d_{wheel}}{d_{roll} + d_{wheel}} = 106.66\,mm$$

(19)

In which:

$$d_{roll} = 150mm \; and \; d_{wheel} = 184.5 \cdot 2 = 369.14\,mm$$

A table showing different dressing parameters set and the relative dressing Aggressiveness number is presented. The higher are speed ratio and radial infeed per wheel revolution, the higher is the Aggressiveness number (and the sharper will be the grinding wheel grains).

speed ratio [-]	radial infeed [µm/rev]	dressing Aggressiveness number [-]
0.8	0.1	4841
0.8	0.3	8386
0.8	0.7	12809
0.8	1	15310
0.8	1.5	18751
0.4	0.1	1614
0.4	0.3	2795
0.4	0.7	4270
0.4	1	5103
0.4	1.5	6250
-0.4	0.1	692
-0.4	0.3	1198
-0.4	0.7	1830
-0.4	1	2187
-0.4	1.5	2679
-0.8	0.1	538
-0.8	0.3	932
-0.8	0.7	1423
-0.8	1	1701
-0.8	1.5	2083

After realizing each condition by dressing, surface grinding on a steel workpiece in 38MnSiVS5 with average hardness 217 HV5 has been performed with the following parameters:

- Number of passes for overcoming transient: 10 passes
- Depth of cut per pass: 0.025 mm
- Wheel step width: 12.83 mm
- Workpiece feedrate: 50 mm/s
- Material removal rate:

$$MRR = width \cdot depth\ of\ cut \cdot feedrate = 12.83 \cdot 0.025 \cdot 50 = 16.0375 \frac{mm^3}{s}$$

- Specific material removal rate:

$$Q' = depth\ of\ cut \cdot feedrate = 1.25 \frac{mm^2}{s}$$

9.1.1 Grinding power and grinding specific energy (SE_g)

First of all, collecting the data from the machine and plotting the grinding wheel power during surface grinding, after 10 passes the transient can be considered over, and therefore the correct grinding power is evaluated.

A measured grinding power (called ‘P1’, green line) is obtained considering the peak value of the last pass, and an idle grinding power (called ‘P2’, red line) is estimated as well. Once they are defined, it is possible to proceed by subtracting P2 from P1 and get the actual grinding power.

For instance, for the case with speed ratio -0.4 and ar=1.5µm/rev, the plot is presented in Figure 61, and the grinding power is given by 1022-193=829W.

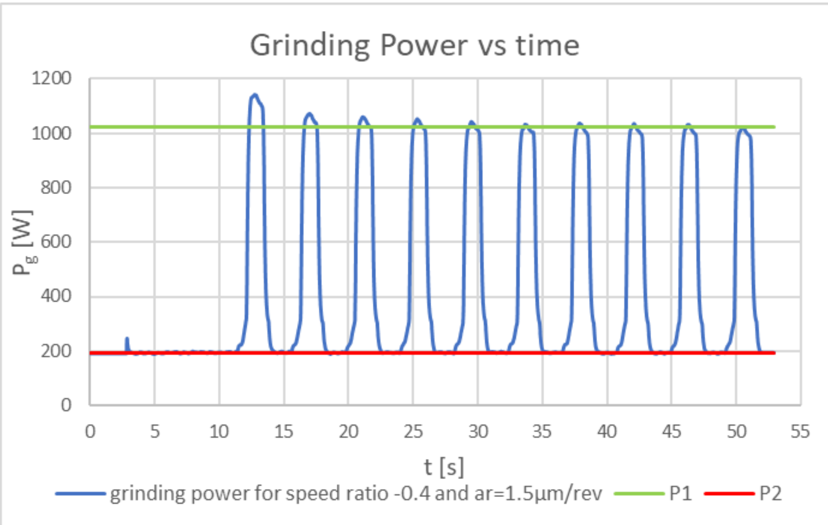

Figure 61: Grinding power is plotted against time for speed ratio -0.4 and radial infeed 1.5 µm/rev

For visualizing the differences between the operations, there are plots for different dressing radial infeeds for same speed ratio. The plot in Figure 62 is for speed ratio 0.8. It is clear such as a more aggressive dressing condition (if speed ratio constant is obtained with higher radial infeed value) would lead to lower grinding power. First passes are to be disregarded because of slight errors on evaluating the zero-position for the grinding operation start.

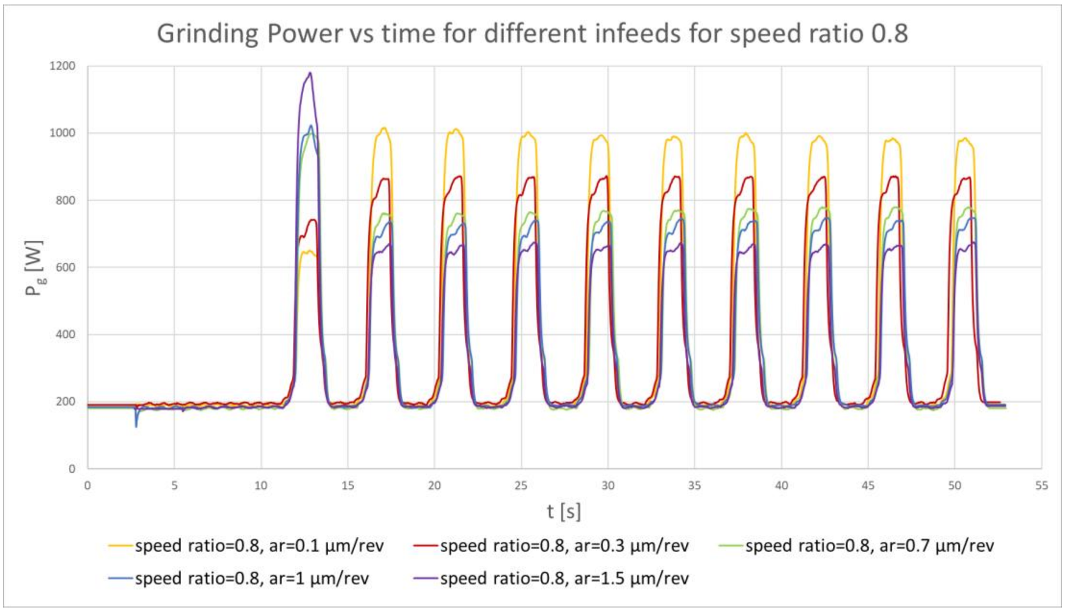

Figure 62:Grinding power is plotted against time for different radial infeeds and speed ratio 0.8

Once the grinding power has been calculated, it has been possible to get the grinding specific energy, obtained by dividing grinding power by grinding material removal rate, as shown previously in (16).
Here there are the grinding results for all the dressing conditions.

speed ratio [-]	radial infeed [µm/rev]	Measured power [W]	P idle [W]	P grinding [W]	SE_g [J/mm^3]	$Aggr_d$ [-]
0.8	0.1	986	188	798	49.76	4841
0.8	0.3	869	194	675	42.09	8386
0.8	0.7	780	179	601	37.47	12809
0.8	1	748	183	565	35.23	15310
0.8	1.5	676	184	492	30.68	18751
0.4	0.1	1213	189	1024	63.85	1614
0.4	0.3	864	182	682	42.53	2795
0.4	0.7	960	189	771	48.07	4270
0.4	1	770	182	588	36.66	5103
0.4	1.5	788	184	604	37.66	6250
-0.4	0.1	1398	191	1207	75.26	692
-0.4	0.3	1048	176	872	54.37	1198
-0.4	0.7	1001	191	810	50.51	1830
-0.4	1	947	181	766	47.76	2187
-0.4	1.5	1022	193	829	51.69	2679
-0.8	0.1	1627	174	1453	90.60	538
-0.8	0.3	1261	191	1070	66.72	932
-0.8	0.7	1050	181	869	54.19	1423
-0.8	1	914	188	726	45.27	1701
-0.8	1.5	929	183	746	46.52	2083

Proceeding with representing all the points in the same chart, the expected trends can be seen by plotting grinding specific energy versus radial infeed for different speed ratios in Figure 63: generally, for each radial infeed, if the speed ratio is lower, the grinding specific energy is higher, and consequently for each speed ratio, the higher is the radial infeed the lower is the grinding specific energy.

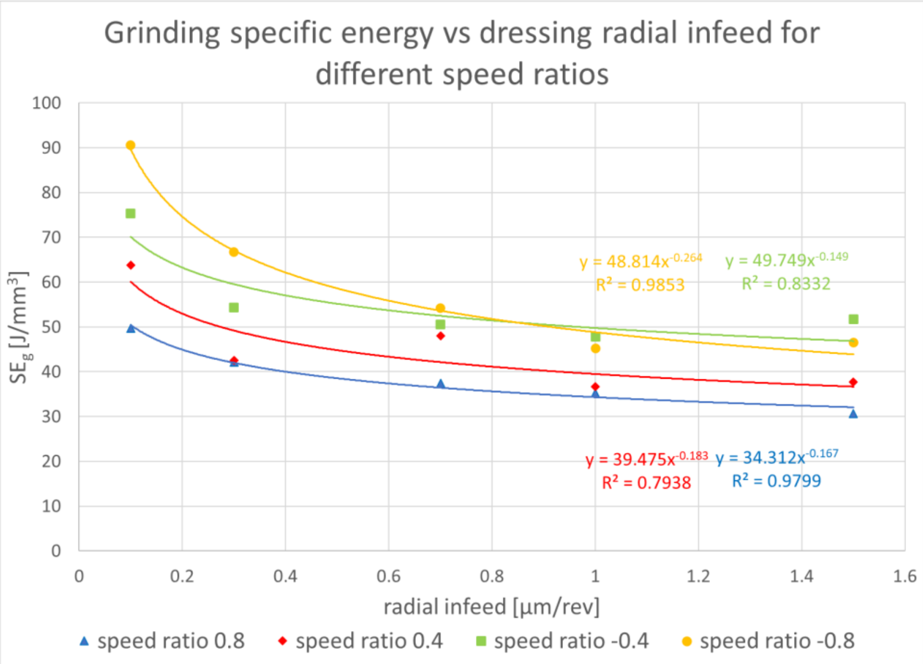

Figure 63: Grinding specific energy vs dressing radial infeed for different speed ratios - power law trends for each speed ratio value

In order to get a better idea of the process, the grinding specific energy can be plotted versus the dressing Aggressiveness number, which is reuniting the main dressing parameters (Figure 64).

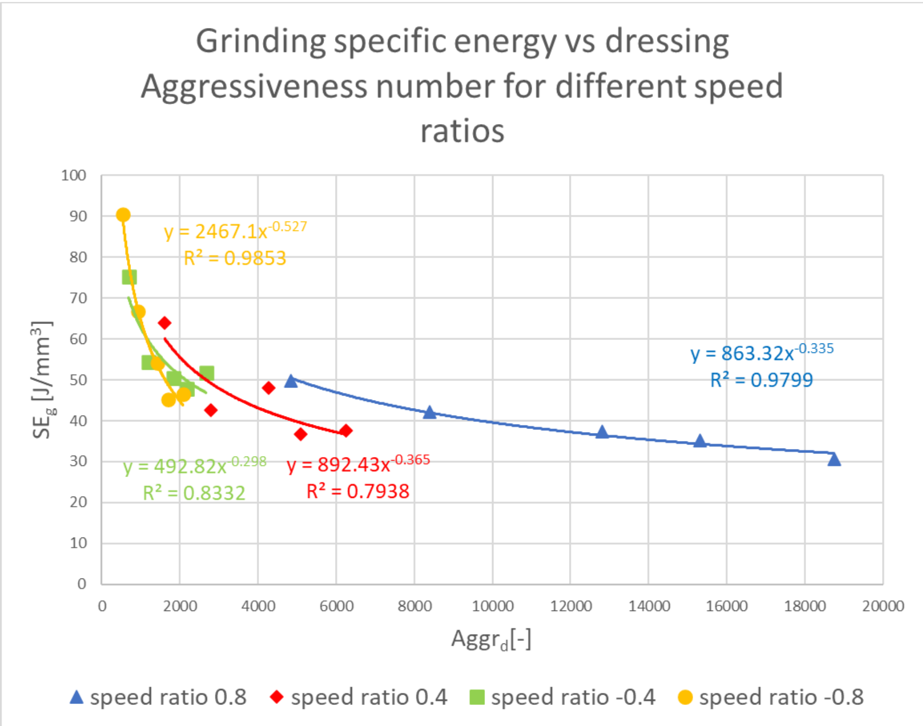

Figure 64: Grinding specific energy is plotted against the dressing Aggressiveness number for different speed ratios - a power-law trend for each speed ratio can be seen

To make the concept even clearer, in Figure 65, for different speed ratios, the data are fit in one trend with a power law equation, which results in an enough-precise approximation. This plot reminds of the one in Figure 43 and Figure 46.

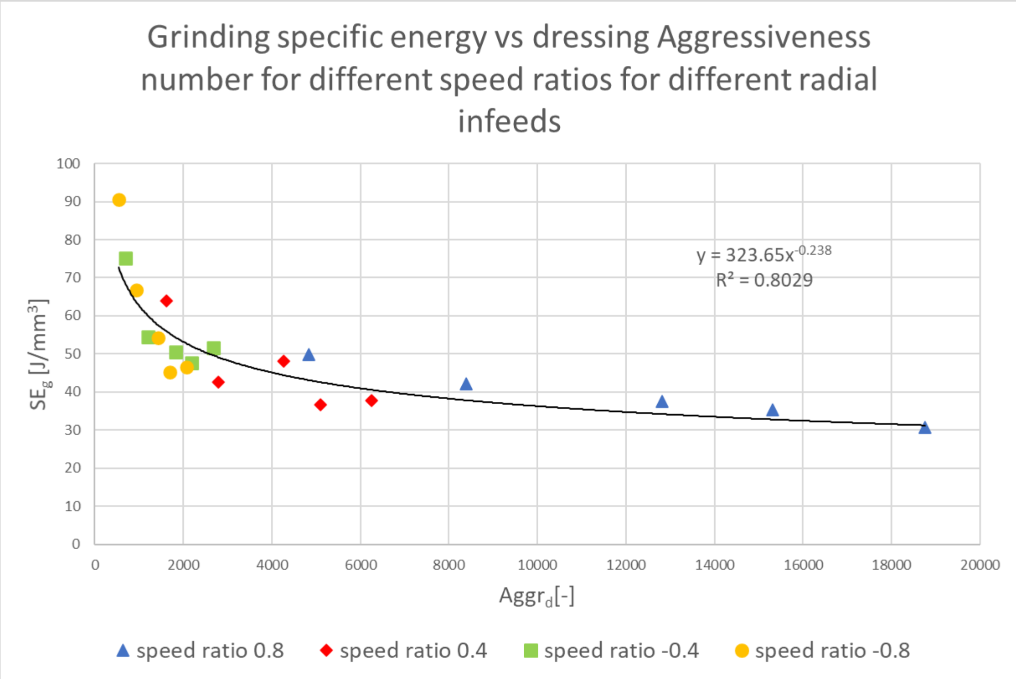

Figure 65: Grinding specific energy is plotted against the dressing Aggressiveness number for different speed ratios - a power-law trend can be observed

Especially, if visualizing in the same plot Malkin and Murray's results (Figure 43) and the experimental results for grinding specific energy versus dressing Aggressiveness number, there are similarities (Figure 66).

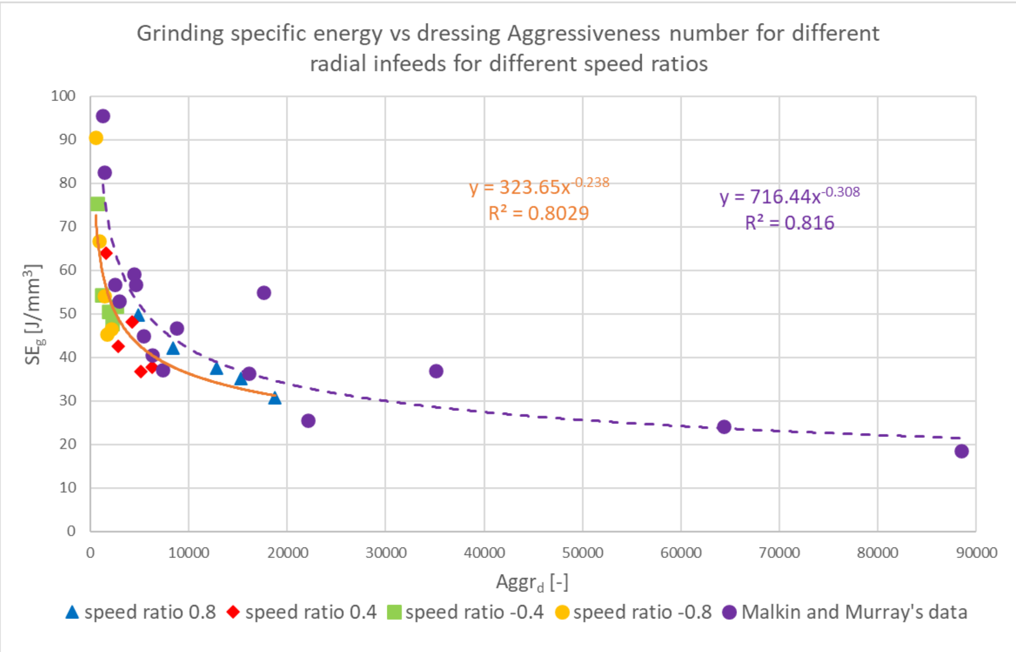

Figure 66: Grinding specific energy is plotted against dressing Aggressiveness number: comparison with Malkin's data

Since Malkin's data were for a larger range of dressing Aggressiveness, by restricting the analysis, an even better correlation is found regardless eventual differences between grinding wheels, dressing rolls and workpiece materials used (Figure 67).

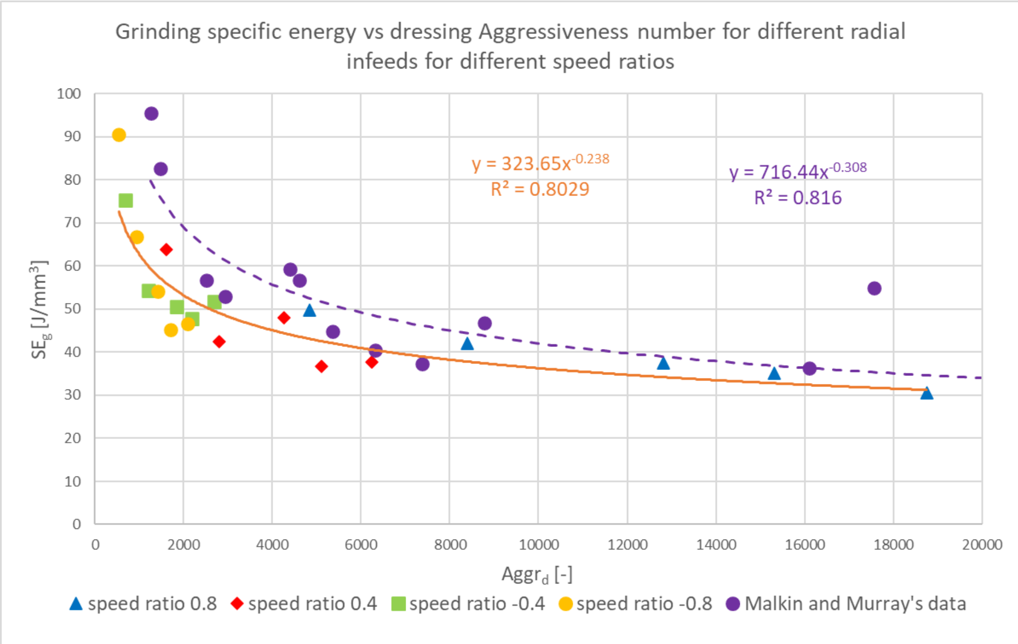

Figure 67: Grinding specific energy is plotted against dressing Aggressiveness number: comparison with Malkin's data in a restricted area

9.1.2 Dressing power and dressing specific energy (SE_d)

By means of the power sensors mounted on grinding wheel spindle and dressing roll spindle, it has been possible to collect data during dressing operation, and hence get the dressing power. The latter has been defined according to the following equations, and by considering the value of power in the plot towards the end of the dressing operation, where eventual transients would be over.

In order to obtain this variable, the charts are including dressing roll power and grinding wheel power during dressing, indeed the total power results as a combination of the two of them.

For instance, for the unidirectional case with speed ratio 0.4 and radial infeed 1.5 µm/rev (Figure 68), the dressing power has been defined in (20), as the difference between (P1-P2) and (P3-P4) since the dressing roll power has an opposite behaviour with respect to the grinding wheel power during dressing.

$$P_{dressing} = (P1 - P2) - (P3 - P4) \tag{20}$$

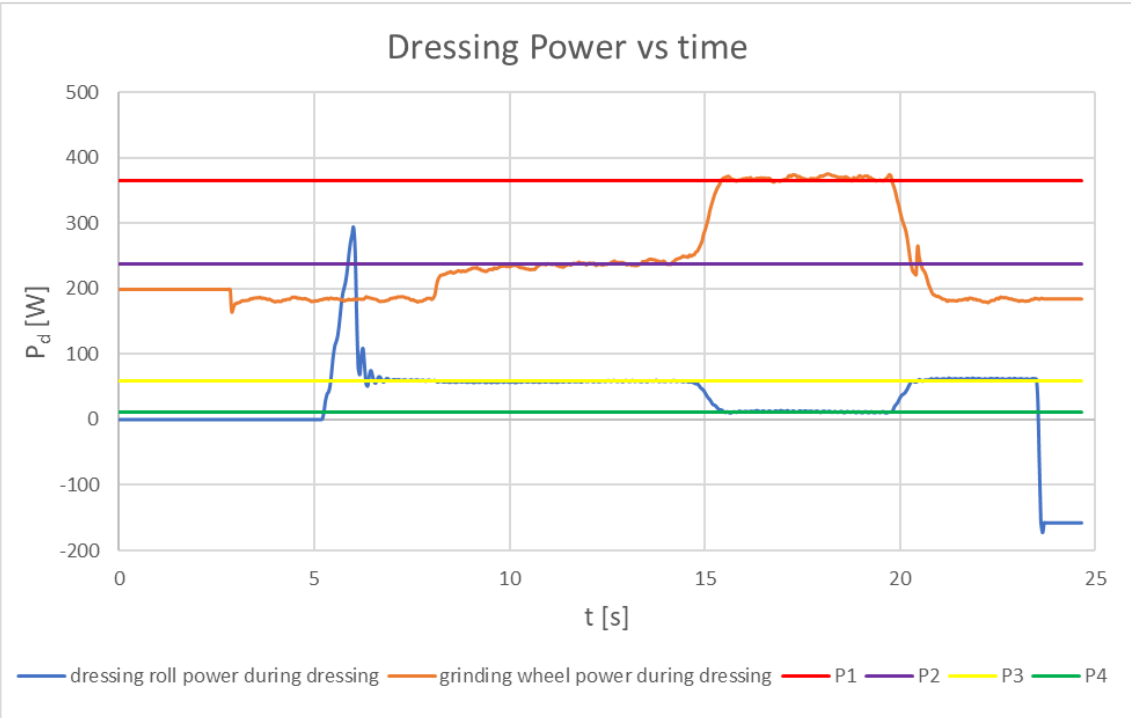

Figure 68: Dressing power is plotted against time with speed ratio 0.4 and radial infeed 1.5 µm/rev

In Figure 69, a similar procedure has been adopted for calculating dressing power for anti-directional dressing mode (speed ratio -0.4 and radial infeed 1.5µm/rev) , however in this case both powers are defined as positive, as it can be seen in (21):

$$P_{dressing} = (P1 - P2) + (P3 - P4)$$

(21)

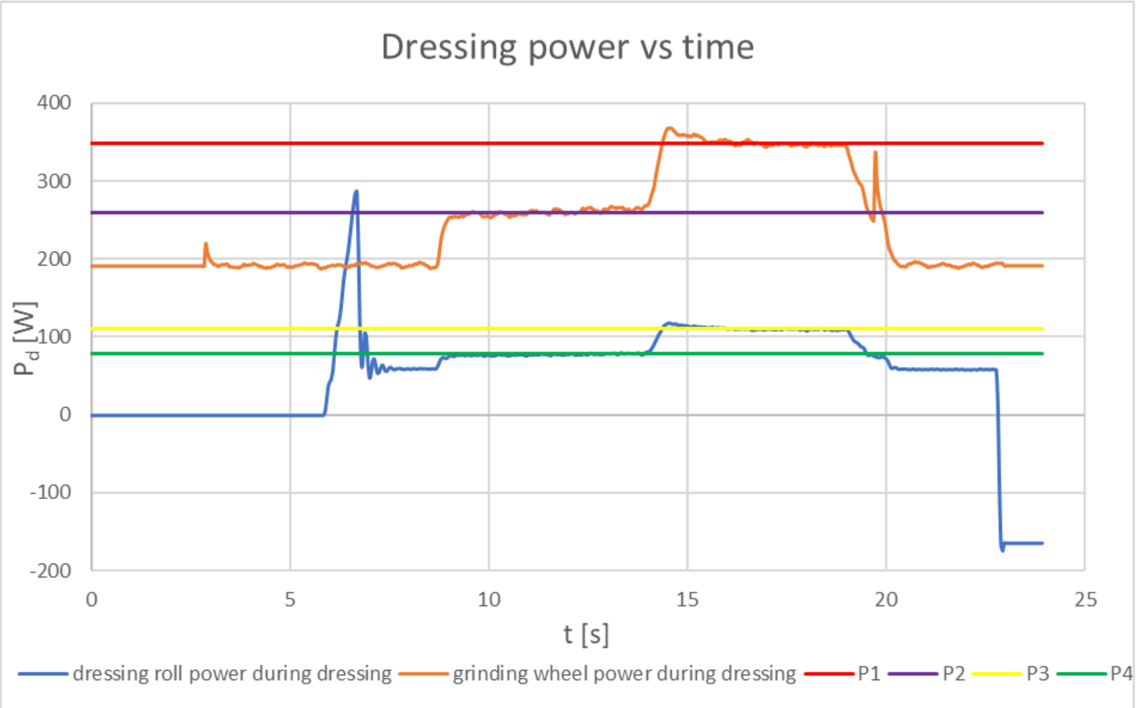

Figure 69: Dressing power is plotted against time with speed ratio -0.4 and radial infeed 1.5 µm/rev

Finally, the dressing specific energy can be defined. It is given by dressing power divided by dressing material removal rate.

The dressing material removal rate for outside diameter (OD) dressing is defined in (22):

$$MRR = 2\pi \cdot grinding\ wheel\ radius \cdot width \cdot \frac{radial\ infeed\ in \frac{\mu m}{s}}{1000} \left[\frac{mm^3}{s}\right]$$

(22)

A table with all the data is reported. Wheel speed was 30m/s and width was 12.83 mm for all cases.

speed ratio [-]	radial infeed [µm/rev]	P total dressing [W]	Wheel rpm [rpm]	Wheel radius [mm]	radial infeed [µm/s]	Dressing MRR [mm^3/s]	SE_d [J/mm^3]	$Aggr_d$ [-]
0.8	0.1	8.5	1579	181.43	2.63	38.49	0.221	4841
0.8	0.3	21.0	1575	181.88	7.88	115.47	0.182	8386
0.8	0.7	35.0	1569	182.56	18.31	269.43	0.130	12809
0.8	1	48.0	1562	183.37	26.04	384.90	0.125	15310
0.8	1.5	82.0	1559	183.72	38.98	577.35	0.142	18751
0.4	0.1	13.5	1581	181.20	2.64	38.49	0.351	1614
0.4	0.3	21.5	1561	183.52	7.81	115.47	0.186	2795
0.4	0.7	53.5	1582	181.09	18.46	269.43	0.199	4270
0.4	1	49.5	1552	184.56	25.87	384.90	0.129	5103
0.4	1.5	86.0	1566	182.92	39.15	577.35	0.149	6250
-0.4	0.1	15.0	1584	180.85	2.64	38.49	0.390	692
-0.4	0.3	30.5	1556	184.11	7.78	115.47	0.264	1198
-0.4	0.7	61.0	1574	182.00	18.36	269.43	0.226	1830
-0.4	1	72.5	1567	182.79	26.12	384.90	0.188	2187
-0.4	1.5	116.5	1586	180.59	39.66	577.35	0.202	2679
-0.8	0.1	33.0	1557	183.99	2.60	38.49	0.857	538
-0.8	0.3	41.5	1577	181.65	7.89	115.47	0.359	932
-0.8	0.7	50.5	1554	184.32	18.13	269.43	0.187	1423
-0.8	1	62.0	1564	183.14	26.07	384.90	0.161	1701
-0.8	1.5	94.5	1571	182.32	39.28	577.35	0.164	2083

All the data are reported in a single chart, but it is not possible to fit them in a single trend even if each one of them has a linear behaviour if considering fixed speed ratio.
Since it is physically clear that for 0 as dressing Aggressiveness, a power of 0 Watts would correspond, by setting the intercept at 0 W it is possible to state that the less aggressive is the condition (lower speed ratio if plotting for different speed ratios), the higher is the slope value of the trendline (Figure 70). Therefore, if having fixed speed ratio, for speeding up the production it would be beneficial to increase radial infeed value, however, if considering anti-directional dressing modes, it would result inconvenient because of high increase rates of the dressing power.

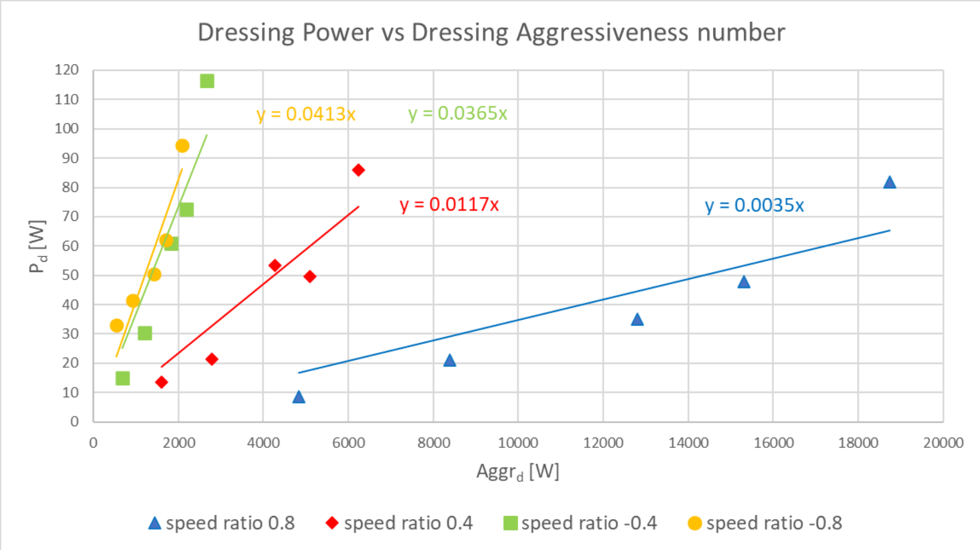

Figure 70: Dressing power is plotted against the dressing Aggressiveness number for different speed ratios - linear trend for each case with intercept 0 Watts

By means of the dressing specific energy, a better-defined behaviour can be observed in Figure 71. In this plot, the dullest dressing case in which burning has occurred (test performed with speed ratio -0.8 and radial infeed as 0.1 µm/rev), has not been considered.

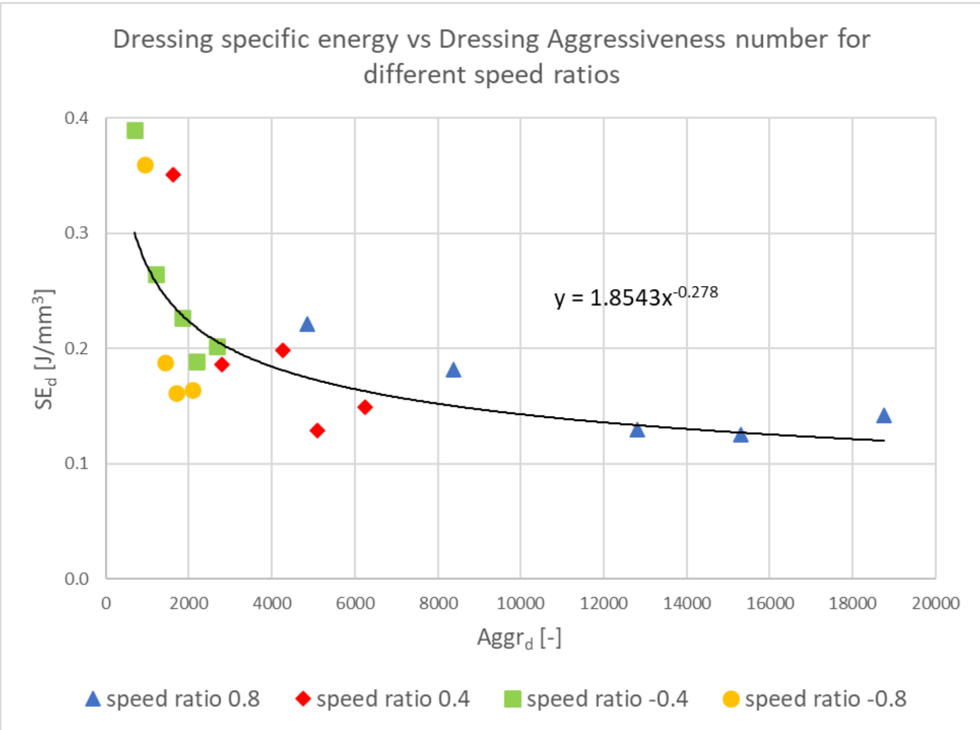

Figure 71: Dressing specific energy is plotted against the dressing Aggressiveness number for different speed ratios – a power law trend can be seen

In Figure 72, there is a plot for different speed ratios of grinding specific energy vs dressing specific energy. A good trend seems to be the linear one. Thus, grinding specific energy and dressing specific energy would appear to be proportional, and 20 J/mm^3 could be defined as the minimum grinding specific energy that is possible to reach by dressing with an “infinite sharp” condition with this diamond dressing roll, Aluminum oxide grinding wheel and steel workpiece.

As for the previous case, considering that during the grinding operation for the dullest dressing condition (for speed ratio -0.8 and radial infeed 0.1 µm/rev) burning occurred, it is better not to consider it for the fitting curve since it led to too high specific energies for the data point itself.
On the other hand, by using a power law fitting curve, the result is shown in the same figure and it leads to a higher R^2 value, hence this is the proposed trend for fitting properly the data points.

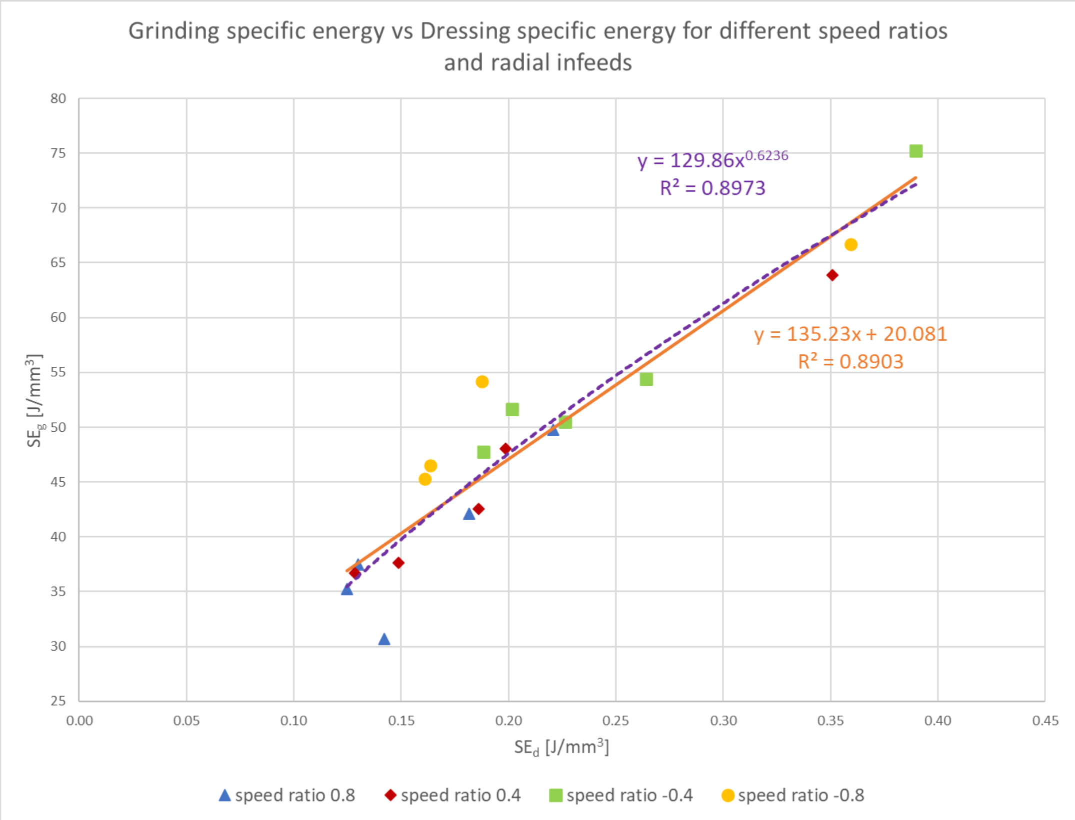

Figure 72: Grinding specific energy is plotted against the dressing specific energy - a linear trend is found

In Figure 73 there is a comparison of the experimental power law trend with the plot shown in Figure 49, coming from Malkin and Murray's analysis on rotary dressing (7.6 Grinding specific energy versus dressing specific energy analysis, Malkin and Murray).

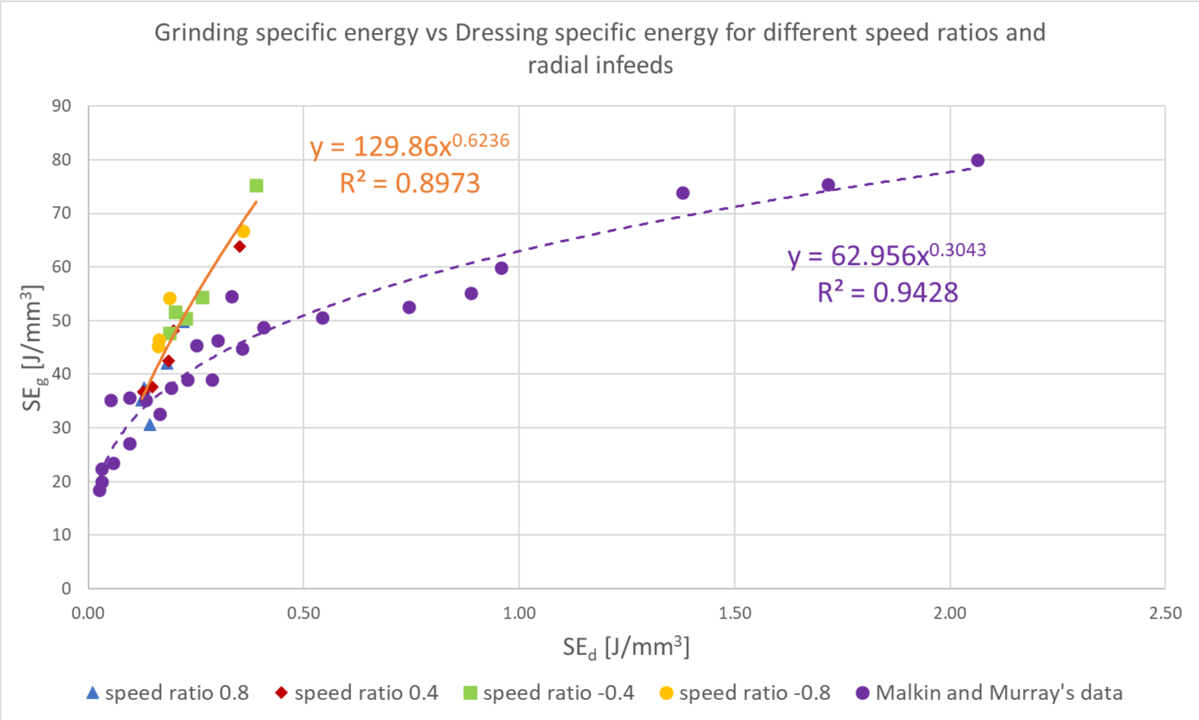

Figure 73: Comparison between experimental data and Malkin and Murray data for SE_g against SE_d

And more specifically in a SE_d values region in which the experimental tests have been focused (Figure 74).

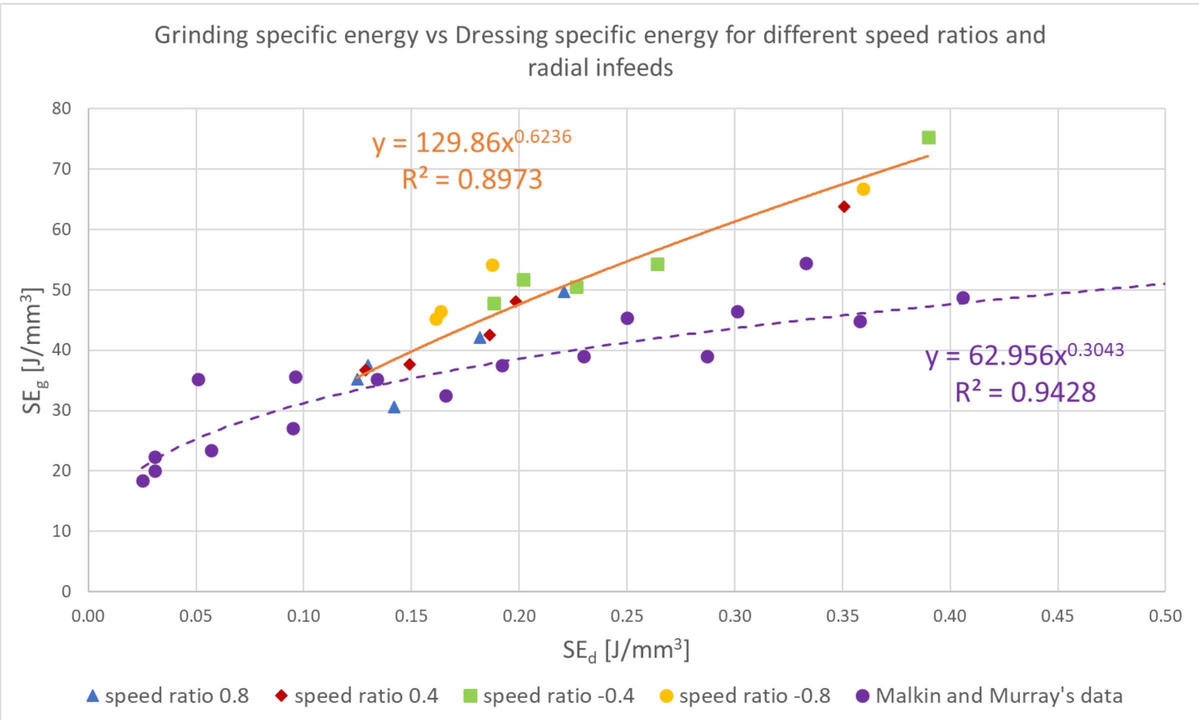

Figure 74: Comparison between experimental data and Malkin and Murray data for SE_g against SE_d, restricted region for SE_d values

9.1.3 Dressing acoustic emission and acoustic emission specific energy (SE_a)

During the dressing operation, the dressing acoustic emission monitoring has been possible with sampling time of 0.004s, as result of acoustic emission sensor presence.
An "idle acoustic emission" has been identified in each case, and it resulted 2.3% for each case.
Here there are two examples of how the acoustic emission has been identified: basically, an acoustic emission value during the operation has been taken, and finally from this value the idle value of 2.3% has been subtracted.
For instance, in Figure 75 and Figure 76 the two cases of speed ratio +0.4 and radial infeed 1.5 µm/rev and speed ratio -0.4 and radial infeed 0.3 µm/rev are reported.

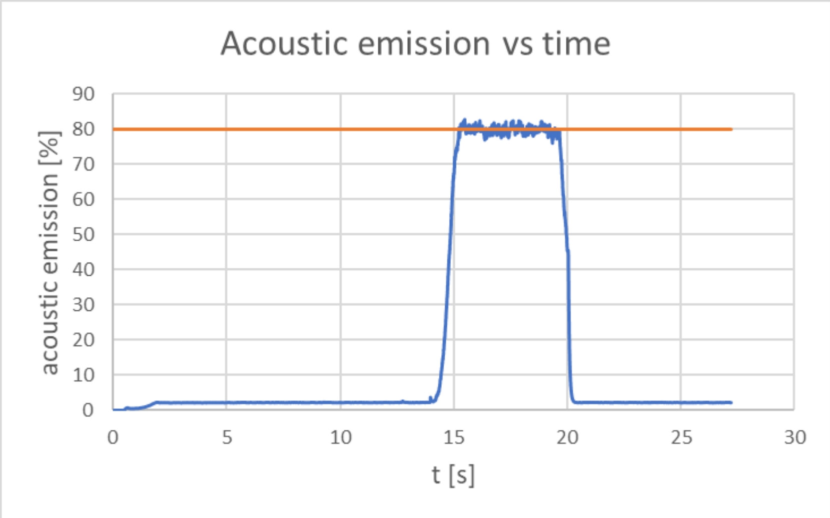

Figure 75: Acoustic emission during dressing is plotted against the time for speed ratio 0.4 and radial infeed 1.5 µm/rev: orange line is the acoustic emission value taken during the operation and P_{idle} is 2.3 %

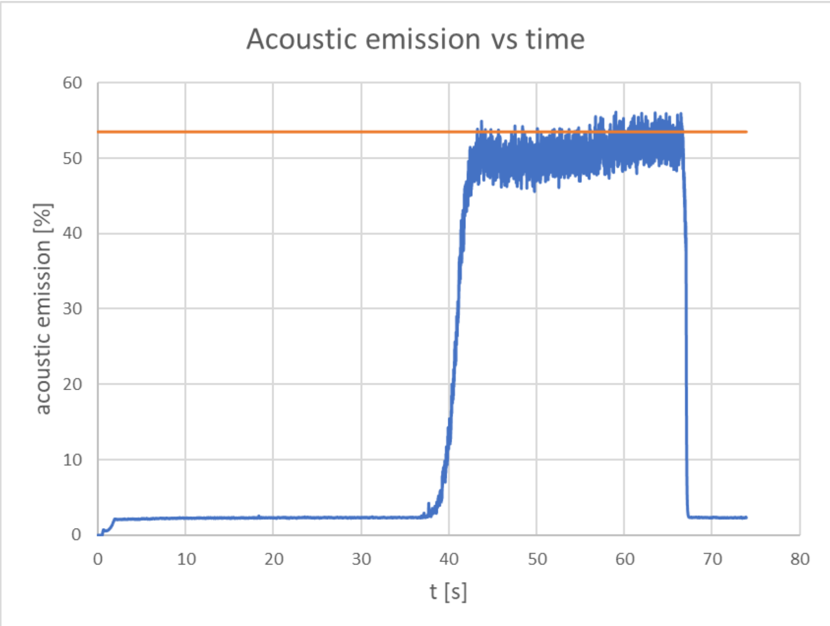

Figure 76: Acoustic emission during dressing is plotted against the time for speed ratio -0.4 and radial infeed 0.3 µm/rev: orange line is acoustic emission value taken during the operation and P_{idle} is 2.3 %

Afterwards, since both dressing material removal rate and the acoustic emission are known for each dressing case, it has been possible to determine *acoustic emission specific energy*, given by acoustic emission over dressing material removal rate, as can be seen in (23):

$$SE_a = \frac{AE}{MRR_d} \left[\frac{\%}{\frac{mm^3}{s}} \right] \tag{23}$$

In the following table, all data are collected.

speed ratio [-]	radial infeed [µm/rev]	Idle acoustic emission [%]	measured acoustic emission [%]	acoustic emission [%]	Dressing power [W]	Dressing MRR [mm^3/s]	SE_d [J/mm^3]	SE_a [%/mm^3*s^{-1}]	SE_g [J/mm^3]
0.8	0.1	2.3	15.9	13.6	8.5	38.49	0.221	0.35	49.76
0.8	0.3	2.3	25.2	22.9	21.0	115.47	0.182	0.20	42.09
0.8	0.7	2.3	37.2	34.9	35.0	269.43	0.130	0.13	37.47
0.8	1	2.3	43.8	41.5	48.0	384.90	0.125	0.11	35.23
0.8	1.5	2.3	54	51.7	82.0	577.35	0.142	0.09	30.68
0.4	0.1	2.3	28.2	25.9	13.5	38.49	0.351	0.67	63.85
0.4	0.3	2.3	38.4	36.1	21.5	115.47	0.186	0.31	42.53
0.4	0.7	2.3	65.3	63	53.5	269.43	0.199	0.23	48.07
0.4	1	2.3	64.5	62.2	49.5	384.90	0.129	0.16	36.66
0.4	1.5	2.3	80	77.7	86.0	577.35	0.149	0.13	37.66
-0.4	0.1	2.3	34	31.7	15.0	38.49	0.390	0.82	75.26
-0.4	0.3	2.3	50.8	48.5	30.5	115.47	0.264	0.42	54.37
-0.4	0.7	2.3	69.6	67.3	61.0	269.43	0.226	0.25	50.51
-0.4	1	2.3	82.2	79.9	72.5	384.90	0.188	0.21	47.76
-0.4	1.5	2.3	99	96.7	116.5	577.35	0.202	0.17	51.69
-0.8	0.1	2.3	35.4	33.1	33.0	38.49	0.857	0.86	90.60
-0.8	0.3	2.3	56	53.7	41.5	115.47	0.359	0.47	66.72
-0.8	0.7	2.3	72.7	70.4	50.5	269.43	0.187	0.26	54.19
-0.8	1	2.3	84.4	82.1	62.0	384.90	0.161	0.21	45.27
-0.8	1.5	2.3	96.8	94.5	94.5	577.35	0.164	0.16	46.52

About the acoustic emission, now it can be plotted versus the dressing power in the scope of finding a correlation between the two of them (Figure 77).
Both a power law trend and a linear trend could be defined, but the power law seems to fit the data in a better way, hence the choice is again for a power law equation for describing the phenomenon.

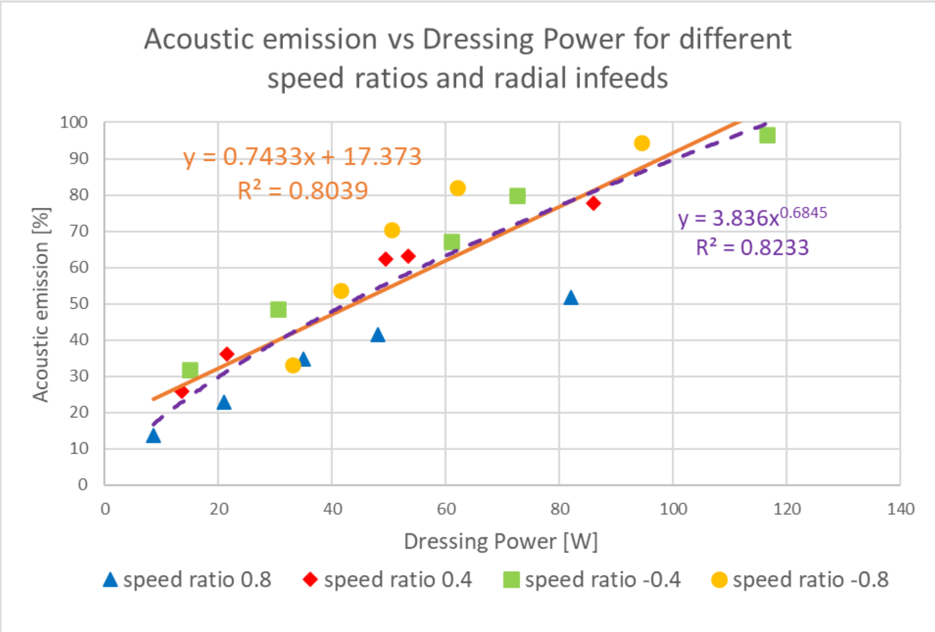

Figure 77: Acoustic emission is plotted against the dressing power for different speed ratios – power law trend fits better the data

If not considering the data coming from speed ratio +0.8 (blue triangles), the R^2 value results higher, as can be seen in Figure 78.

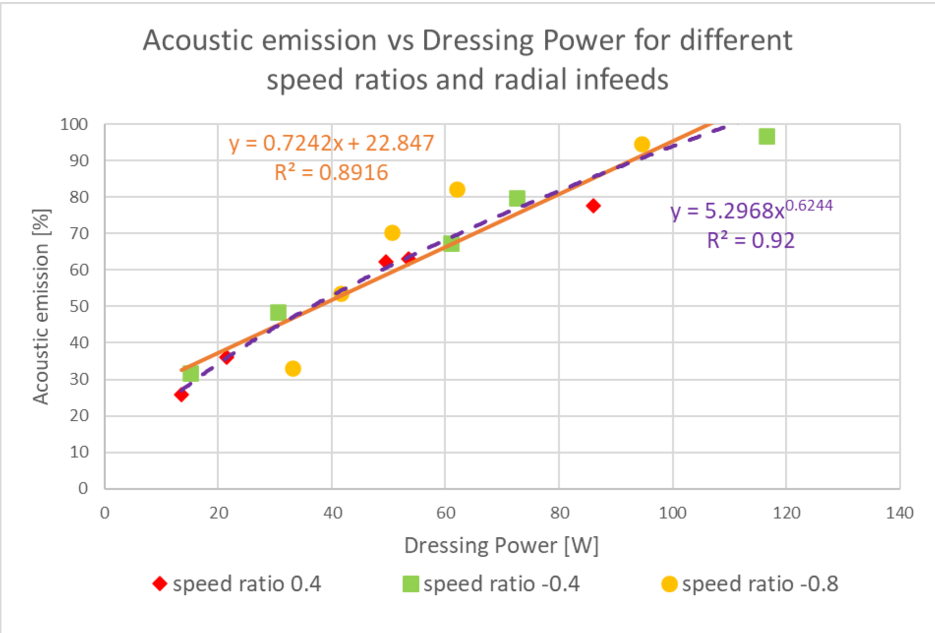

Figure 78: Acoustic emission is plotted against the dressing power for different speed ratios, without +0.8 – power law trend fits better the data

Nevertheless, it would be possible to define a “calibrated power”, $P_{AE,c}$ in order to get a power in Watts by knowing the acoustic emission value: this calculation could be done by setting 0 as intercept of a linear trend, and taking the slope of this line as a conversion factor. The distortion between this trend and a power law trend would not be evident, as shown in Figure 79. In conclusion, for sake of simplicity there is the option to define this linear trend with intercept 0, and the more interesting conclusion is that the conversion factor would result close to 1, hence 45° slope for the trendline.

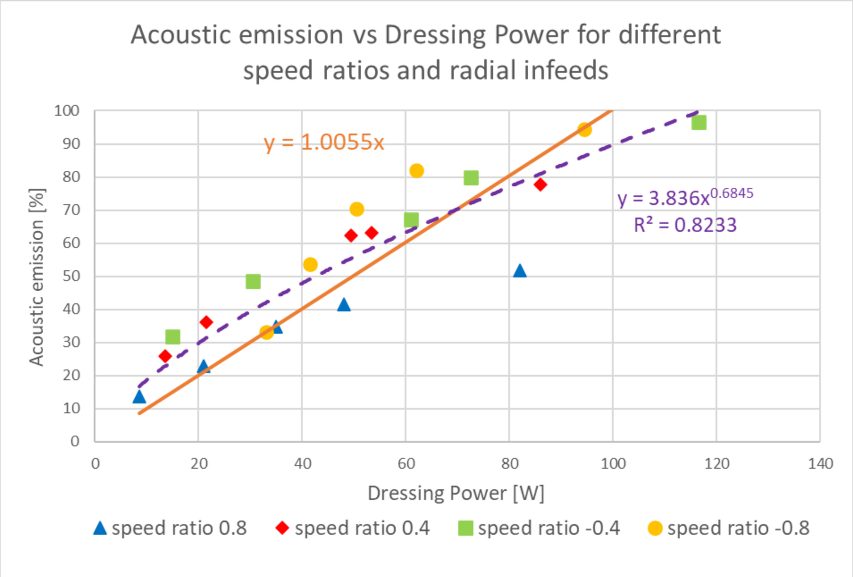

Figure 79: Acoustic emission is plotted against dressing power for different speed ratios – linear trendline with zero as intercept and power law trend

By means of the dressing Aggressiveness number, a similar plot to Figure 70 can be presented for dressing acoustic emission instead of dressing power versus dressing Aggressiveness number.
Therefore, in Figure 80 linear trends with acoustic emission 0% as intercept, for different speed ratios, are shown.

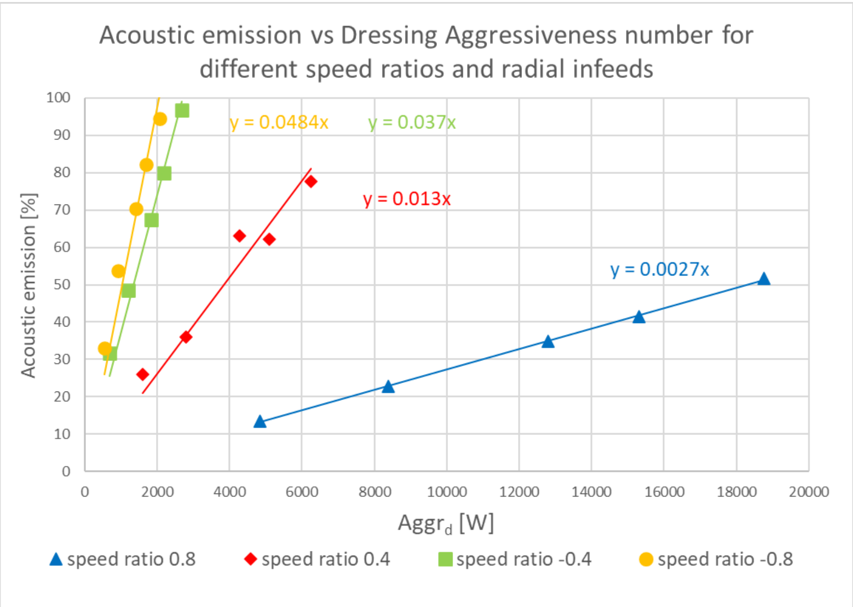

Figure 80: Acoustic emission is plotted against the dressing Aggressiveness number for different speed ratios - linear trend for each case with 0% as intercept

From Figure 80 it can be noticed as the slopes result very similar to the ones coming from the plot for dressing power vs dressing Aggressiveness number (Figure 70).

In addition, in the next figure it is proposed the dressing specific energy plotted against the acoustic emission specific energy. A linear trendline can be recognized with an intercept value of 0.0999. Therefore, the chart in Figure 81 shows that the dressing specific energy and the acoustic emission specific energy are proportional. Furthermore, in the same Figure a power law trend is proposed and chosen as the best fitting curve since the R^2 value is proven to be higher. Nevertheless, the linear trend is still a possible choice for easier understanding.

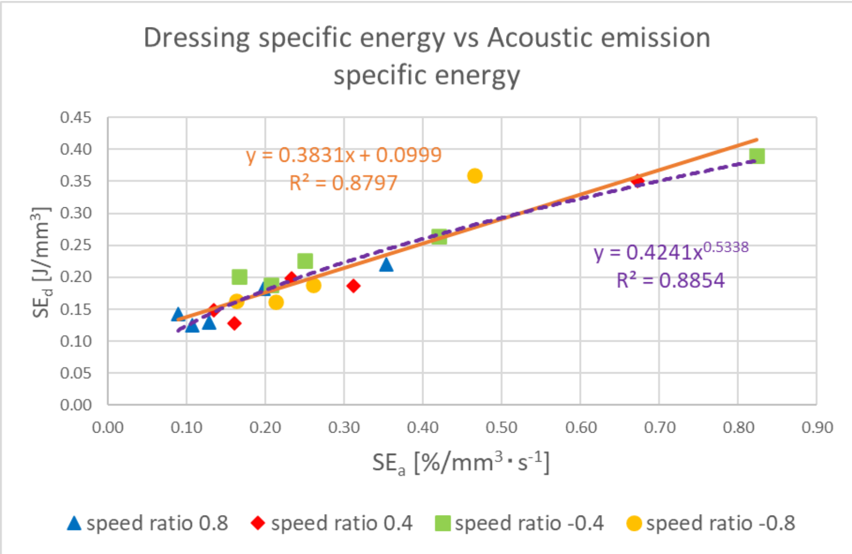

Figure 81: Dressing specific energy is plotted against the acoustic emission specific energy for different speed ratios – linear trend and power law trend

In addition, in Figure 82 there is a plot for grinding specific energy vs acoustic emission specific energy. A power law is fitting properly the data as well as a linear trend, that is convenient for simplified analysis.

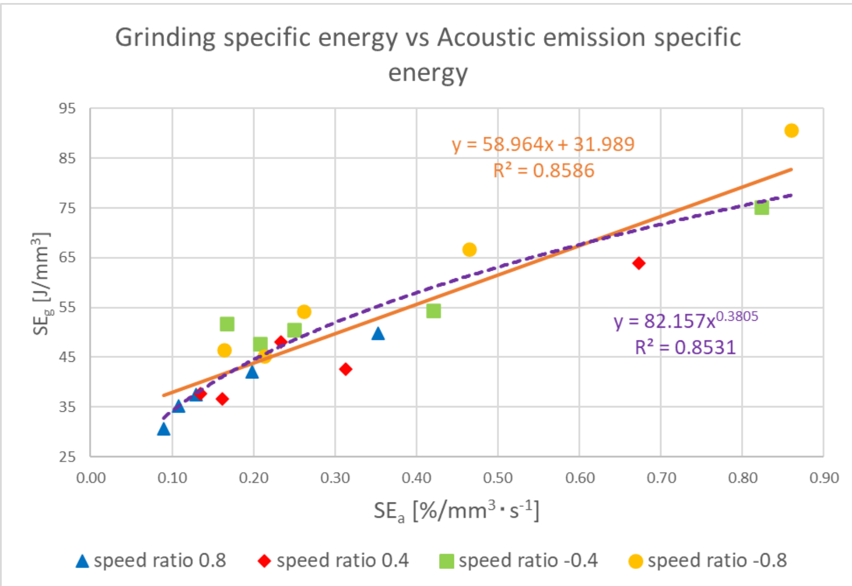

Figure 82: Grinding specific energy is plotted against the acoustic emission specific energy for different speed ratios - a power law trend and linear trend can be identified

In Figure 83, it is displayed a plot including acoustic emission specific energy and dressing specific energy in the same chart, plotted versus dressing Aggressiveness number.

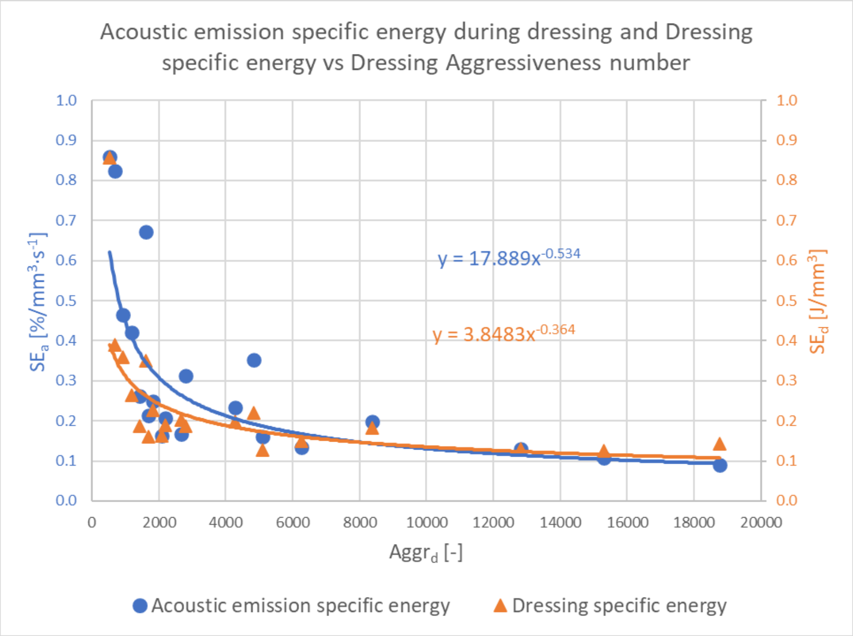

Figure 83: Acoustic emission specific energy and dressing specific energy are plotted against the dressing Aggressiveness number

Finally, there are plots for dressing roll power during dressing, grinding wheel power during dressing and acoustic emission value during dressing vs time. In Figure 84 and in Figure 85, examples for unidirectional dressing and anti-directional dressing are shown. It can be seen that acoustic emission and dressing power have the same behaviour, thus acoustic emission could be used instead of dressing power for the same analyses.

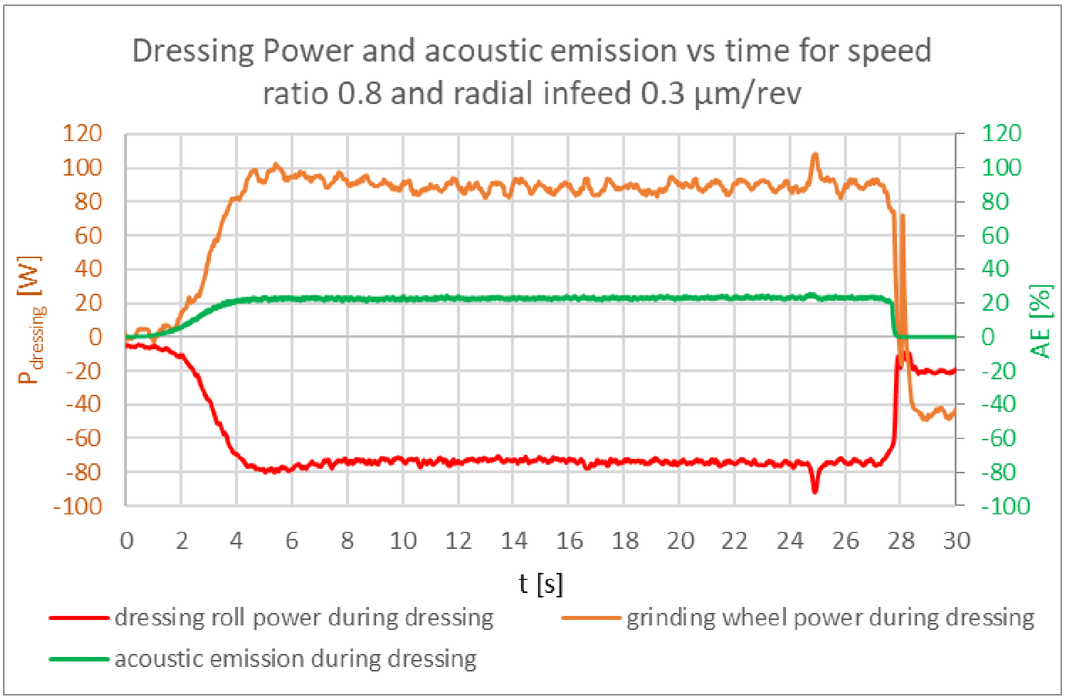

Figure 84: Dressing power and acoustic emission are plotted against the time for speed ratio 0.8 and radial infeed 0.3 µm/rev

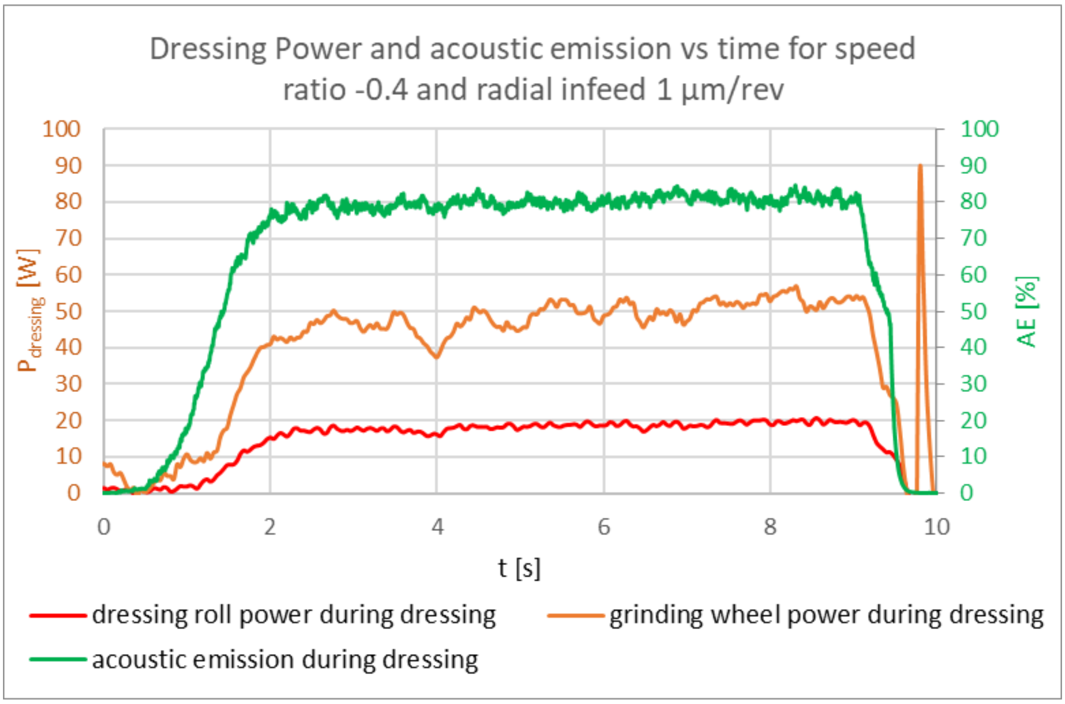

Figure 85: Dressing power and acoustic emission are plotted against the time for speed ratio -0.4 and radial infeed 1 µm/rev

9.1.4 Tangential forces, normal forces, grinding wheel spindle displacement

In an effort to calculate tangential forces during dressing, the total dressing power has been considered and divided by a Δspeed, defined based on dressing mode (unidirectional with minus in the following equation and anti-directional with plus).

It would have been possible to consider the amount of dressing power generated in the grinding wheel during the dressing operation, and divide it by the grinding wheel speed, obtaining again a tangential force.

The first mentioned definition has been preferred because data are coming from both spindles, and therefore the method results more robust.

The used equation is (24):

$$F_{T_{dressing}} = \frac{P_{total_{dressing}}}{V_s \pm V_r} \; [N] \tag{24}$$

In the following there is a table showing all different tangential forces, normal forces and grinding wheel spindle deflections during the dressing operation.

The wheel speed as mentioned is 30m/s and the grinding wheel spindle stiffness is K=30000N/mm.

The normal force is calculated through (25):

$$F_{N_{dressing}} = 1.5 \cdot F_{T_{dressing}} \; [N] \tag{25}$$

With the ratio between normal dressing force and tangential dressing force defined as stated by Barbara Linke in [16].

Basically, in this paper it is proven that this ratio is varying between 1.35 and 5, depending on the speed ratio, and it is equals to 1.5 for most of the cases.

The grinding wheel spindle displacement is gotten from (26):

$$h = \frac{F_{N_{dressing}}}{K} \cdot 1000 \; [\mu m] \tag{26}$$

speed ratio [-]	radial infeed [µm/rev]	P total dressing [W]	F_T[N]	F_N[N]	grinding wheel spindle displacement during dressing [µm]
0.8	0.1	8.5	1.42	2.13	0.071
0.8	0.3	21.0	3.50	5.25	0.175
0.8	0.7	35.0	5.83	8.75	0.292
0.8	1.0	48.0	8.00	12.00	0.400
0.8	1.5	82.0	13.67	20.50	0.683
0.4	0.1	13.5	0.75	1.13	0.038
0.4	0.3	21.5	1.19	1.79	0.060
0.4	0.7	53.5	2.97	4.46	0.149
0.4	1.0	49.5	2.75	4.13	0.138
0.4	1.5	86.0	4.78	7.17	0.239
-0.4	0.1	15.0	0.36	0.54	0.018
-0.4	0.3	30.5	0.73	1.09	0.036
-0.4	0.7	61.0	1.45	2.18	0.073
-0.4	1.0	72.5	1.73	2.59	0.086
-0.4	1.5	116.5	2.77	4.16	0.139
-0.8	0.1	33.0	0.61	0.92	0.031
-0.8	0.3	41.5	0.77	1.15	0.038
-0.8	0.7	50.5	0.94	1.40	0.047
-0.8	1.0	62.0	1.15	1.72	0.057
-0.8	1.5	94.5	1.75	2.63	0.088

Once knowing the normal forces, plots for absolute acoustic emission decrease, relative acoustic emission decrease and acoustic emission slope (defined respectively with (27), (28), (29)) vs normal force during dressing, are displayed in Figure 86-Figure 90.

$$Absolute\ AE\ decrease = AE\ before\ dwelling\ starts - AE\ end\ of\ dwelling\ [\%] \tag{27}$$

$$Relative\ AE\ decrease = \frac{AE\ before\ dwelling\ starts - AE\ end\ of\ dwelling}{AE\ before\ dwelling\ starts} \cdot 100\ [\%] \tag{28}$$

$$AE\ slope = \frac{AE\ before\ dwelling\ starts - AE\ end\ of\ dwelling}{considered\ \Delta t} \left[\frac{\%}{s}\right] \tag{29}$$

The data points in the next plots are taken from the table below.

speed ratio [-]	radial infeed [µm/rev]	$Aggr_d$ [-]	considered Δt [s]	absolute decrease [%]	slope [%/s]	relative decrease [%]	F_N[N]
0.8	0.1	4841	0.412	1.34	3.26	8.25	2.13
0.8	0.3	8386	0.392	2.93	7.47	11.57	5.25
0.8	0.7	12809	0.364	10.31	28.33	28.33	8.75
0.8	1	15310	0.416	14.38	34.57	33.64	12.00
0.8	1.5	18751	0.368	19.57	53.17	37.69	20.50
0.4	0.1	1614	0.400	3.45	8.63	11.82	1.13
0.4	0.3	2795	0.420	7.48	17.81	18.88	1.79
0.4	0.7	4270	0.312	20.30	65.06	32.71	4.46
0.4	1	5103	0.364	22.74	62.47	34.12	4.13
0.4	1.5	6250	0.368	32.18	87.45	41.54	7.17
-0.4	0.1	692	0.272	7.08	26.03	18.94	0.54
-0.4	0.3	1198	0.344	13.33	38.75	25.27	1.09
-0.4	0.7	1830	0.352	26.20	74.43	34.19	2.18
-0.4	1	2187	0.372	35.28	94.84	41.89	2.59
-0.4	1.5	2679	0.336	43.78	130.30	45.53	4.16
-0.8	0.1	538	0.388	7.69	19.82	19.12	0.92
-0.8	0.3	932	0.352	14.47	41.11	23.71	1.15
-0.8	0.7	1423	0.368	31.34	85.16	40.23	1.40
-0.8	1	1701	0.380	36.52	96.11	41.08	1.72
-0.8	1.5	2083	0.404	45.12	111.68	46.16	2.63

For AE absolute decrease against normal force (Figure 86), for each speed ratio a linear trend is visible, and moreover the intercepts are all close to zero as expected.

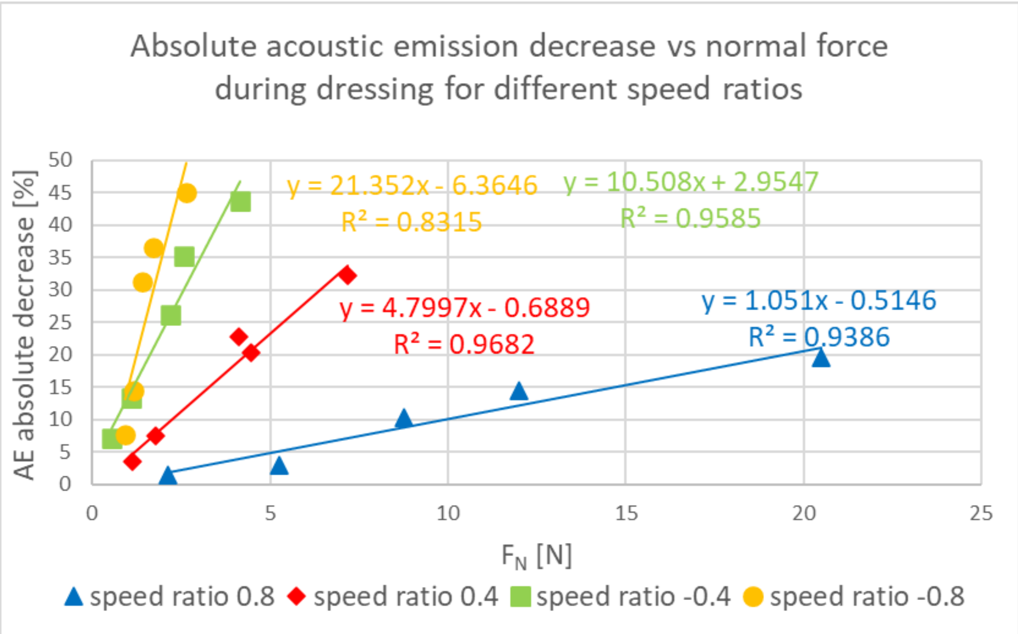

Figure 86: Absolute acoustic emission decrease is plotted against the normal force during dressing for different speed ratio - linear trend for each speed ratio

By reporting AE absolute decrease versus F_N for different speed ratios and imposing as 0% the intercept on the acoustic emission axis, Figure 87 is proving that for lower speed ratios (thus duller conditions in general), the line slope in the plot has higher value.

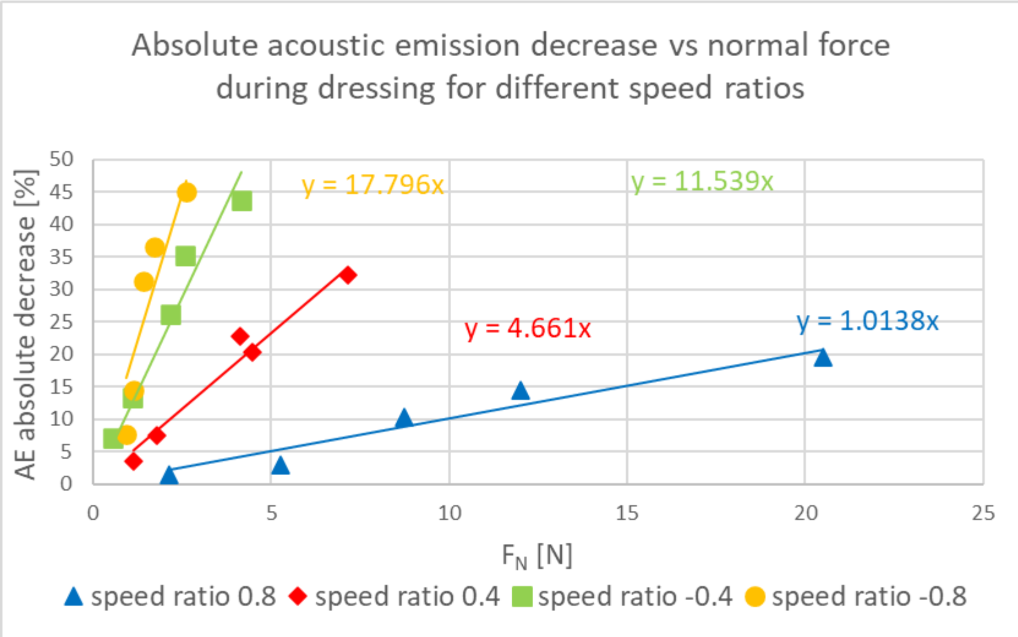

Figure 87: Absolute acoustic emission decrease is plotted against the normal force during dressing for different speed ratios - linear trends for each speed ratio and intercepts set at 0%

For AE relative decrease, for each speed ratio a power law trend is recognized (Figure 88):

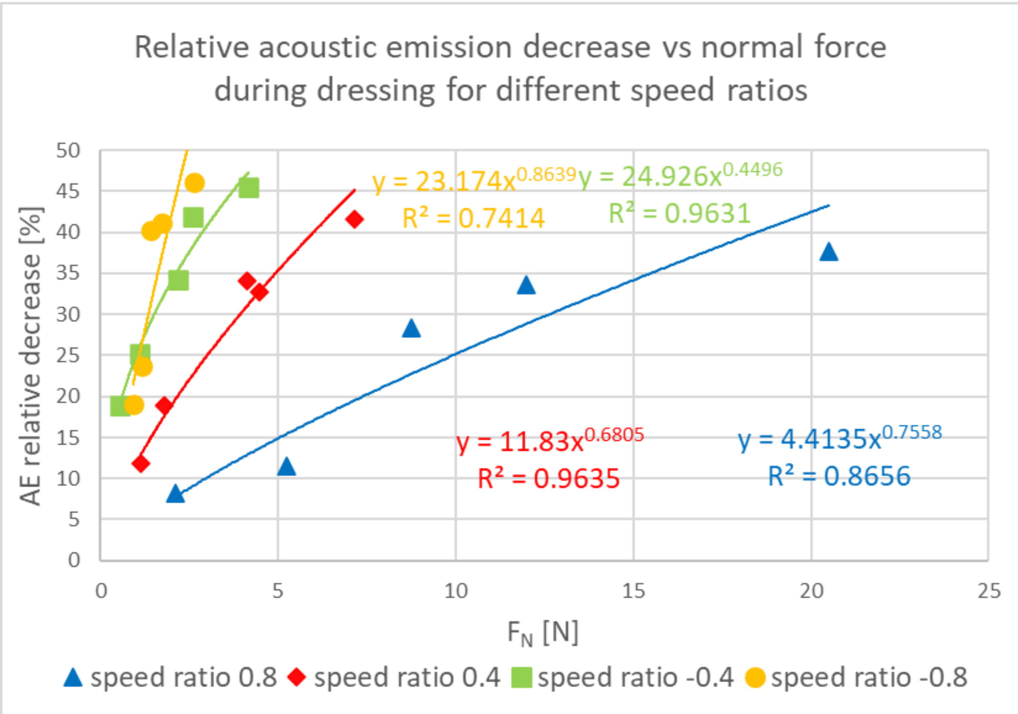

Figure 88: Relative acoustic emission decrease is plotted against the normal force during dressing for different speed ratios - power law trend for each speed ratio

For AE slope for each speed ratio a linear trend is evident, and furthermore the intercepts are all close to zero (Figure 89):

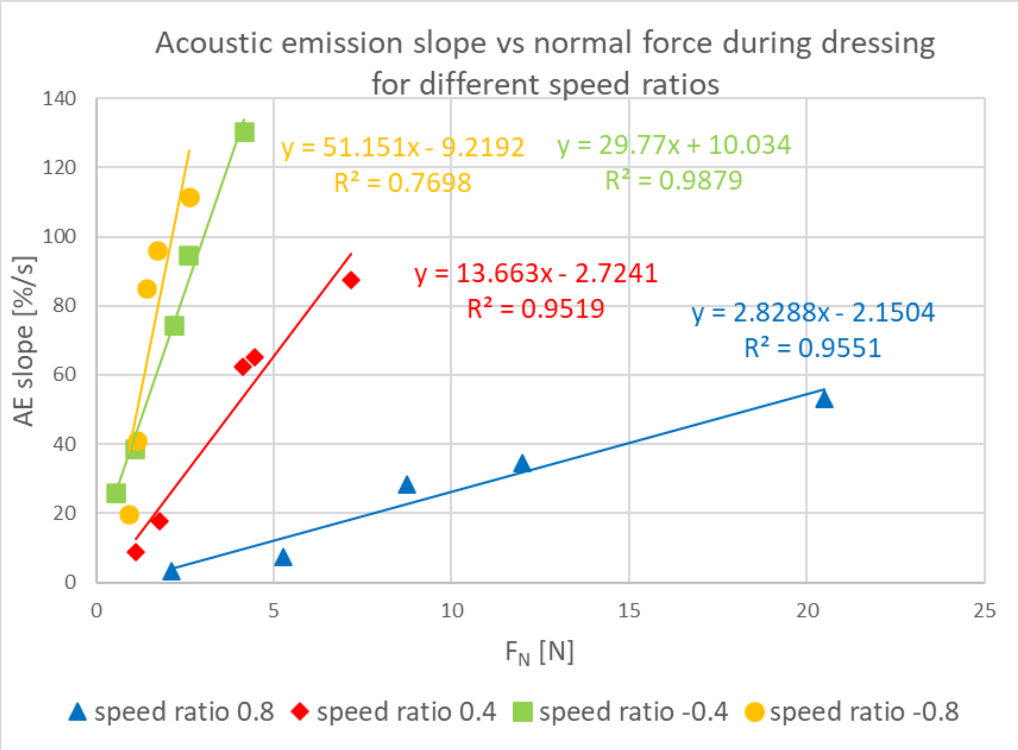

Figure 89: Acoustic emission slope is plotted against the normal force during dressing for different speed ratios - linear trend for each speed ratio

In Figure 90, given the previous statement, plots for the same variables as in Figure 89 are displayed and the intercept is set at 0%/s. As for Figure 87, higher slopes are associated to lower speed ratios.

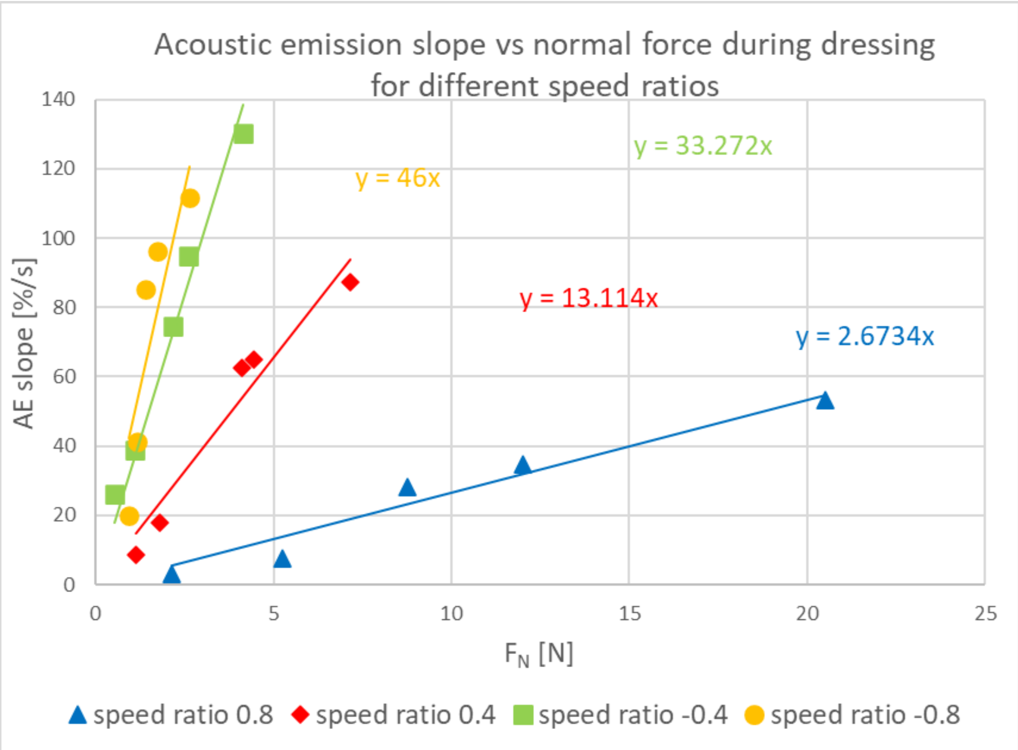

Figure 90: Acoustic emission slope is plotted against the normal force during dressing for different speed ratios - linear trend for each speed ratio and intercepts set at 0 %/s

9.2 Different dressing and grinding conditions effects on grinding specific energy (SE_g)

The following tests have been run by using four different grinding aggressiveness conditions and five different dressing conditions, for the total of 20 data points. The grinding parameters have been kept constant apart from varying the depth of cut per pass to differ grinding Aggressiveness.

In particular, the grinding parameters were:

- Workpiece feedrate: 50mm/s
- Number of passes for different depths of cut: 8 for 0.05mm, 10 for 0.025mm, 15 for 0.01mm and 20 for 0.005mm.

The grinding Aggressiveness number ([10]) for surface grinding is defined in the following equation (30):

$$Aggr_g = \sqrt{\frac{a_e}{d_{wheel}} \cdot \frac{v_{workpiece}}{v_{wheel}}} \; [-] \tag{30}$$

The parameters and results are summarized in the following table.

Speed ratio [-]	radial infeed [µm/rev]	$Aggr_d$ [-]	depth of cut per pass [mm]	$Aggr_g$ [-]	Grinding MRR [mm^3/s]	Grinding power [W]	SE_g [J/mm^3]
0.8	1	15370	0.05	19.63	32.08	912	28.43
0.8	1	15370	0.025	13.88	16.04	554	34.54
0.8	1	15370	0.01	8.78	6.42	308	48.01
0.8	1	15370	0.005	6.21	3.21	182	56.74
0.4	1	5123	0.05	19.64	32.08	1106	34.48
0.4	1	5123	0.025	13.89	16.04	612	38.16
0.4	1	5123	0.01	8.78	6.42	330	51.44
0.4	1	5123	0.005	6.21	3.21	253	78.88
-0.4	1	2195	0.05	19.65	32.08	1280	39.91
-0.4	1	2195	0.025	13.90	16.04	696	43.40
-0.4	1	2195	0.01	8.79	6.42	407	63.45
-0.4	1	2195	0.005	6.21	3.21	303	94.47
0.4	0.1	1620	0.05	19.66	32.08	1430	44.58
0.4	0.1	1620	0.025	13.90	16.04	761	47.45
0.4	0.1	1620	0.01	8.79	6.42	399	62.20
0.4	0.1	1620	0.005	6.22	3.21	292	91.04
-0.4	0.1	694	0.05	19.67	32.08	3208	100.02
-0.4	0.1	694	0.025	13.91	16.04	1132	70.58
-0.4	0.1	694	0.01	8.80	6.42	449	69.99
-0.4	0.1	694	0.005	6.22	3.21	284	88.54

The goal was to find out the behaviour of grinding specific energy plotted vs grinding Aggressiveness number. In Figure 91 there is a first image for representing how specific energy is varying going from sharper to duller condition. Clarifying, sorting from sharper to duller condition, there are:

1) speed ratio 0.8 and radial infeed 1 µm/rev;
2) speed ratio 0.4 and radial infeed 1 µm/rev;
3) speed ratio -0.4 and radial infeed 1 µm/rev;
4) speed ratio 0.4 and radial infeed 0.1 µm/rev;
5) speed ratio -0.4 and radial infeed 0.1 µm/rev.

Therefore, it is possible so state that duller conditions once again lead to higher heat generation and burning risk, especially associated with more aggressive grinding conditions.

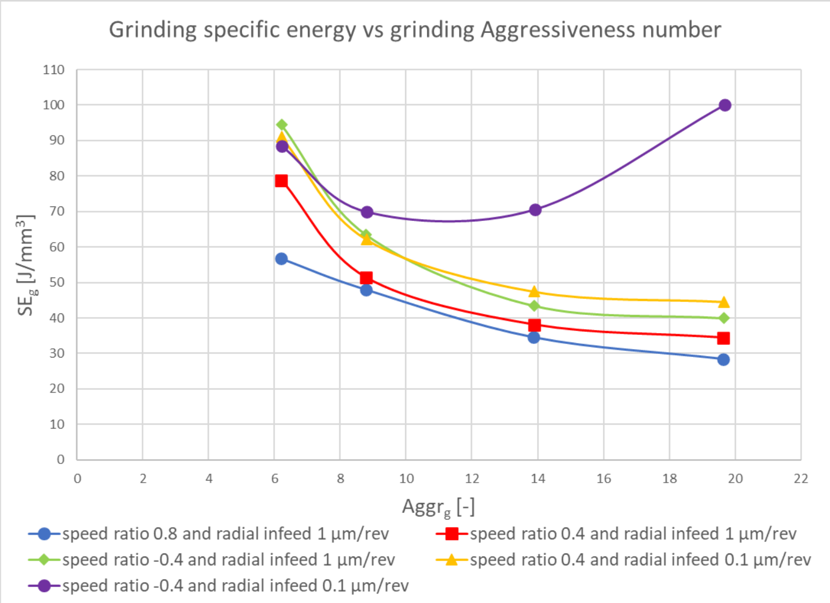

Figure 91: Grinding specific energy is plotted against grinding Aggressiveness number for different dressing parameters

For almost all dressing conditions, a power law trend can be recognized as shown in Figure 92.

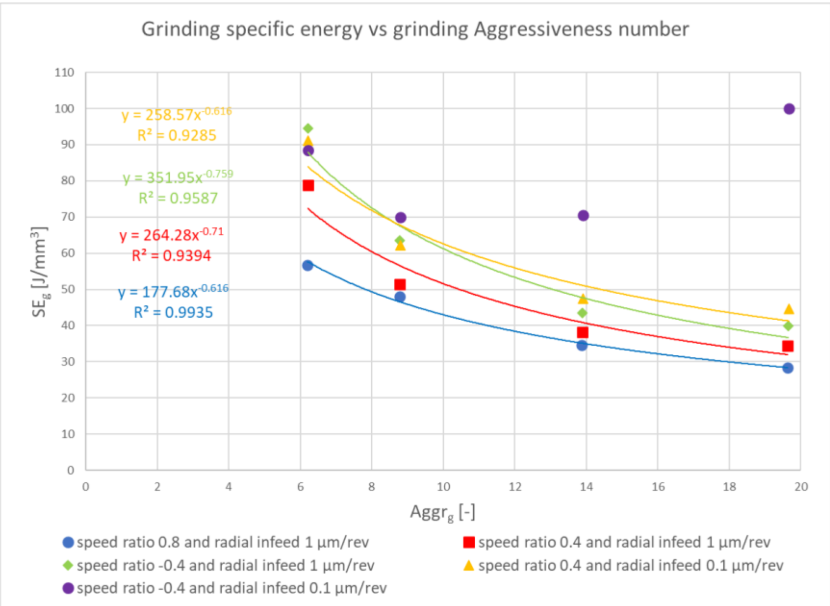

Figure 92: Grinding specific energy is plotted against grinding Aggressiveness number for different speed ratios and radial infeeds: power laws can be seen

For the dullest dressing condition combined with the two most aggressive grinding conditions (larger depths of cut: 0.025mm and 0.05mm), burning has been detected as can be seen in Figure 93, hence no trend is reported for this case (purple data points).

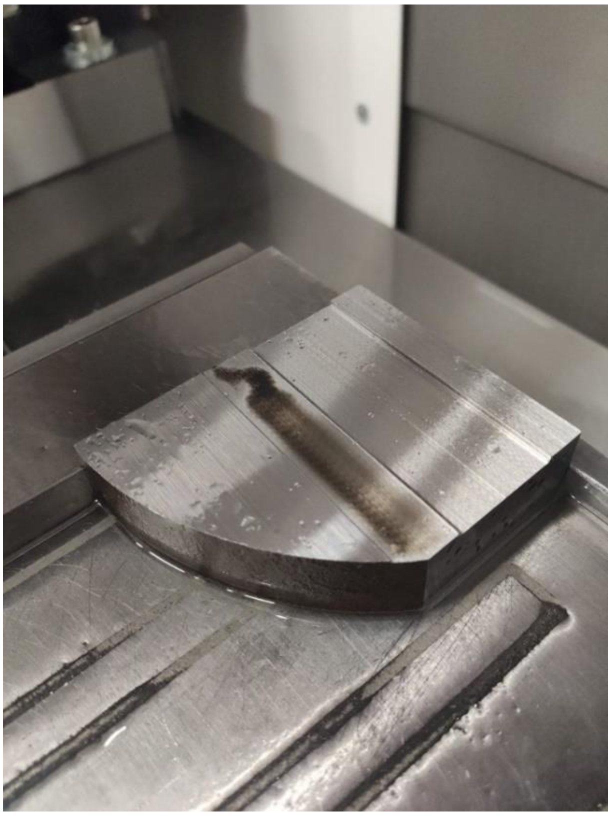

Figure 93: Burning occurred for the dullest dressing condition combined with the most aggressive grinding condition in this case (left track)

9.3 Dwell time effect on dressing acoustic emission signal

New tests have been run by performing a sharp and a dull dressing condition, respectively +0.8 as speed ratio and 1 µm/rev as radial infeed, and -0.8 as speed ratio and 0.1µm/rev as radial infeed. Six data points have been collected by using 3 different dwell times for each dressing condition; in particular: 0, 10 and 100 dwell revolutions of grinding wheel.

In Figure 94 and Figure 95, plots are displayed showing a comparison for each dressing condition.

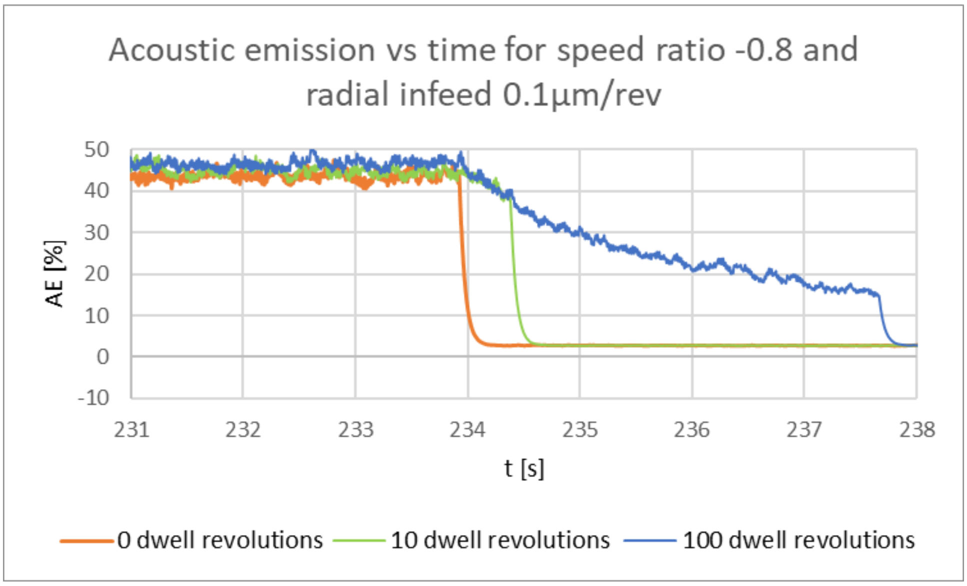

Figure 94: Acoustic emission is plotted against time for speed ratio -0.8 and radial infeed 0.1 µm/rev with 0, 10 and 100 dwell revolutions

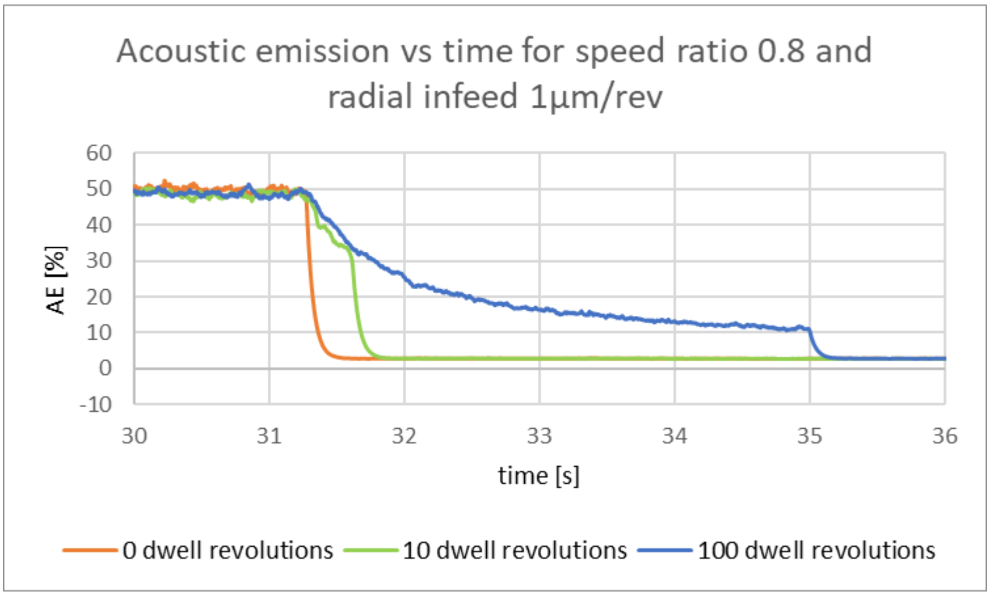

Figure 95: Acoustic emission is plotted against time for speed ratio 0.8 and radial infeed 1 µm/rev with 0, 10 and 100 dwell revolutions

10. Scanning electron microscope (SEM) analysis

Scanning electron microscope (SEM) analysis has been carried out to analyse the topography of the grinding wheel surface: the grinding wheel step has been dressed with speed ratio 0.8 and 1 μm/rev of radial infeed on one half, and for speed ratio -0.8 and 0.1 μm/rev of radial infeed on the other half. Furthermore, the step, 12.83 mm wide, has been ground in the central part for a width of 6.415 mm, with the aim of analysing and identifying differences between the ground and not ground regions processed with different parameters. Hence, overall, four different conditions can be identified: dull dressing, dull dressing + grinding, sharp dressing + grinding, sharp dressing. These regions are indicated in Figure 99, Figure 100.

10.1 SEM analysis setup

With the purpose of getting a sample small enough to fit in the scanning electron microscope, a chunk of the grinding wheel step has been broken away with a hammer. The sample has been coated with a thin gold layer in order to proceed with the analysis properly, since made of Aluminum oxide, a ceramic material therefore non-conductive material. Without applying the coating, it would have been challenging to obtain relevant and clear SEM images, considering that an accumulation of charge (electrons) would have occurred and it would have disturbed the detection of secondary electrons.
The interaction between the electrons of the beam and the atoms of the sample describes a volume of interaction that is gradually larger with increasing beam voltage. For the SEM analysis two different types of electrons have been used:

- secondary electrons, which are the electrons linked to the outermost atomic levels; they are emitted with an energy between 0 and 50 eV.
- Backscattered electrons, reflected with an energy ranging from 50 eV up to incidence energy.

The first are used for studying surface morphology of the samples, instead the latter are carrier mainly of topographical signals.

In the next image (Figure 96) the SEM station (Philips XL30 ESEM) at Chalmers is shown, and in the screen in the middle it is possible to see SE, BSE images and moreover an internal camera useful for checking the specimen position. Different holders have been used with the purpose of facilitating the view with high tilt angles.
Contrast and brightness have been adjusted time by time to have the best possible image.
Different magnifications will be presented, and the high tension has been set to 20kV.

Figure 96: Chalmers scanning electron microscope

10.2 SEM analysis images

In the following there are reported the most relevant SEM images of the sample.

In Figure 97, it is shown a comparison between the dull and sharp parts of the grinding wheel step. As expected, the part of the wheel dressed with speed ratio -0.8 and 0.1 µm/rev of radial infeed (on the left) exhibits a quite flat surface overall; instead the other side dressed with speed ratio 0.8 and 1 µm/rev of radial infeed (on the right) reveals an irregular and sharp surface.

In addition, by looking at the red circles it can be noticed that in the left SEM image (dull condition) there are more flat surfaces areas than in the SEM image on the right (sharp condition), for the same considered mm^2.

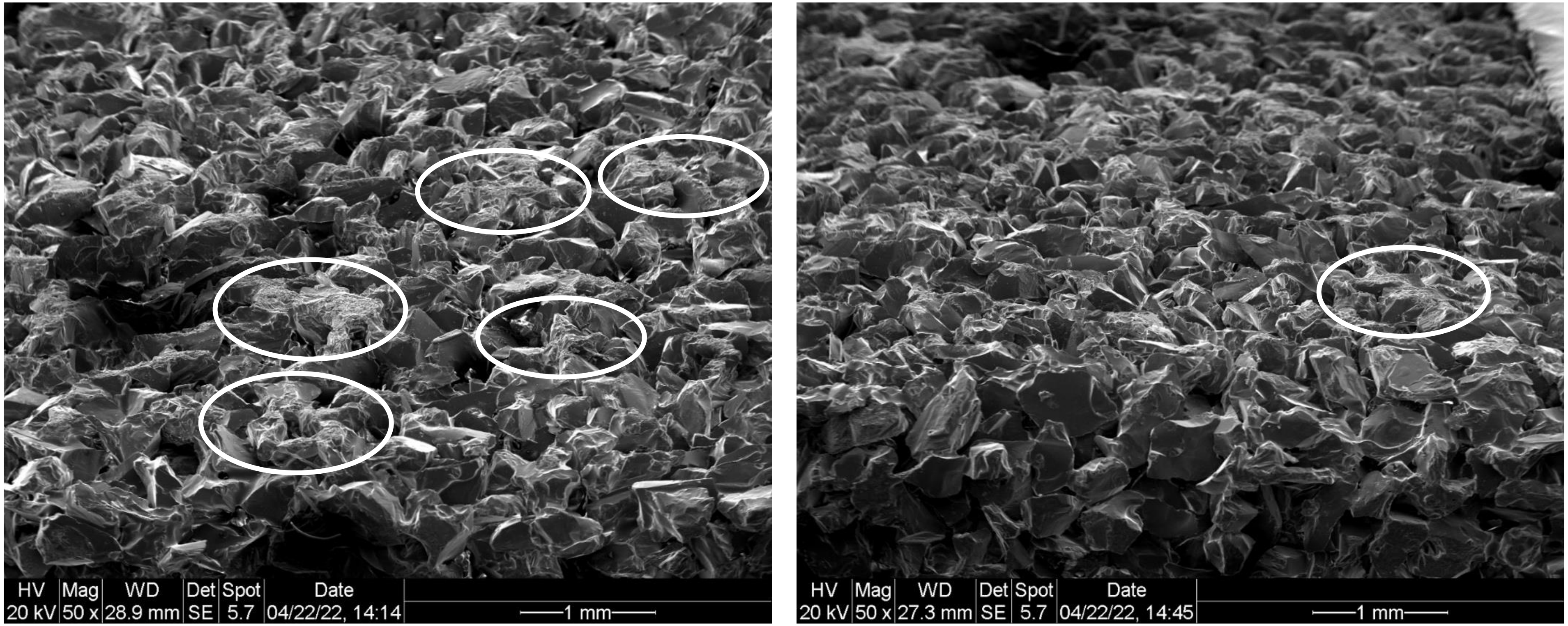

Figure 97: Comparison between the dull (on the left) and sharp (on the right) regions of the grinding wheel step (low tilt angle)

In Figure 98 a significant zoom of Figure 97 is presented to better exhibit the dull and sharp areas of the grinding wheel step dressed with different conditions.

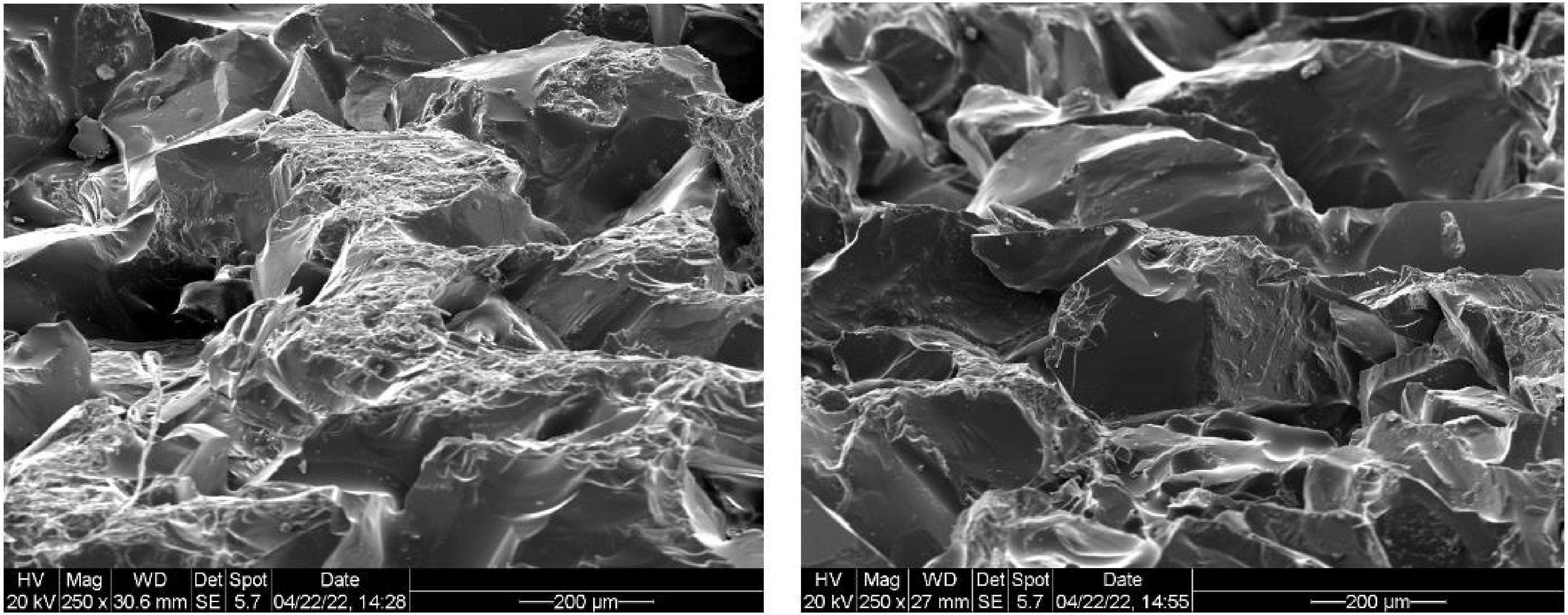

Figure 98: Comparison between dull (on the left) and sharp (on the right) regions of the grinding wheel step with high magnification

The differences between the regions of the grinding wheel step can be seen in Figure 99, in which the dressed and dressed-ground parts are defined and distinguished, taking into account an overview of the sample with a high tilt angle. Figure 100 shows the same image with 90° observing angle. In these pictures the steel presence on the ground part can be recognized by means of backscattered electrons, in particular in the second one it is clear as for duller dressing condition, the steel presence (material loading) will be larger, thus the heat generation as well.

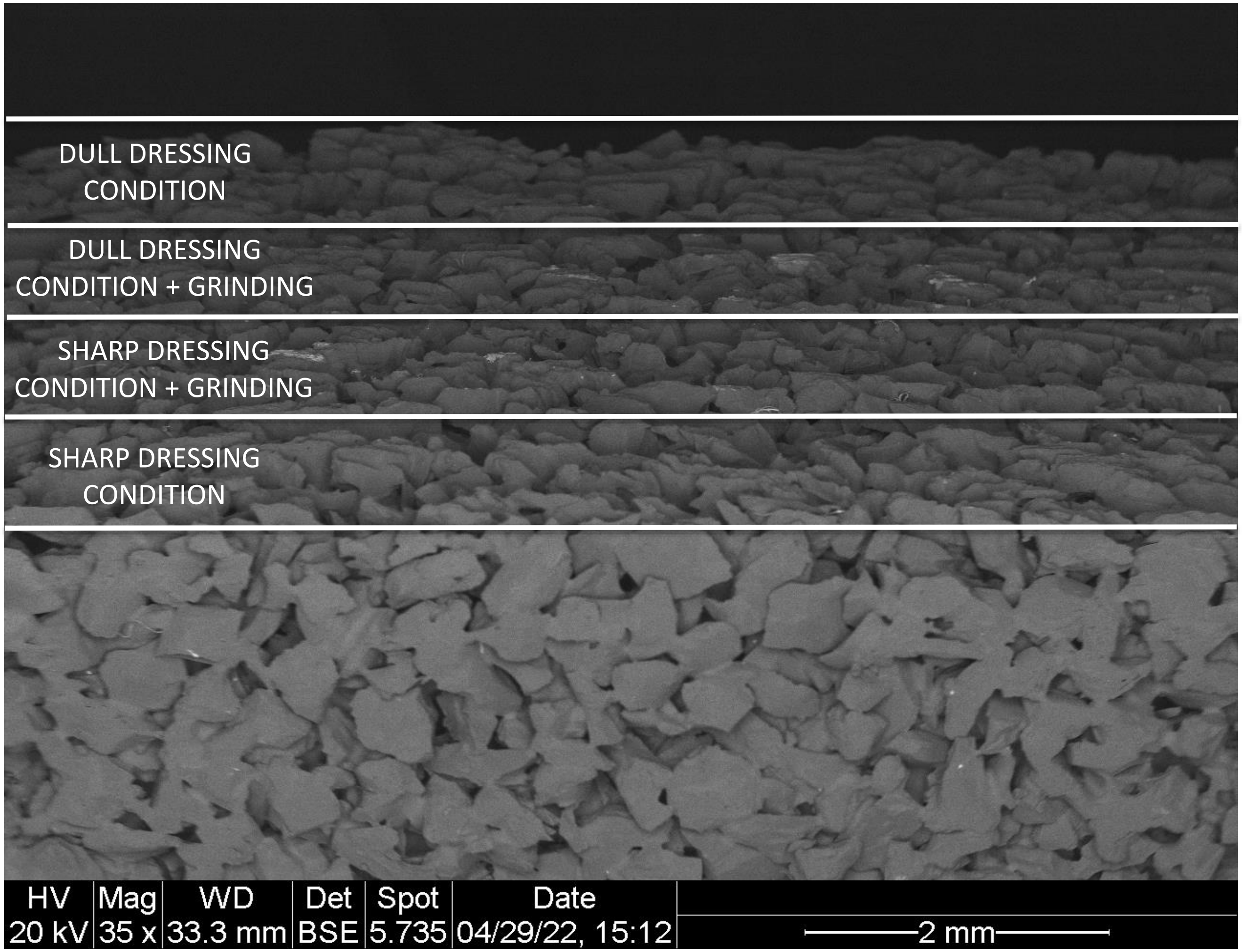

Figure 99: Distinction of the 4 sections of the grinding wheel step – sharp dressing condition, sharp condition + grinding, dull dressing condition + grinding, dull dressing condition

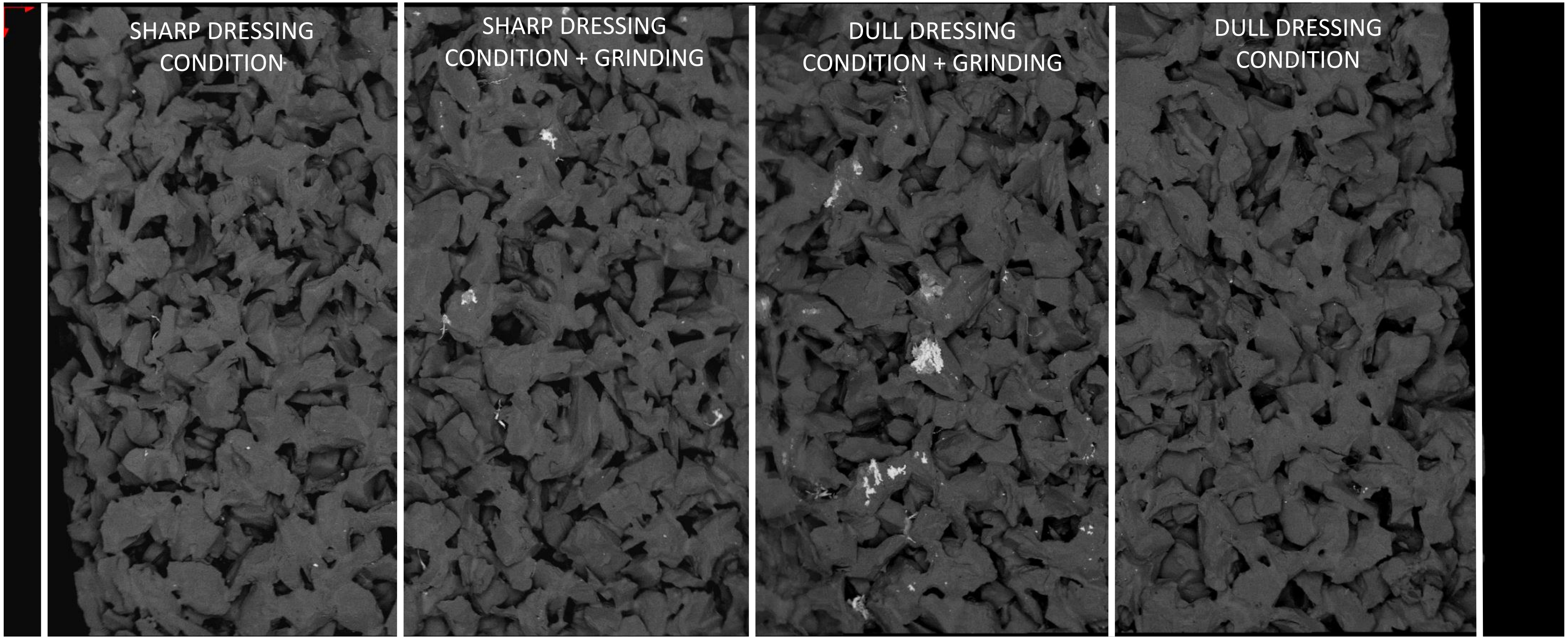

Figure 100: Distinction of the 4 sections of the grinding wheel step using 90° observing angle – sharp dressing condition, sharp condition + grinding, dull dressing condition + grinding, dull dressing condition

In the next pages, several SEM images (obtained with high tilt angle) of the dull and sharp parts of the grinding wheel step are reported, showing furthermore for both conditions the areas in which steel is present with a larger magnification and reporting a comparison between BSE and SE of each zoom area as well (proceeding from left to right BSE and then SE).

In Figure 101, the sharp part of the sample is shown with high tilt angle, and in Figure 102 - Figure 106 the zoomed areas showing steel presence are proposed.

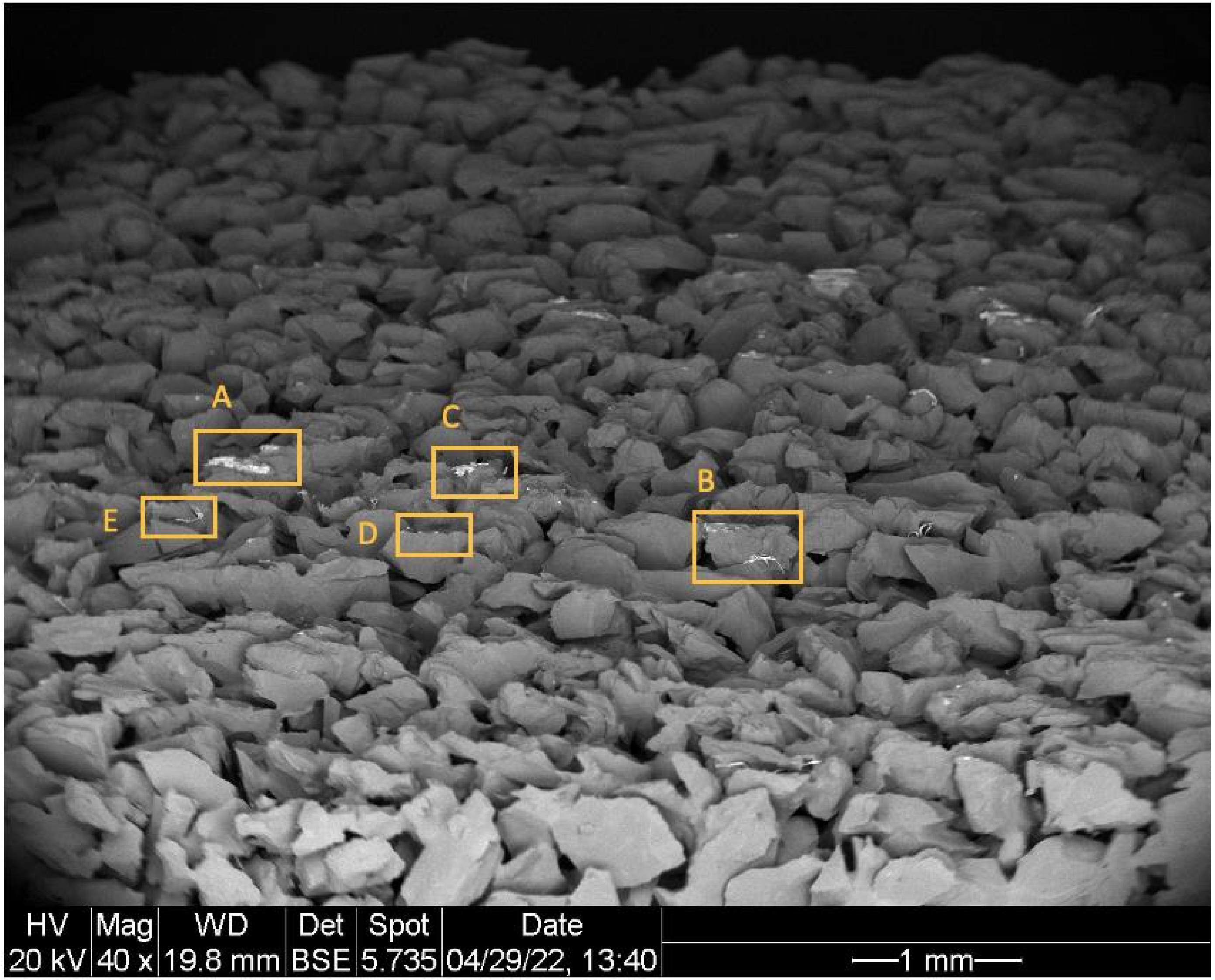

Figure 101: Sharp part of the grinding wheel step (high tilt angle)

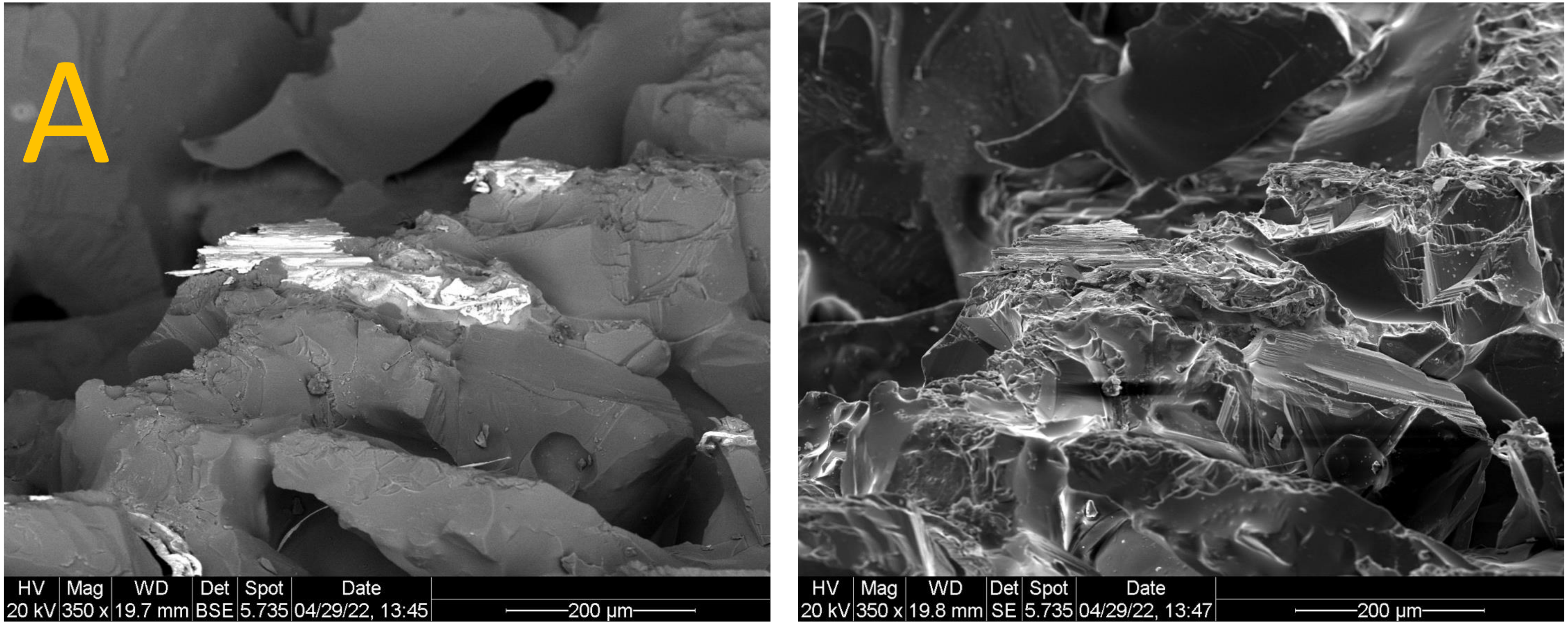

Figure 102: Zoom sharp part rectangle A - comparison BSE and SE

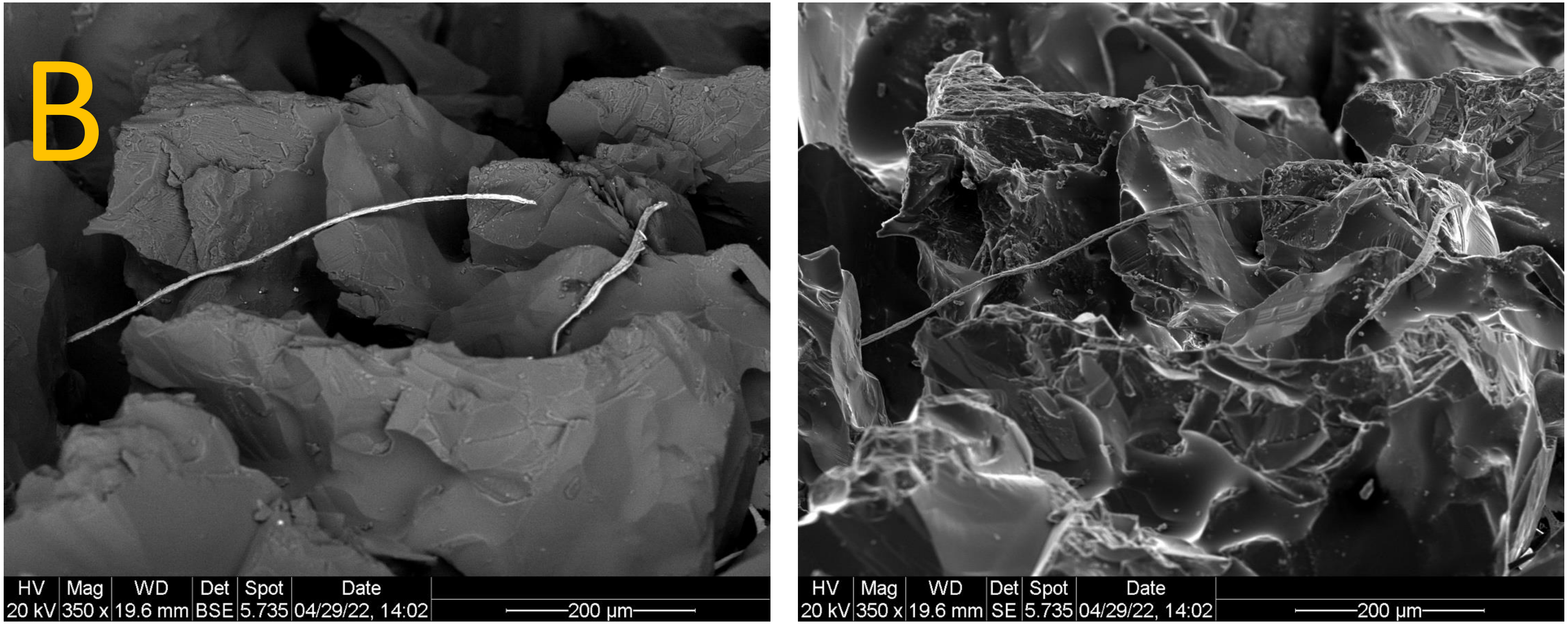

Figure 103: Zoom sharp part rectangle B - comparison BSE and SE

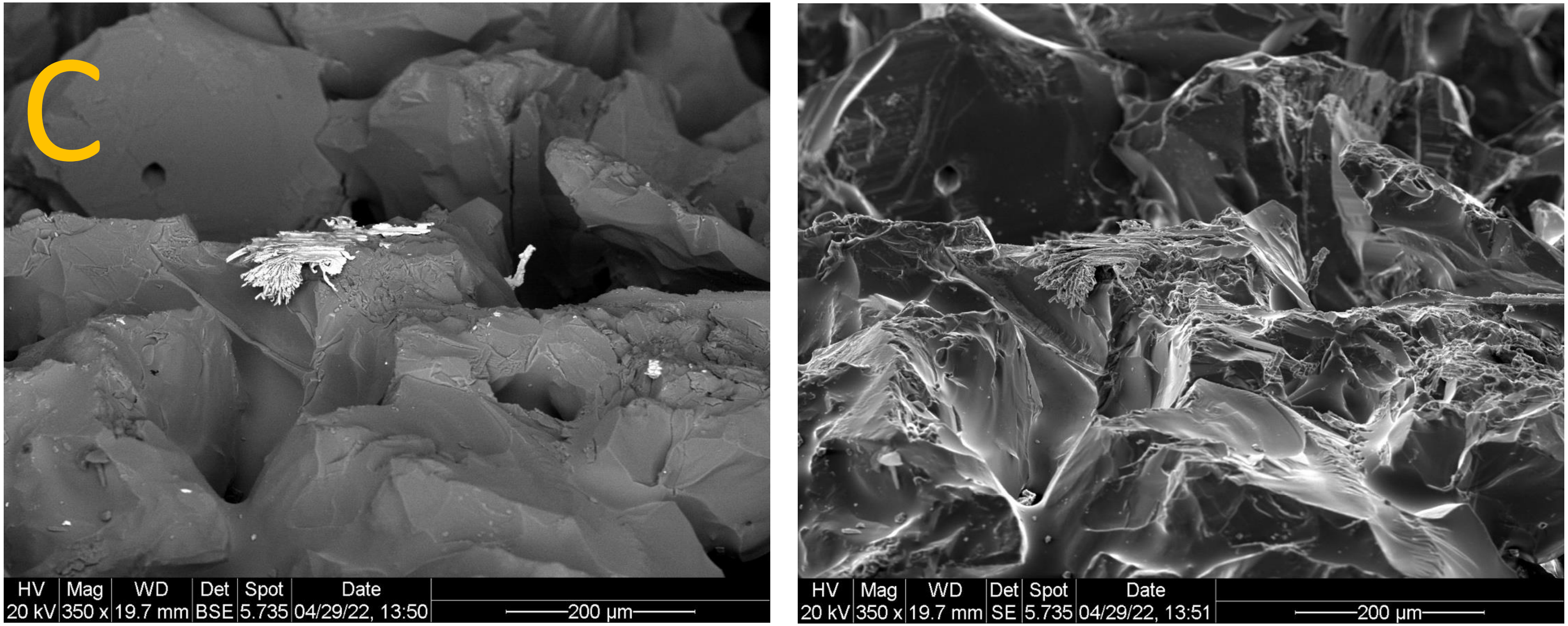

Figure 104: Zoom sharp part rectangle C - comparison BSE and SE

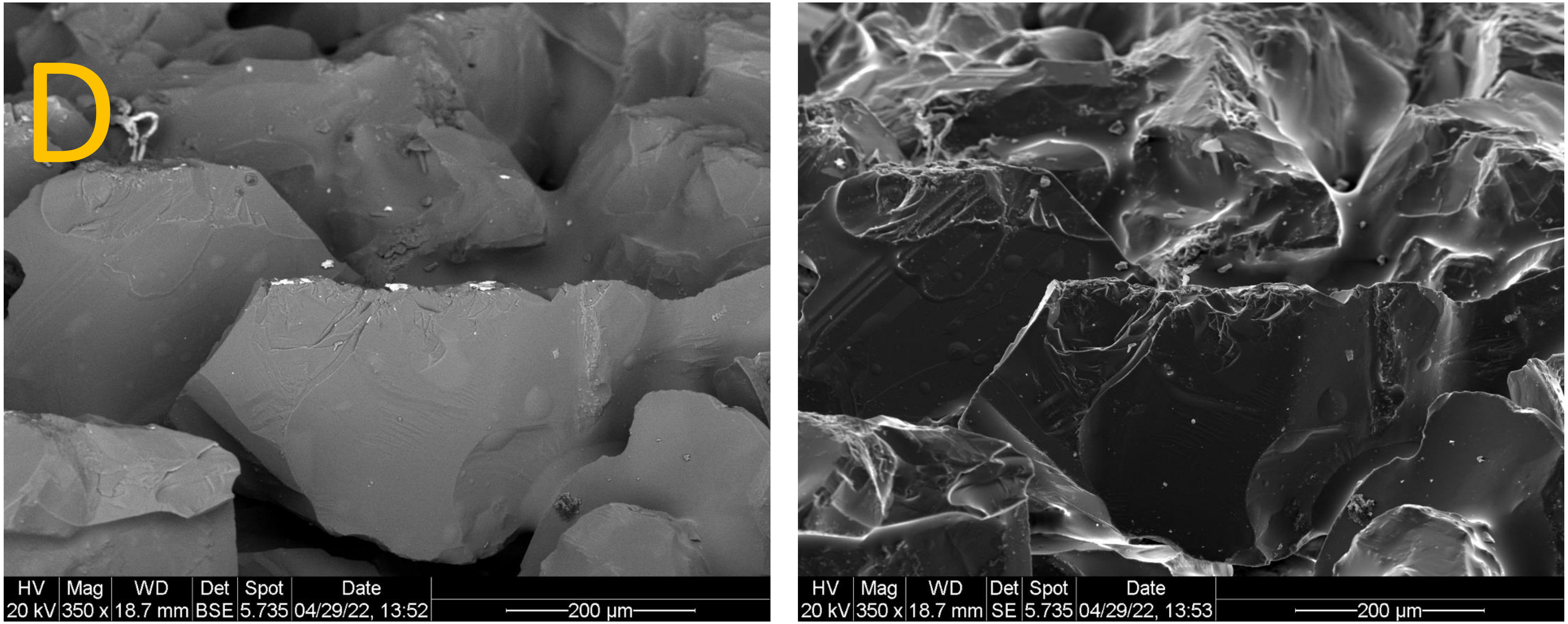

Figure 105: Zoom sharp part rectangle D - comparison BSE and SE

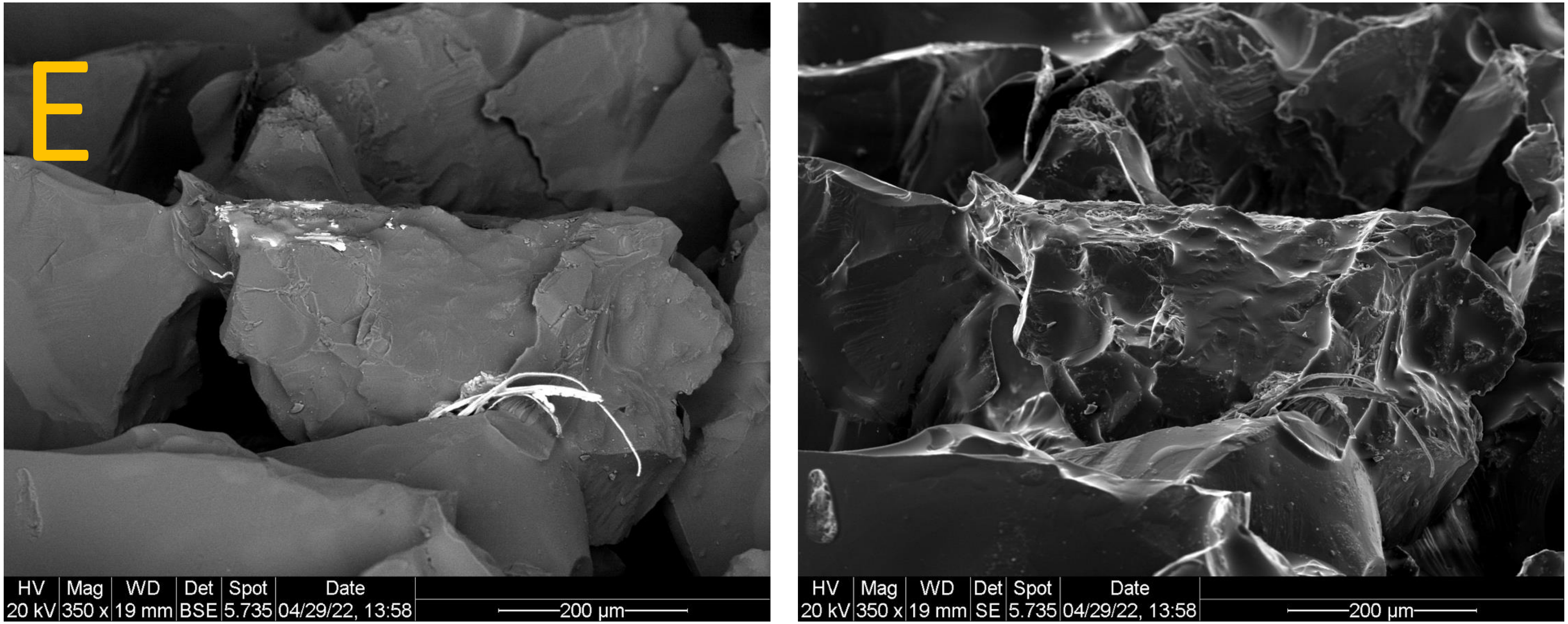

Figure 106: Zoom sharp part rectangle E - comparison BSE and SE

In Figure 107 there is a zoom of the sharp dressing condition of the step taken with high tilt angle, which shows the differences between BSE and SE of a very irregular grains area.

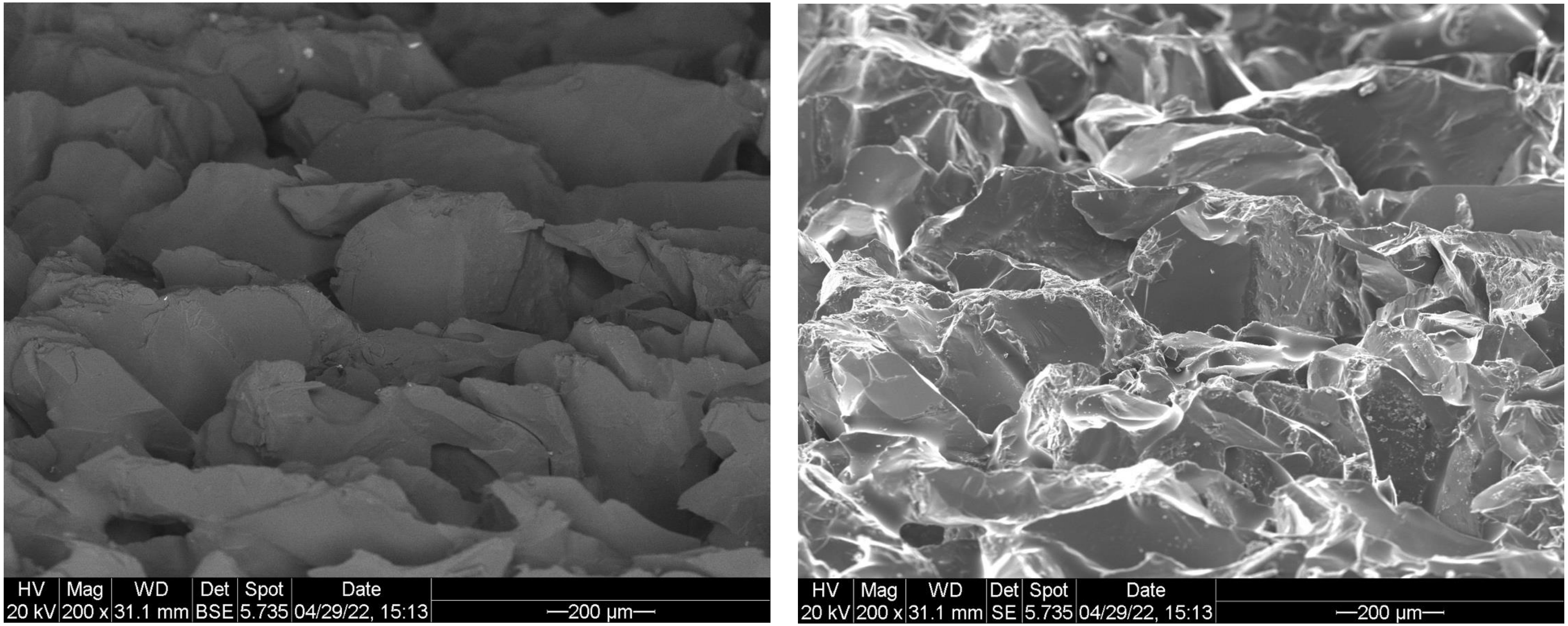

Figure 107: Very irregular grains area, sharp part of the grinding wheel step - comparison BSE and SE

In Figure 108, a picture of the dull dressing condition of the sample got with high tilt angle is presented, and in the figures below (Figure 109 - Figure 113), the zoomed areas revealing steel presence are shown as well.

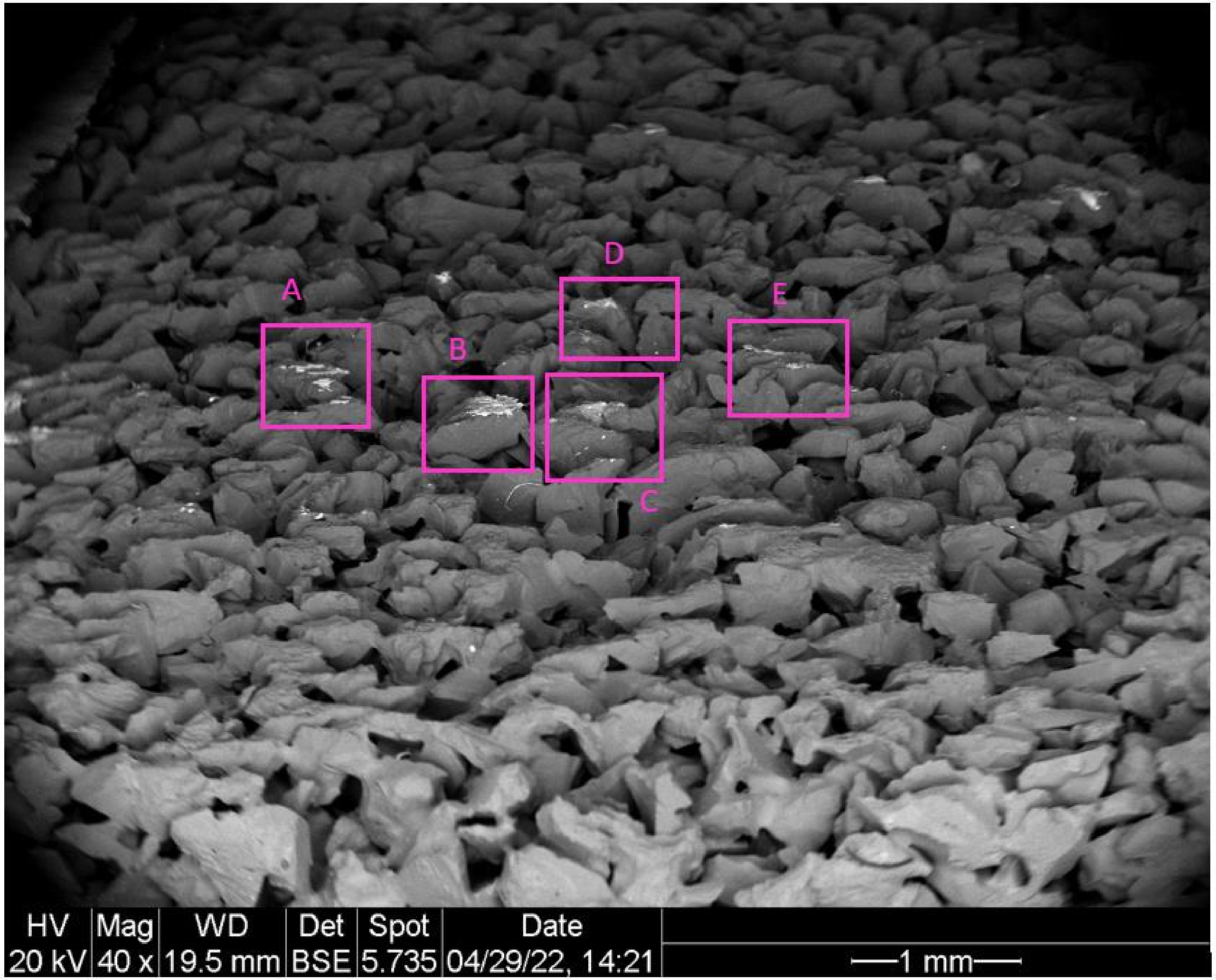

Figure 108: Dull part of the grinding wheel step (high tilt angle)

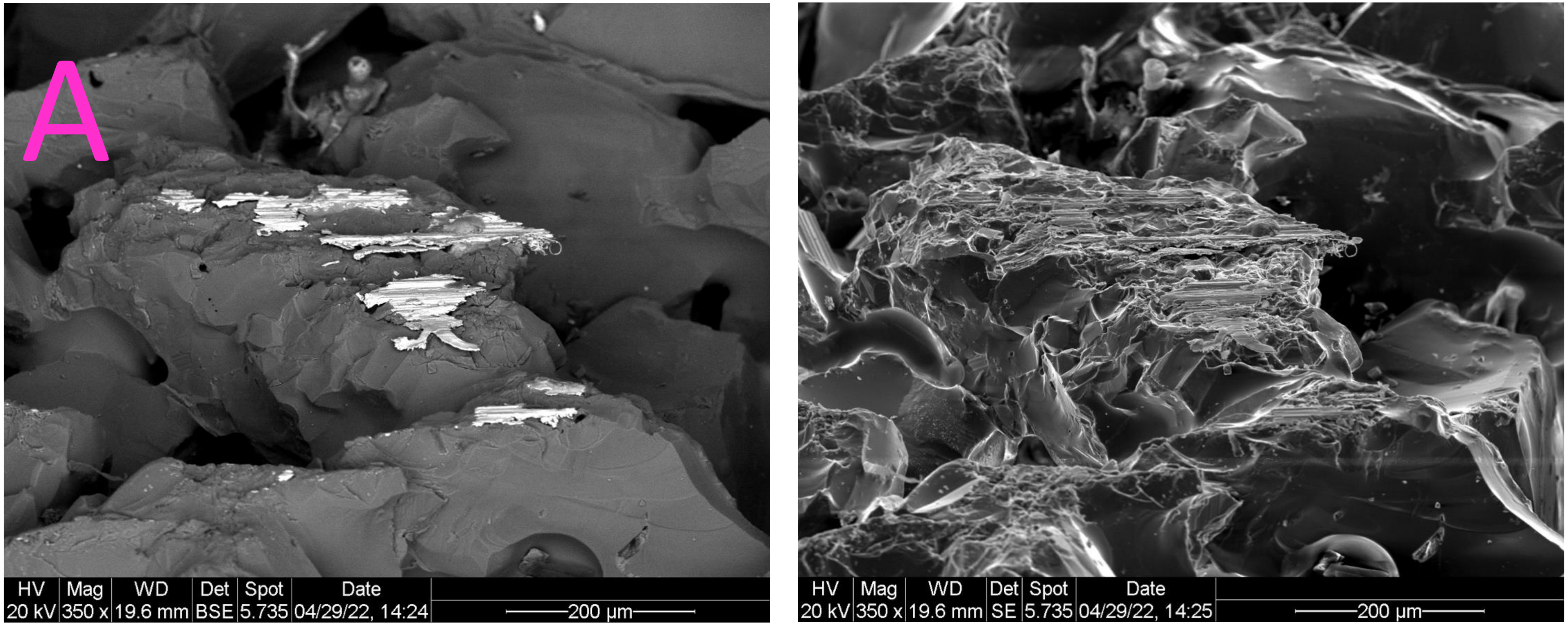

Figure 109: Zoom Dull part rectangle A - comparison BSE and SE

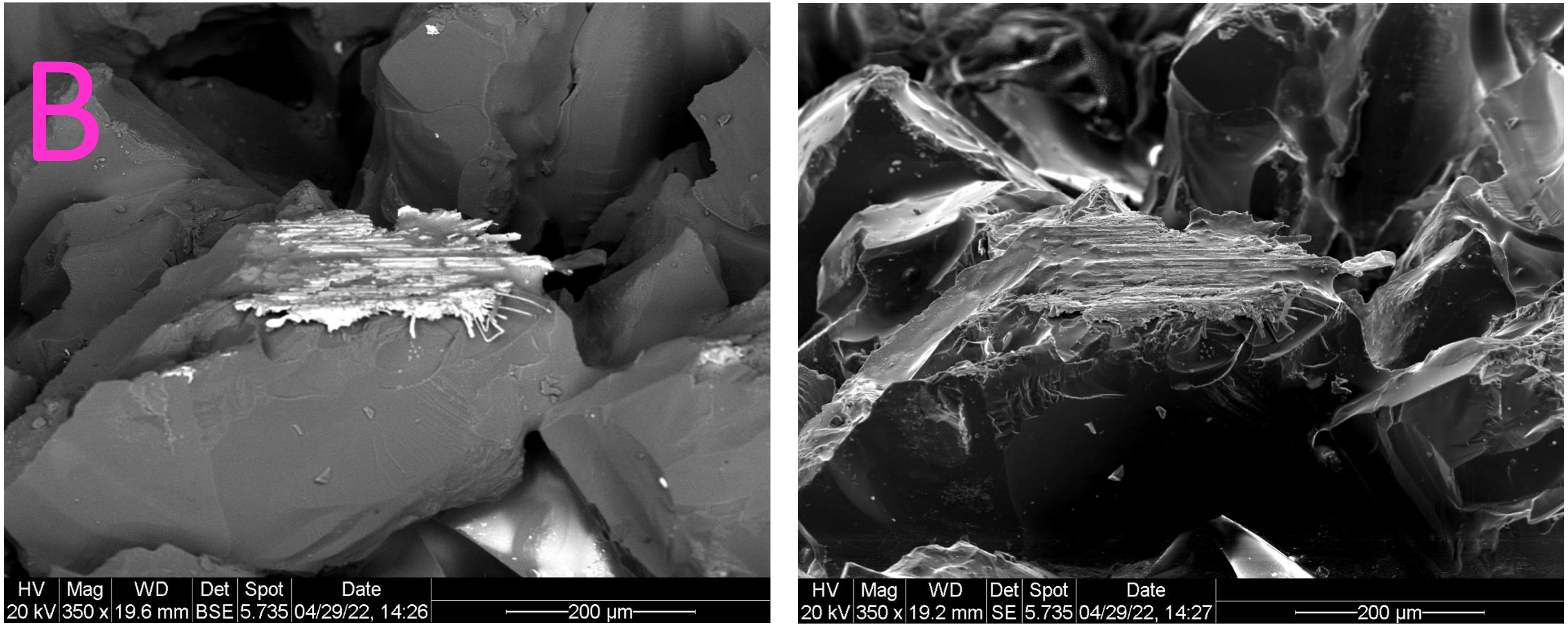

Figure 110: Zoom Dull part rectangle B - comparison BSE and SE

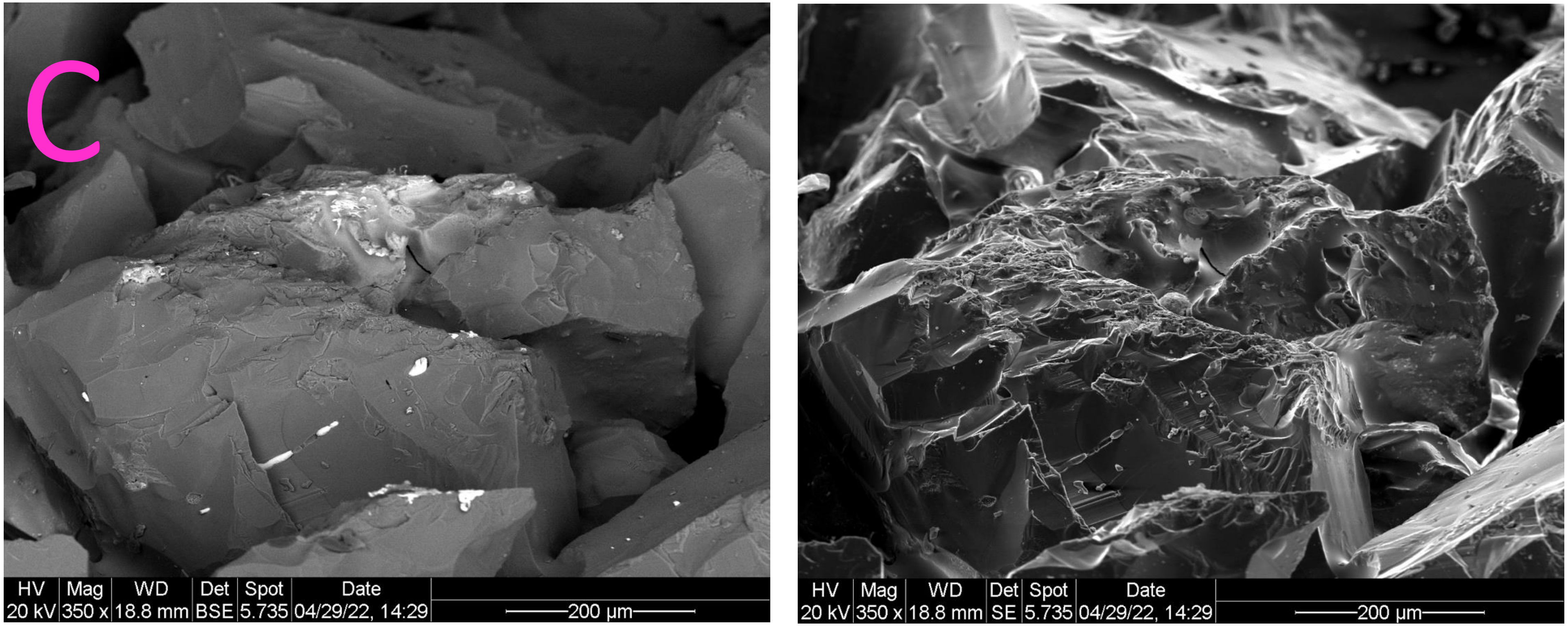

Figure 111: Zoom Dull part rectangle C - comparison BSE and SE

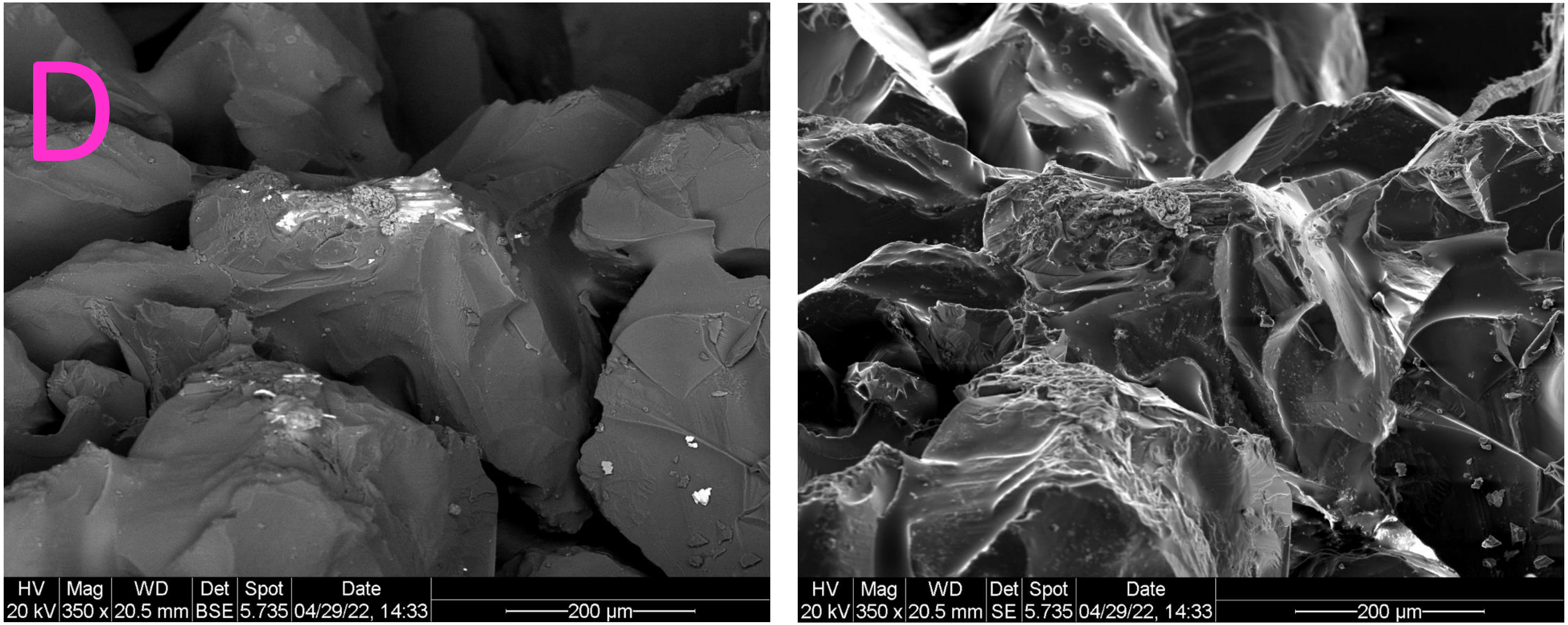

Figure 112: Zoom Dull part rectangle D - comparison BSE and SE

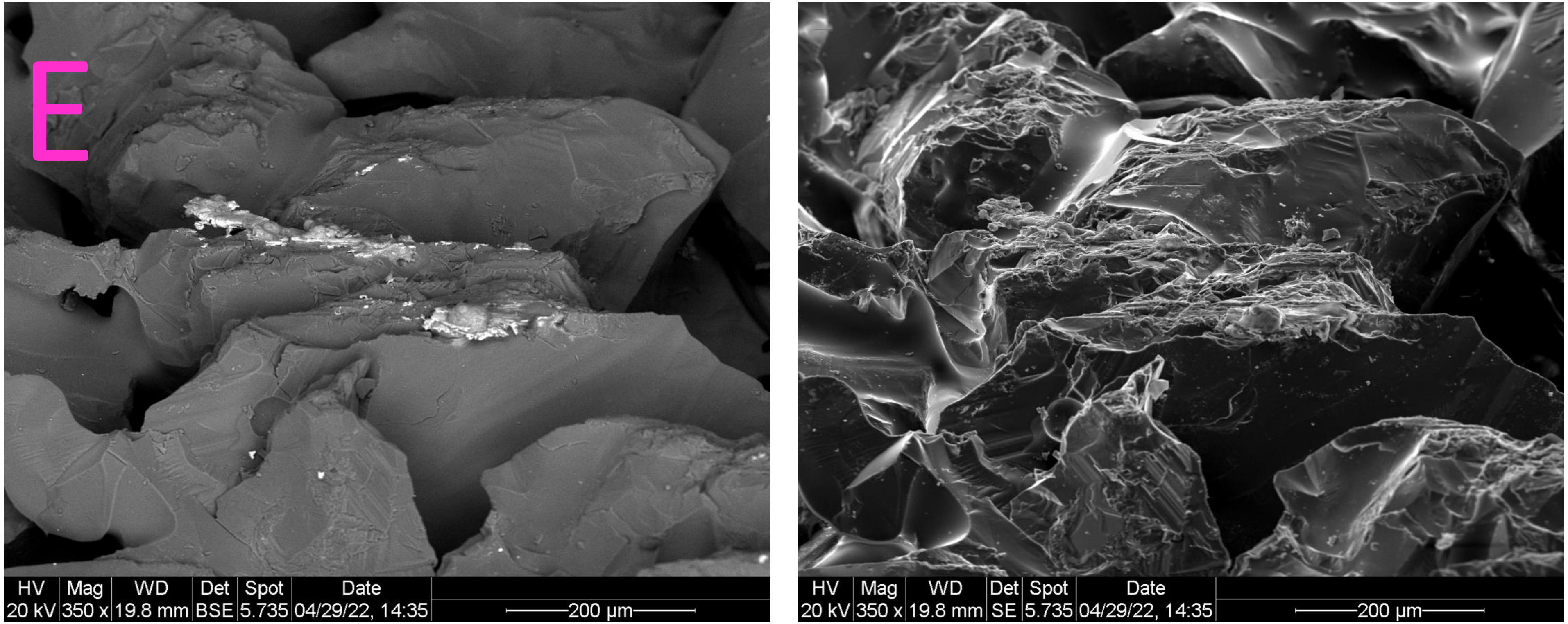

Figure 113: Zoom Dull part rectangle E - comparison BSE and SE

In conclusion, in Figure 114 there is an interesting zoom of the dull part of the step, which shows the comparison between BSE and SE of a very flat surface, taken with high tilt angle.

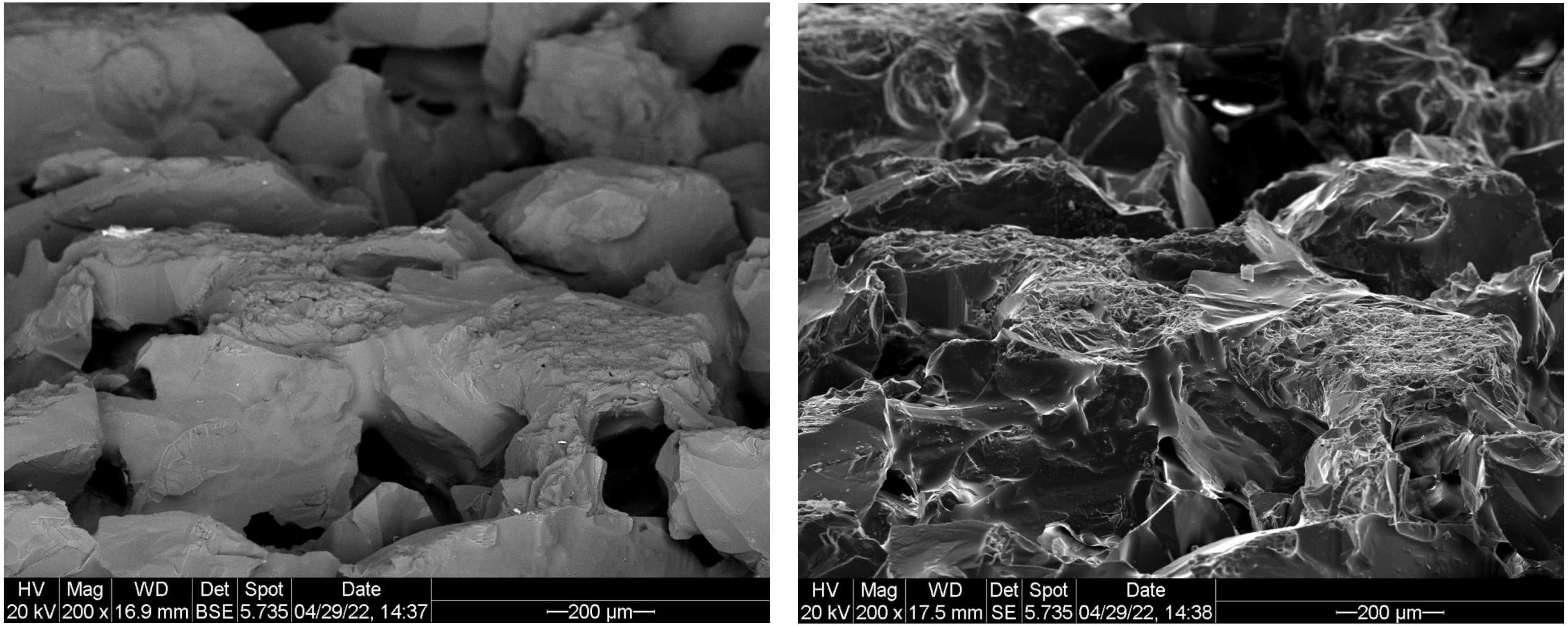

Figure 114: Very flat area, dull part of the grinding wheel step - comparison BSE and SE

11 Experimental results discussions and conclusions

A discussion about the experimental job performed in this study for plunge-roll dressing of vitrified grinding wheels is here presented as well as key results and conclusions. Moreover, problems during the tests and possible further developments are mentioned.

11.1 Consistency with Malkin and Murray's results

First of all, some of the results are comparable with Malkin and Murray's experiments, in particular plots for grinding specific energy versus dressing Aggressiveness number (this one coming for Malkin and Murray's data however with a further analysis for plotting SE_g against $Aggr_d$), and for grinding specific energy against dressing specific energy, the charts are re-proposed in the following (Figure 115).

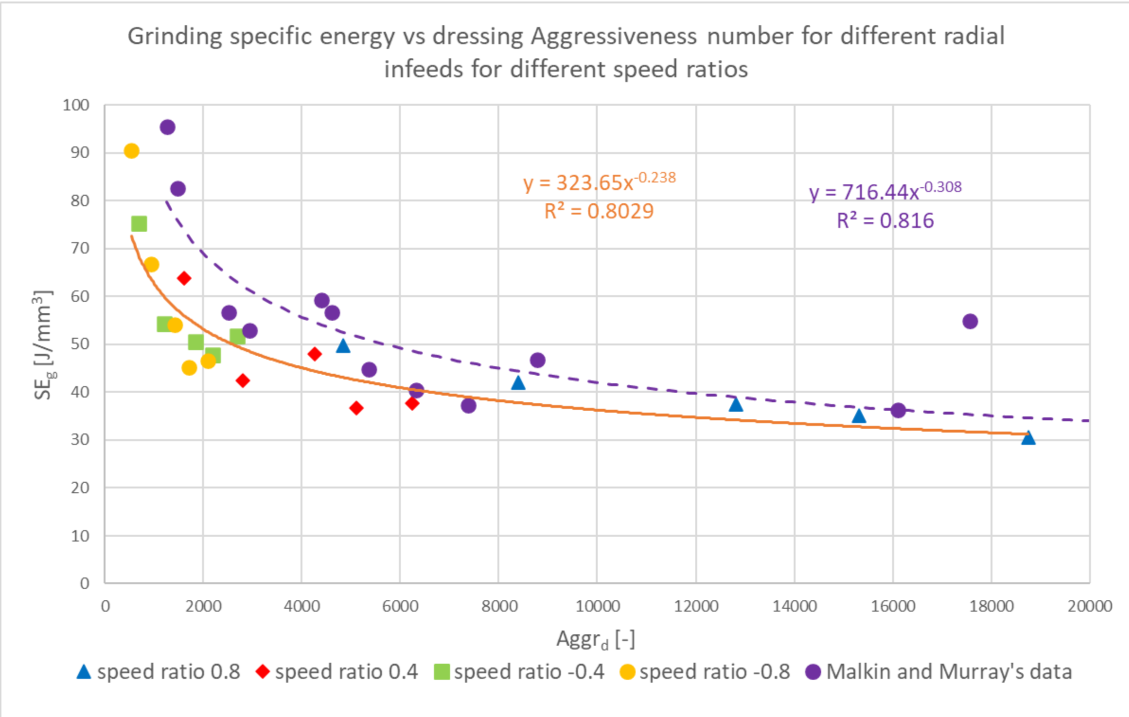

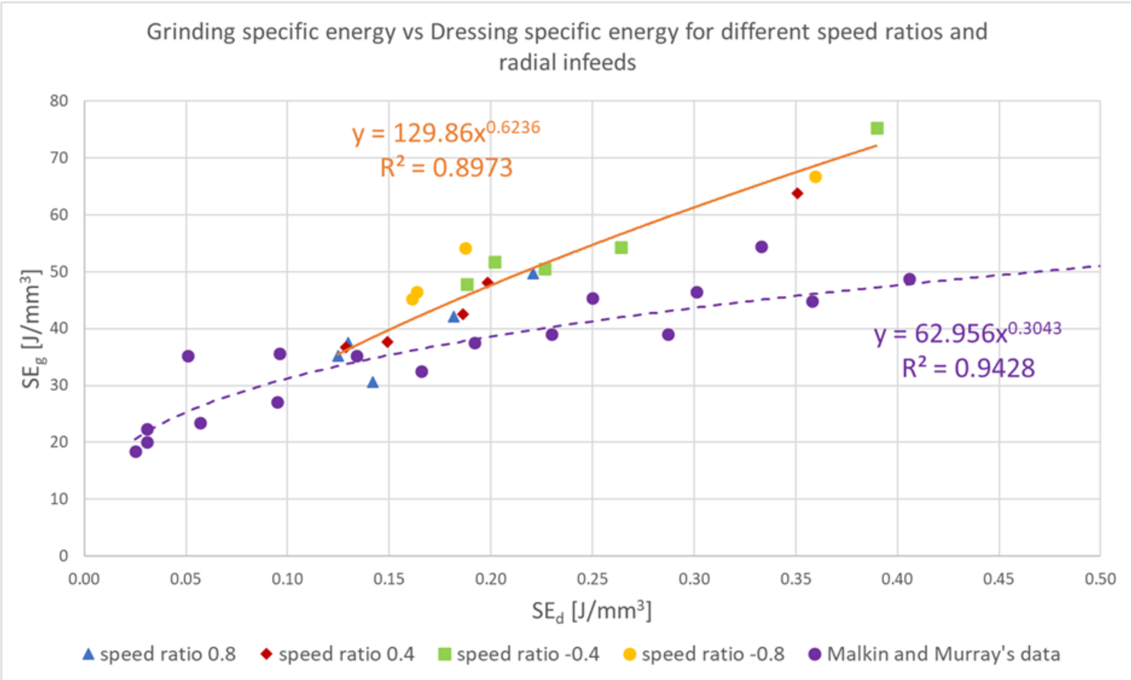

Figure 115: experimental plots similar to Malkin and Murray's results

This is proving that in general, even if for different conditions and tools such as dressing roll, grinding wheel, steel workpiece, the behaviours of the involved variables are consistent overall.
Indeed, in the first, case data points for grinding specific energy versus dressing Aggressiveness number have the same behaviour as well as similar values.
Speaking about the second plot in Figure 115, for grinding specific energy versus dressing specific energy, the situation is a bit different: considering the behaviour it is possible to state both for Malkin and Murray's results both for the new experiments that for higher dressing specific energy, higher grinding specific energy corresponds, but by looking at the data points value it is more difficult to find a clear similarity. This is due to many factors involved in the operations performed such as: material type, grit size and type for grinding wheel grits, coolant type, grinding parameters just to mention a few. Therefore, in this case the primary finding is that for given grinding operation, grinding specific energy increases with dressing specific energy.
In order to get a better idea of the reasons for the difference in these values, more tests with a larger variety of dressing parameters as well as different grinding conditions and various grinding wheel types should be run.

11.2 Dressing Aggressiveness number usefulness for industry purposes and burning preventing

A second important point is the utility of defining a dressing Aggressiveness number for industry purposes.

One of the main strengths of this dimensionless number is that by simply looking at the equation for plunge-roll dressing it is possible to adjust the parameters (speed ratio and radial infeed per wheel revolutions) in order to speed-up the production and still avoid burning.

$$Aggr_d\ [-] = \frac{1}{1-\underline{\left(\frac{v_r}{V}\right)}} \cdot \sqrt{\frac{\underline{a_{eff}}}{d_{eq}}} \cdot 10^6$$

Moreover, once the grinding conditions is fixed, it is possible to establish a "rule" to foresee thermal damages, indeed burning as previously mentioned is caused by a combination of too dull dressing (low dressing Aggressiveness number) and too large grinding Aggressiveness (e.g. high workpiece feedrate, large depth of cut).

In the following picture, for fixed grinding conditions, only one dressing condition (the dullest) led to burning, thus a threshold can be established.

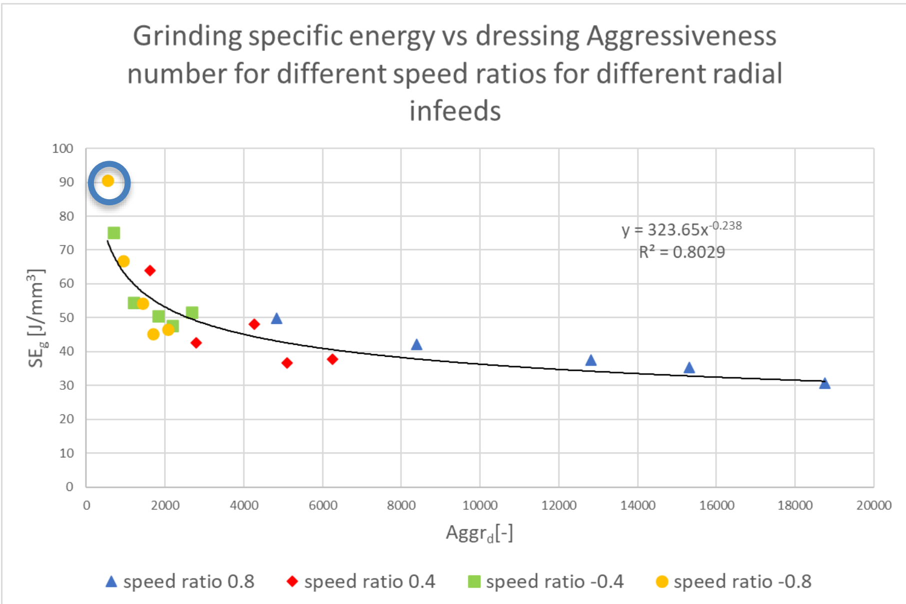

Figure 116: grinding specific energy versus dressing Aggressiveness number, burning threshold

A similar reasoning for variable dressing and grinding conditions is displayed in the next plot, and once again, burning can be easily detected in Figure 117.

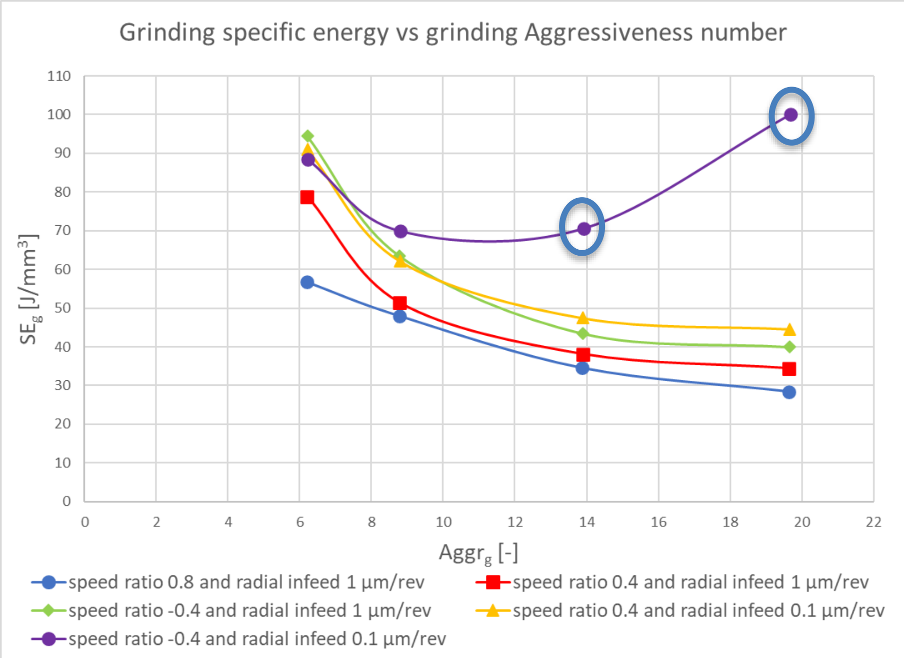

Figure 117: grinding specific energy against grinding Aggressiveness number, burning occurred

11.3 Wheel sharpness assessment

Once again, a key point is that through the dressing Aggressiveness number it is possible to assess the wheel sharpness, in fact for establishing if the dressing condition is dull or sharp, thus if the grinding wheel would have more or less flattened areas, the same plot as the one shown in Figure 116 can be utilized: as stated several times already, duller dressing condition will lead to higher specific energy, and vice-versa for sharp condition. In conclusion, by knowing at $Aggr_d$ or SE_g it would be possible to have an accurate idea of the dressing conditions (if knowing the type of dressing process involved).

Additionally, the SEM images have revealed consistent differences between dull and sharp condition, and as it can be seen in the following comparison (Figure 118) between two of the zooms on dull and sharp areas with steel loading, in the dull condition the steel presence results higher and the material is basically molten, indicating larger rubbing and plowing with respect to cutting, hence higher heat generation. On the other hand, in the sharp case, some chips are visible by means of the backscattered electrons, therefore the grains edges are sharper, and cutting is occurring.

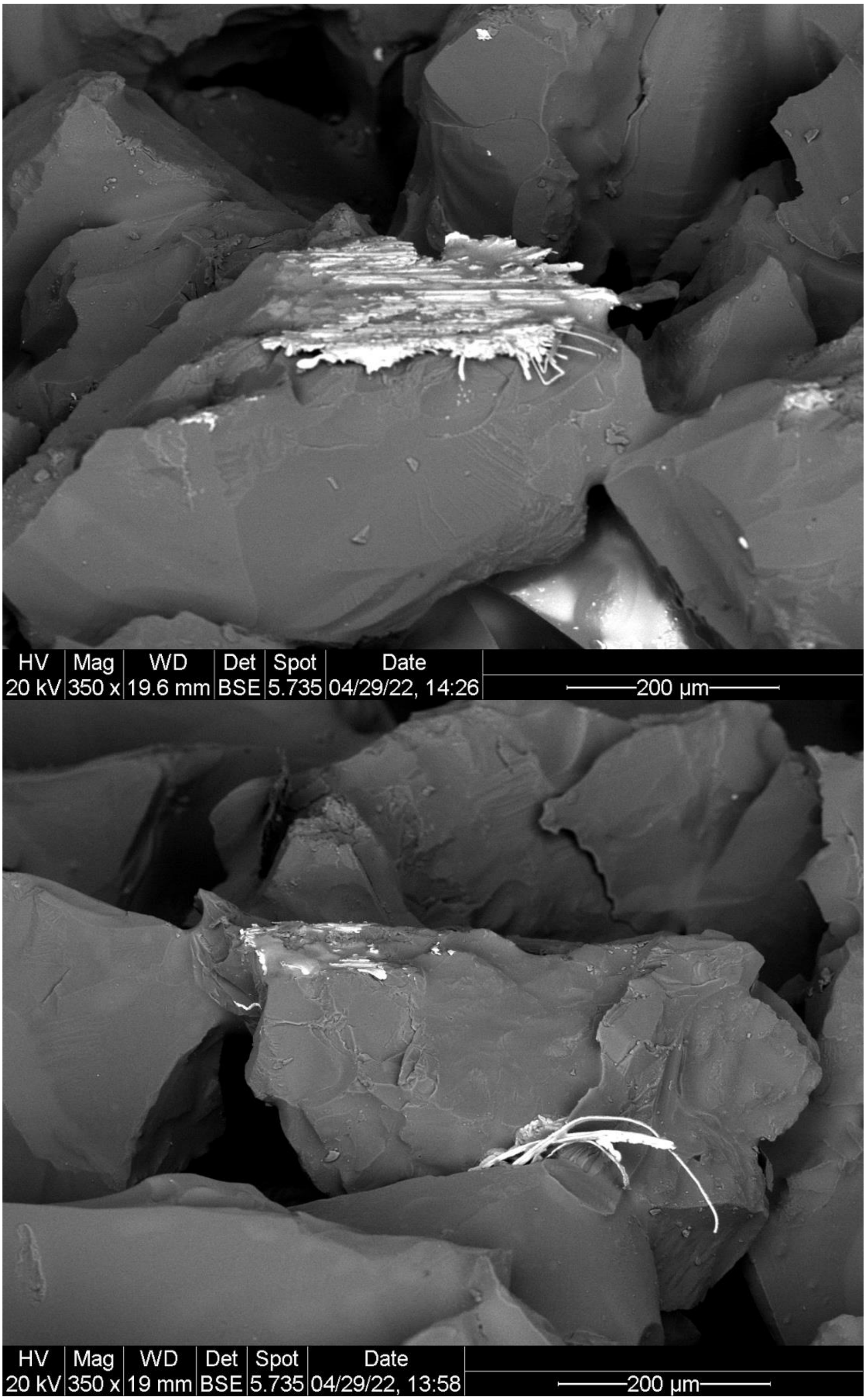

Figure 118: dull (above) and sharp (below) conditions comparison

11.4 Acoustic emission signal during dressing

Acoustic emission has been another important study factor in the tests.
By means of the acoustic emission sensor mounted in the machine, it was possible to collect AE data coming from the dressing operations and draw conclusions.
First, it has been proven that it was possible to find a correlation between acoustic emission and dressing power (Figure 77), or an even better between the corresponding specific energies (Figure 81).
In Figure 84 and Figure 85 there is a proof that dressing power and acoustic emission have the same behaviour during the process.
Finally, there is the possibility of defining an acoustic emission calibrated power, and in Figure 79 it has been noticed that the accuracy will not be too low with respect to the one coming from following a power law trend, the one with the highest R^2. The acoustic emission value was given in percentage of a certain Volt value, not known; nevertheless, it is possible to say that the Volt value was "calibrated" as well to have a correlation between AE and dressing power giving a possible linear proportionality with slope close to 1: hence a percentage value of acoustic emission would correspond to the same value in Watts for the dressing power.

11.5 Problems and further developments

1) Surface roughness measurements

   One of the main problems has been measuring the surface roughness on the ground workpiece. A profilometer was functioning and ready to be used, tests have been performed, however with unexpected results: not a defined behaviour for surface roughness of the workpiece for different dressing conditions. The probable reason for that was chatter, that has been found on the ground track on the workpiece. The chatter was not easy to detect, nevertheless it was enough to invalidate the surface roughness measurements. The reasons that could have caused the phenomenon are:

   - magnetic chuck not strong enough to withstand grinding forces (a new one is expected to arrive soon).
   - Run-out tolerance and possible clearances while mounting dressing roll on the dressing station spindle.

2) Number of cutting points evaluation

   An effort has been done for measuring somehow the number of cutting points of the grinding wheel for different dressing conditions (one extremely sharp and one extremely dull).

   The idea was to get the number of cutting points per mm^2 for the two conditions, or at least look for some kind of differences. The grinding wheel step has been dressed with -0.8 as speed ratio and 0.1 µm/rev as radial infeed on the left, and with +0.8 as speed ratio and 1 µm/rev as radial infeed on the right.

   The following image (Figure 119) is showing the results after applying a black spray painting on the grinding wheel step and rolling the grinding wheel on a white paper sheet. No clear difference between the two conditions have been identified.

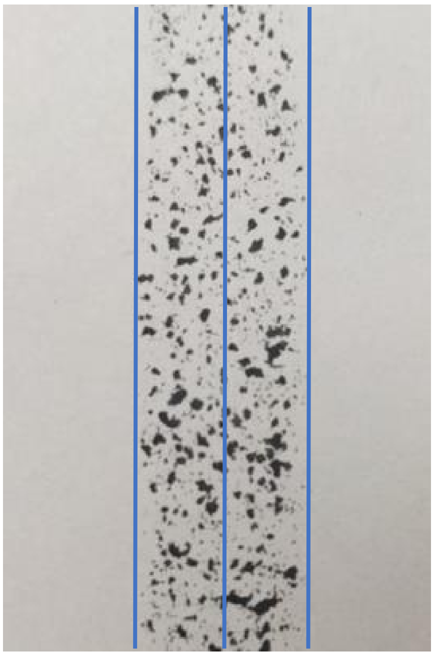

Figure 119: number of cutting points for dull (left half) and sharp (right half) dressing conditions on the grinding wheel step

The specimen has been sent to a laboratory with availability of an optical system, the tests have not been run yet though.

3) Future studies and improvements

The study of course is not complete, and the development possibilities are several.
For instance, not enough data points for dressing and different dwell times have been testes, it would be interesting to look for a correlation between dressing condition and number of dwell revolutions to achieve a proper spark out of the grinding wheel.
Furthermore, studies have been performed on Aluminum oxide grinding wheels, however it would be relevant to run similar tests on CBN grinding wheels. The problem has been the cost, since superabrasives are expensive, and working with the same dressing roll and disk used for the conventional abrasive grinding wheel on this type of wheel would cause larger wear rate, hence higher expenses for dressing tools as well.
In addition, it would be of interest to try dressing conditions with even higher dressing Aggressiveness. As seen in the comparison plots in Figure 115, the experiment area was restricted with respect to the one considered by Malkin and Murray, indeed the maximum dressing Aggressiveness in the two cases were about 20000 and about 90000, hence the study could be extended by using even higher dressing Aggressiveness, simply by increasing the radial infeed per wheel revolution.

Figure index

References

[1] M. P. Groover, Principles of modern manufacturing.

[2] Amstead, Ostwald and Begeman, Manufacturing processes.

[3] S. Kalpakjian and S. R. Schmid, Manufacturing engineering and technology, Pearson, 2006.

[4] S. Malkin and C. Guo, Grinding Technology - Theory and Applications of Machining with Abrasives, 2008.

[5] Creep-feed grinding - Continuous dressing.

[6] P. Krajnik, F. Hashimoto, B. Karpuschewski, E. J. d. Silva and D. Axinte, “Grinding and fine finishing of future automotive powertrain components”.

[7] J. Badger, The grinding book.

[8] T. Murray and S.Malkin, “Effects of Rotary Dressing on Grinding Wheel Performance”.

[9] S.Malkin and T.Murray, “Mechanics of Rotary Dressing of Grinding Wheels”.

[10] J. Badger, P. Krajnik and R. Dražumerič, “Application of the dimensionless Aggressiveness number in abrasive processes”.

[11] J. Badger, S. Murphy and G. E. O'Donnel, “Acoustic emission in dressing of grinding wheels: AE intensity, dressing energy, and quantification of dressing sharpness and increse in diamond wear-flat size,” *International Journal of Machine Tools and Manufacture 125,* 2018.

[12] S.Malkin and T.Murray, “Comparison of single point and rotary dressing of grinding wheels”.

[13] “PLANOMAT HP | BLOHM,” [Online]. Available: https://www.blohm-machines.com/en/grinding-machines/detail-view/product/planomat-hp/.

[14] P. Beyer, “Hybrid technology for dressing systems”.

[15] “Basic of bonded abrasives - Hermes”.

[16] B. Linke, “Wirkmechanismen beim Abrichten keramisch gebundener Schleifscheiben”.